FREIBURGER SCHRIFTEN
ZUR HYDROLOGIE

Band 22

Karl Ludwig & Manfred Bremicker (Eds)

The Water Balance Model LARSIM - Design, Content and Applications

Institut für Hydrologie der Universität Freiburg i.Br.

Karl Ludwig & Manfred Bremicker (Eds)

The Water Balance Model LARSIM - Design, Content and Applications

Drucklegung unterstützt durch / Publication supported by:

Förderverein Hydrologie an der Albert-Ludwigs-Universität
Freiburg im Breisgau

FREIBURGER SCHRIFTEN ZUR HYDROLOGIE

Band 22

Karl Ludwig & Manfred Bremicker (Eds)

The Water Balance Model LARSIM – Design, Content and Applications

2006

Institut für Hydrologie der Universität Freiburg i. Br.

Freiburger Schriften zur Hydrologie

Herausgegeben von / Edited by:

Prof. Dr. Christian Leibundgut
Prof. Dr. Siegfried Demuth
Dr. Jens Lange

Institut für Hydrologie, Universität Freiburg i. Br.

Schriftleitung / Editorial office:

Ingeborg Vonderstraß

Verlag und Vertrieb / Published and saled by:

Institut für Hydrologie
Universität Freiburg i. Br.
im Selbstverlag
Anschrift / Address: Fahnenbergplatz, D-79098 Freiburg i. Br.
Germany

ISSN 0945-1609

Preface – About LARSIM

LARSIM is an acronym for **L**arge **A**rea **R**unoff **Si**mulation **M**odel. It is a hydrologic model, which describes continuous runoff processes in catchments and river networks. LARSIM is based on an earlier river basin model for single flood and low-flow episodes, from which it inherited the general model structure. Hydrological processes are simulated in a series of subarea elements connected by flood routing elements in a predetermined sequence. LARSIM simulates the hydrologic processes for one element for a defined time period. The resulting output hydrograph is the input information for the next element according to the general model structure rules. The model structure can be grid based or based on hydrologic subcatchments.

Since about a decade hydrological system data (e.g. land use, soil types, topography and channel data) needed for model input is digitally available for large areas in a high spatial resolution. At the same time computer speed and capacity have evolved significantly. This has made it possible to apply the model to large areas using a high-resolution grid, e.g. 1x1 km grid subareas for catchments of several thousands of square kilometres.

These features allow applications to a great variety of problems using different time and space scales. LARSIM has been used for simulations of flood protection planning, land use changes, and effects of climate change on water resources. An important function is its application to operational forecasts of floods, low flow and water temperature.

The use of the model by different water authorities, which articulated their particular wishes for further development and additional model features in a highly cooperative way, especially helped to develop a practically useful model. Particularly its application as a routine tool for operational forecasts of runoff and other hydrologic parameters (soil moisture, snow cover) resulted in a very reliable and stable model code.

The description of LARSIM in this paper is to a great extent based on a German description of the model and examples of its application in BREMICKER 2000 (Freiburger Schriften zur Hydrologie, Band 11). The more recent model developments regarding snowmelt, soil water budget, water temperatures and operational forecast methods have been added here.

Current developments of LARSIM are aiming at the simulation and forecast of oxygen content of water and also at applications to long-term forecasts for different purposes.

Karl Ludwig, Manfred Bremicker

Karlsruhe, Germany, September 2006

Freiburger Schriften zur Hydrologie

Band 22 / Volume 22

Contributors:

Manfred Bremicker [1)]
Martin Ebel [2)]
Kai Gerlinger [2)]
Ingo Haag [2)]
Annette Luce [2)]
Karl-Gerd Richter [2)]
Angela Sieber [1)]

[1)] State Institute for Environment, Measurement and Nature Conservation Baden-Württemberg. Karlsruhe, Germany www.lubw.baden-wuerttemberg.de

[2)] Ludwig Consulting Engineers. Karlsruhe, Germany www.ludwig-wawi.de

Contents

Summary

In this paper, the hydrologic basis of the water balance model LARSIM and application examples are presented. LARSIM allows a process- and area-detailed simulation of the water cycle. It uses system data, which are readily available in most cases.

Fundamental approaches used in LARSIM are described in detail for the following hydrological subprocesses: interception, actual evapotranspiration, snow accumulation, metamorphosis of snow and snow melt, soil water and groundwater storage, lateral water transport to streams (run-off concentration), water temperature and routing in channel networks. Furthermore, procedures for regionalisation of model parameters of LARSIM and methods of spatial interpolation of meteorological input data are discussed.

Various applications of LARSIM are described: the impact of climate change on water balance in south-western Germany, water budget of the Baltic Sea catchment in connection with coupled atmosphere-hydrology simulations, hydrologic effects of land use change and the operational forecasts of low flow, flood and water temperature by the Flood Forecast Centre (HVZ) of the federal state of Baden-Württemberg (Germany).

1 Introduction

Water balance models are programs to quantify the spatial and temporal distribution of important hydrometeorologic data and hydrologic conditions like precipitation, evaporation, seepage, water storage in the catchment and runoff (SINGH 1995). They combine different water balance components (Fig. 1.1).

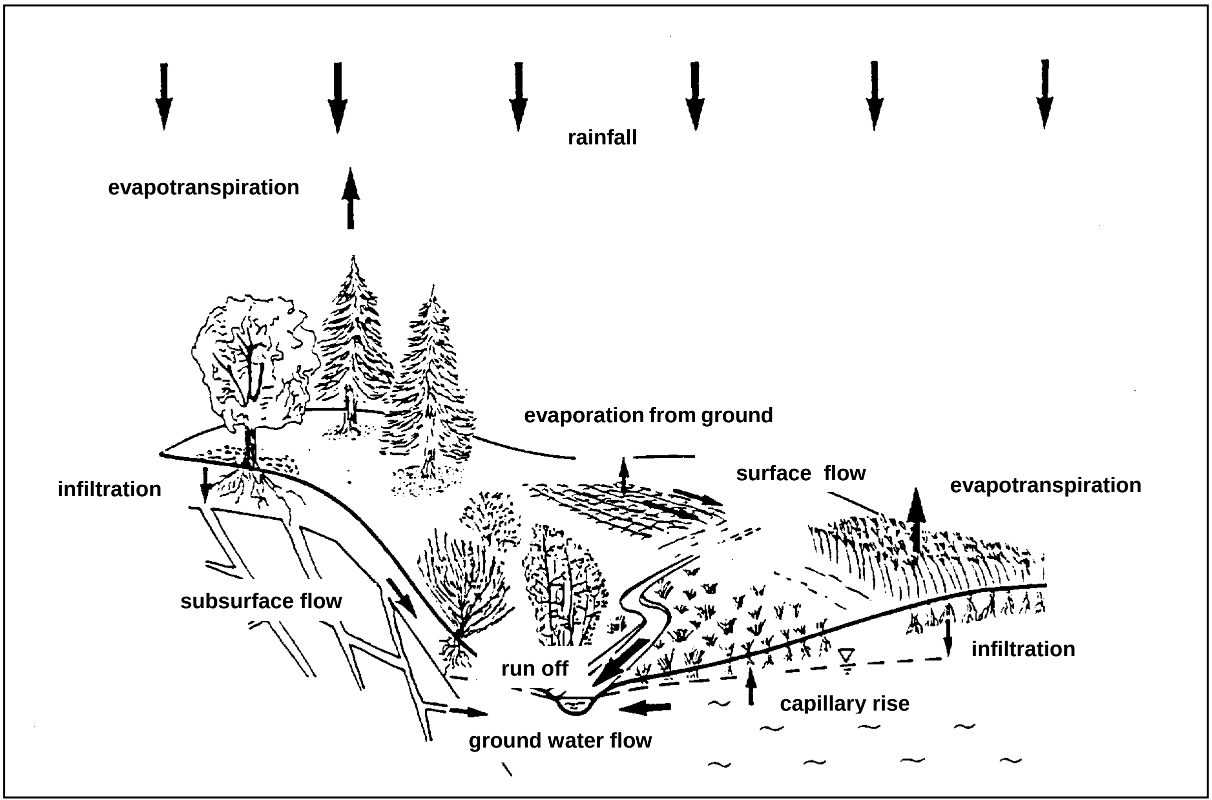

Fig. 1.1 Water balance components (WOHLRAB et al. 1992, modified)

Water balance models are an extension of conventional precipitation-runoff models (e.g. single flood models). They allow continuous, process-oriented simulations and forecasts of the *entire* runoff process. They include components of water balance, as e.g. groundwater recharge or snow cover and allow their time-space-dependent description and display.

Water balance models can be used for different purposes as:

- *Display of the current system state*

  E.g. as basis for evaluation of critical situations for water management, description of input parameters for water quality models and groundwater models.

- *Simulation (prognosis/scenarios) of changed system states*

  E.g. for calculating effects of climate changes or changes in land use on the water balance, especially flood and low-flow characteristics or groundwater recharge.

- *Forecasts*

  E.g. operational low-flow forecast, continuous daily discharge forecast, flood or temperature forecasts.

Input parameters for water balance models are on one hand system data like elevation, land use, soil parameters as field capacity and channel geometry, and on the other hand hydrometeorologic time series like precipitation, air temperature, air humidity, wind speed, global radiation, water temperature and discharge.

Since CRAWFORD AND LINSLEY (1966) developed the Stanford Watershed Model, a variety of water balance models were designed, which could simulate more details of the hydrologic processes, because of several improvements. An overview over such models can be found in SINGH (1995), SINGH AND FREVERT (2002) and UBA (1995), an overview over various applications in BWK (1998), a summary of the state of research in SCHULLA (1997).

This document deals with the program LARSIM (**L**arge **A**rea **R**unoff **Si**mulation **M**odel). Since it's development in the context of the research program BALTEX (BALTEX 1995, BREMICKER 1998), this water balance model is applied both in scientific practice and research (e.g. GATHENYA 1999; GERLINGER AND TUCCI 1999; BAUER 1999; LFU 1999b,c,d; BREMICKER 2000; EBEL et al. 2000; BREMICKER et al. 2004; GERLINGER 2004; HAAG et al. 2005; BREMICKER et al. 2006).

LARSIM allows a process- and area-detailed simulation of the medium-scale mainland water cycle. It uses system data, which at time are generally available in most cases.

2 Concept of the water balance model LARSIM

In hydrological modelling, reasonable process descriptions and solution approaches depend, among other factors, on the intended spatial resolution (BECKER 1992). Therefore, some basic considerations regarding scale and model set-up are given first.

2.1 Scales and process description in hydrology

In general, with increasing scale more details of hydrological systems and processes can be described, which cannot be discerned in smaller scales (DYCK 1980: 47). As a consequence, hydrological characteristics acquired from studies within medium-sized or small scales cannot be transferred to large scales (DYCK 1980: 49 and BECKER 1995).

To classify these varying spatial (and - closely connected - temporal) scales, three categories, micro-, meso- and macro-scale have been defined (BECKER 1986 and PLATE 1992). As these scales can only roughly be specified, intermediate stages of scales (transitions) are frequent, depending on the model purpose (Table 2.1).

Tab. 2.1 Scales in hydrology (BECKER 1992)

Scales in hydrology		Characteristic lengths*	Characteristic areas*
Main scale categories	**Transition categories**		
Macro-scale	-	> 100 km	> 10 000 km^2
	Lower extended macro-scale section	30 - 100 km	1 000 - 10 000 km^2
Meso-scale	Upper extended meso-scale section	10 - 30 km	100 - 1 000 km^2
	-	1 - 10 km	1 - 100 km^2
	Lower extended meso-scale section	0.1 - 1 km	0.01 - 1 km^2
Micro-scale	Upper extended micro-scale section	30 - 100 m	0.001 - 0.01 km^2
	-	< 30 m	< 0.001 km^2

* the figures only indicate orders of size, they are no exact limits

According to PLATE (1992) and BECKER (1992), the spatial range of scales and the corresponding hydrological models can be described as follows:

- In the *micro-scale*, processes can be described which occur in small, homogeneous subareas of a catchment. The characteristic size subarea is usually smaller than one hectare. Generally, physical laws can describe micro-scale processes appropriately. The corresponding physical constants can be determined in laboratories.
- In the *meso-scale*, larger areas of usually heterogeneous structure are considered. A typical example for this scale is a catchment of some square kilometres with different land uses, soil types, slopes and expositions. A meso-scale model cannot fully describe all aspects of such a heterogeneous area by physical laws, but rather summarizes elementary characteristics in groups. Another property of meso-scale models is, that some parameters have to be calibrated according to the natural conditions rather than being deduced from physical measurements or basic constants.
- In the *macro-scale*, catchment areas larger than 10 000 km² are summarized. Models of this type aim at large-area effects, e.g. due to climatic changes. In most cases, macro-scale-models are relatively simple concept models (BECKER 1995), whose parameters have to be adjusted by calibration, analogous to the meso-scale models. Due to different model structures, parameters will not be comparable with lower-scale models.

It must be considered that a model's classification (micro-, meso-, or macro-scale) does not depend on the overall size of the observed area, but on the characteristic size of subareas, for which the process descriptions are designed. Therefore, in area-detailed models, these process descriptions are often made on a subarea level. In the water balance model LARSIM, the hydrological processes are described on a meso-scale level. This scale includes subarea sizes ranging from a few hectares up to several hundred square kilometres.

2.2 Concept of LARSIM for the BALTEX project

In its first version LARSIM was developed in the research project BALTEX (for the Baltic Sea catchment including the Elbe river, total area about 2 Mio. km^2, BALTEX 1994 and 1995) to improve the description of the land-bound water cycle in the regional climate model REMO (JACOB 1995) and to be used as general hydrological component in a coupled atmosphere-hydrology model.

Water balance models available at that time and described in the literature did not seem suitable for different reasons (BREMICKER 1998; BREMICKER 2000). The basic concept for the development of LARSIM was to use relatively simple, but as far as possible physically based (sub-) models, which could be applied on a basis of readily available spatial system data to describe the land-bound water transport in the meso-scale.

This water balance model as component of a combined atmosphere-hydrology model should enable:

- improved modelling of the lower boundary conditions for the atmosphere model (e.g. soil moisture, snow cover, runoff in rivers),
- verification of essential components of the water cycle (e.g., evapotranspiration, soil water

storage and freshwater fluxes to the ocean) which could be used in the combined hydrology-(ocean)-atmosphere model and thus

- making possible a decisively improved coupling of atmosphere models including land bound processes and ocean models.

According to this, a model should be developed with a grid structure identical to the climate models of that time (several hundred square kilometres). Additional guidelines for the model concept were:

- Only feasible approaches described in the current literature should be used.
- Hydrological subprocesses, which should be represented, were: interception, evapotranspiration, snow accumulation, snow compaction, snowmelt, soil water storage, discharge concentration in the area and flood-routing in channels.
- The temporal process resolution should be at least one day (possibly shorter).
- As evapotranspiration is an essential factor; the used method should be as accurate as possible.
- Hydrologic processes, which play a minor role in Central Europe, should be omitted (e.g. evaporation from ice-covered lakes).
- The Xinanjiang-method implemented by DÜMENIL AND TODINI (1992) in the climate model REMO should be used as the basic soil water model to establish a defined interface for the coupling of LARSIM and REMO.
- Geometrical channel data should be used for flood routing in rivers, to discern subarea and river flood-routing parameters in the model calibration.
- Retention in subareas should depend on characteristics of travel time.
- Only hydro-meteorological data, which are available from readily accessible data sources, should be used.
- Simulations of reservoirs (lakes) and river diversions should be possible.
- Alternatively, a subarea structure based on grids or on hydrologic subareas should be possible (Fig. 2.1).

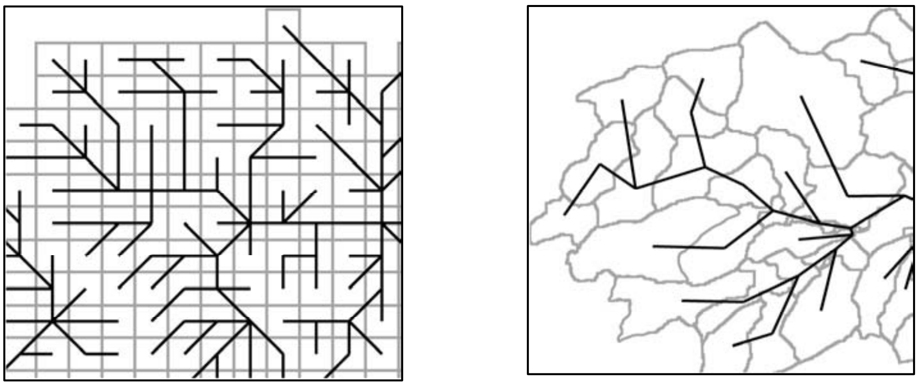

Fig. 2.1 Possible model structure in LARSIM: subareas grid-based (left) **or based on hydrologic subcatchments** (right)

In addition, the following computing specifications should be considered:

- The import routines for system data and time series as well as the program execution structures applied in the flood simulation model FGMOD (LUDWIG 1978, 1982, IFW 1982) should be used as program base.
- LARSIM should be compatible with FGMOD, i.e. LARSIM should also be able to compute FGMOD applications such as flood forecasts.
- Program language had to be FORTRAN 77 / 90, so that executable program versions could be compiled for Windows, Unix and VMS.
- LARSIM should be able to execute simulations for large model (high resolution or large-scale) systems (e.g. for the Neckar catchment with about 15 000 subareas, 16 land use classes and 8 760 calculation intervals) on commercial PCs with calculation times of at most 1 hour.

Due to the classification by BECKER (1995), LARSIM represents a deterministic concept model, a "distributed model" for area-detailed application (Fig. 2.2). LARSIM is not limited to the simulation of larger areas but can also be applied to a whole range of different catchment sizes (see application examples in Section 6).

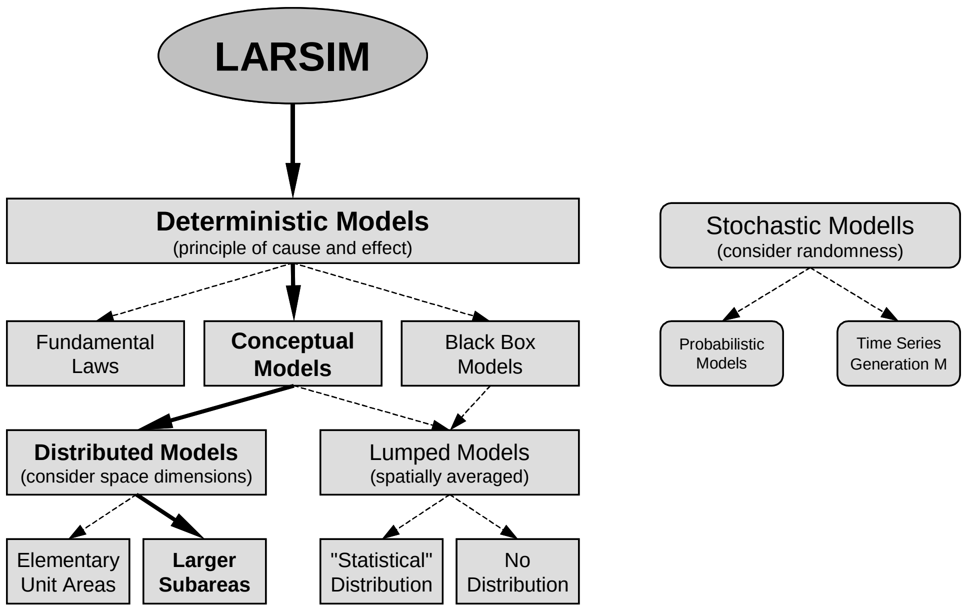

Fig. 2.2 Classification of LARSIM in general categories for hydrologic models (BECKER 1995, modified)

3 Components of LARSIM

LARSIM describes the following water balance subprocesses using deterministic models: interception, evapotranspiration, snow accumulation, compaction and melt, soil water retention, storage and lateral water transport, as well as flood-routing in channels and retention in lakes. Additionally, there are procedures for correction and conversion of measured meteorological data. Anthropogenic factors like water transfer and discharge regulation by reservoirs or dams, as well as water temperatures can be simulated by the model.

Interception, evapotranspiration, snow processes and soil water storage are modelled separately for each single land use category (usually of much smaller scale than subareas) in a subarea to account for essential effects of heterogeneous land use on evaporation (Table 3.1). The model can be operated on grid-based subareas or on subareas according to hydrologic subcatchments (see Fig. 2.1).

Tab. 3.1 Hydrological processes in LARSIM and their spatial allocation

Hydrological process		Allocated spatial resolution in LARSIM
Interception	Area	Per land use category of a subarea
Snow accumulation, snow compaction and snow melt		
Evapotranspiration		
Soil water storage with runoff generation separated in direct runoff, interflow and groundwater runoff		
Discharge concentration in the drainage area	Area	Subarea
Flood-routing	Line	Channel section
Retention in lakes or controlled water release	Point	Lake, storage dam, reservoir

Output results of hydrologic submodels for the different types of land use and field capacities without regarding their spatial allocation within the subarea are added to produce the total output of each subarea. This corresponds to the Grouped Response Unit (GRU) approach (KOUWEN et al., 1993) which has been used by several hydrological models, such as VIC (NIJSSEM et al. 1997) and WATFLOOD (SOULIS et al. 2004). The underlying idea is, that the spatial allocation within a subarea will not play an essential role on the water balance of a catchment, which is normally made up of a relatively great number of subareas. The number of subareas has to be determined according to the problem under investigation. Each subarea contains a limited number of distinct GRUs. Soil water budget is computed for each GRU, and runoff generated from the different GRUs in the subarea is then summed.

In LARSIM, the runoff resulting from the different GRU of a subarea is separated into three (or four) soil storages, one for direct runoff, one for interflow and one for groundwater runoff [1].The water release from these three (or four) storages, which forms the total runoff from a subarea, is routed through channels or lakes.

Provided that no measured discharge hydrographs are imported into the model, the runoff components mentioned above can be separately modelled and displayed during the water transport in channels. A scheme of the model and its various components is shown in Figure 3.1.

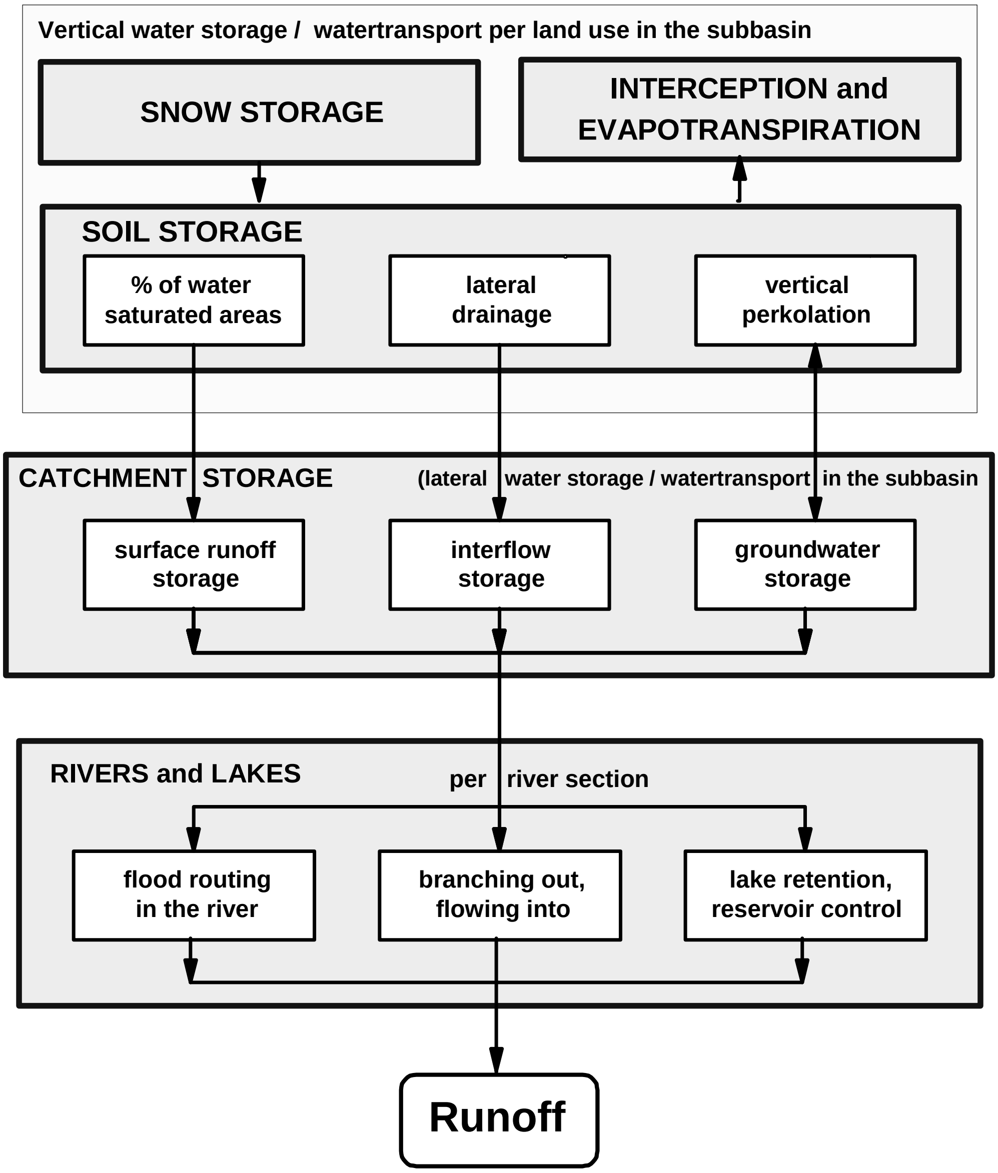

Fig. 3.1 Scheme of the water balance model LARSIM

[1] Here, the terms direct runoff, interflow and groundwater runoff are used as synonyms for flow systems reacting at different rates within the saturated and the unsaturated underground. A comprehensive bibliographical study about such flow systems can be found in LEIBUNDGUT AND UHLENBROOK (1997).

Calculation modes of LARSIM

Besides the use of LARSIM as a water balance model with a *continuous* simulation, the program can also be used as an *event-based* flood forecast model because of its compatibility with the event-based simulation and forecast model FGMOD.

If LARSIM is used as a flood forecast model, it is not necessary to model evaporation and soil water balance. For an event-based simulation, LARSIM only requires precipitation as meteorological input. If snow plays an essential role, air temperature and wind speed are needed as further input data.

For continuous water balance modelling, additional time series of the following data are necessary: global radiation, duration of sunshine, relative air humidity, dew point temperature, air pressure, water temperatures and water temperature (singular) sources. Measured values usually only serve as a verification of results, but can also be imported as input parameters, if desired.

Time intervals

In LARSIM calculations are based on equidistant time intervals. Several time intervals can be chosen (Table 3.2).

Tab. 3.2 Calculation time intervals in LARSIM

Computation mode of LARSIM	Possible time intervals	
	Simulation mode	Forecast mode (operational forecast)
Event-based modelling (flood forecast model)	5, 15, 30 minutes, 1 to 8 hours, 12 hours, 1 day	5, 15, 30 minutes, 1 to 8 hours, 12 hours, 1 day
Continuous water balance modelling	1 hour, 1 day	1 hour, 1 day

The hydrometeorological input data must be available (or prepared for) the calculation time intervals with the exception of data, which are usually measured at defined time points with larger differences as the model time interval (e.g. daily measurements of precipitation, temperature etc.).

For all hydrological processes the chosen time interval is used. Only in case that time intervals are shorter than a day, the calculation of evaporation is based on daily values, which are equally distributed to the selected calculation time intervals. The result is a constant (daily mean) value for the potential evapotranspiration or actual evapotranspiration. Interception evaporation is treated accordingly (depending on the content of the interception storage between zero and the potential evapotranspiration). As interception evaporation varies in the course of a day, actual evapotranspiration also varies.

3.1 Interception storage

Precipitation is partly stored on leaf surfaces of the vegetation as interception. This interception storage has a maximum capacity, which is described by a function of leaf area indices for different kinds of vegetation according to the approach of DICKINSON (1984):

$$K_{Inz} = 0.2\ mm \cdot LAI \tag{3.1}$$

K_{Inz}	[mm]	capacity of interception storage
LAI	[-]	leaf area index

The leaf area index (LAI) depends on the predominant plants (for the different land use categories) and varies over the year. It describes the population's leaf area in proportion to the ground area. LAI values are system data and can be selected specifically for the area under investigation.

LAI values used for the Neckar basin are shown in Table 3.3. Monthly LAI values for different land uses were defined from literature sources, in which references of DISSE (1995), HOYNINGEN-HUENE (1983), MAURER (1997) and THOMPSON et al. (1981) were analysed. As land use classes, viniculture, fallow, vegetationless surface and wetlands were not available, the corresponding leaf area indices were estimated.

If the interception storage is full, the leaves pass on any further precipitation directly to the ground. The interception storage is drained by evaporation. Thus, water from the interception storage is not available for the soil water storage. Evaporation of water from the interception storage is defined by the potential evapotranspiration used within the model (see Section 3.5).

If interception evaporation occurs, the current evapotranspiration for a population with wet leaf surfaces is calculated according to the approach of WIGMOSTA et al. (1994) as follows:

$$E_{ai} = \frac{\left(E_{pot} - E_{izp}\right)}{E_{pot}} \cdot E_a + E_{izp} \tag{3.2}$$

E_{ai}	[mm/d]	current evapotranspiration for vegetation with wet leaf surfaces (content of interception storage > 0)
E_{pot}	[mm/d]	potential evapotranspiration (calculated according to Eq. 3.29 with over-all surface resistance rs = 0)
E_{izp}	[mm/d]	interception evaporation
E_a	[mm/d]	current evapotranspiration for vegetation with dry leaf surfaces (Eq. 3.29)

Tab. 3.3 Monthly values for the leaf area index LAI in the water balance model for the river Neckar (Germany)

Land use	Leaf area index LAI											
	Jan.	Feb.	Mar.	Apr.	May	Jun.	July	Aug.	Sep.	Oct.	Nov.	Dec.
Sealed*	10	10	10	10	10	10	10	10	10	10	10	10
Fields**	0.4	0.4	0.3	0.7	3.0	5.2	4.6	3.1	1.3	0.2	0.0	0.0
Viniculture	1.0	1.0	1.0	1.5	2.0	3.5	4.0	4.0	4.0	1.5	1.0	1.0
Intensive orchards	2.0	2.0	2.0	2.0	3.0	3.5	4.0	4.0	4.0	2.5	2.0	2.0
Fallow (overgrown)	2.0	2.0	3.0	4.0	5.0	5.0	5.0	5.0	5.0	3.0	2.5	2.0
Unsealed, no vegetation	0.0	0.0	0.0	0.0	0.0	0.0	0.0	0.0	0.0	0.0	0.0	0.0
Intensive pasture	2.0	2.0	3.0	4.0	5.0	6.0	6.0	5.0	5.0	3.0	2.5	2.0
Wetlands	2.0	2.0	3.0	4.0	5.0	5.0	5.0	5.0	5.0	3.0	2.5	2.0
Extensive pasture	2.0	2.0	3.0	4.0	5.0	5.0	5.0	5.0	5.0	3.0	2.5	2.0
Sparsely populated forest	2.0	2.0	3.0	5.5	6.5	7.5	7.5	7.5	6.5	4.0	2.5	2.0
Coniferous forest	11	11	11	11	11	11	11	11	11	11	11	11
Deciduous forest	0.5	0.5	1.5	4.0	7.0	11	12	12	11	8.0	1.5	0.5
Mixed forest	3.0	3.0	4.0	6.0	8.0	11	11.5	11.5	11	9.0	4.0	3.0
Water	0.0	0.0	0.0	0.0	0.0	0.0	0.0	0.0	0.0	0.0	0.0	0.0

* fictive value, to account for moistening and syncline losses on sealed areas

** average for miscellaneous crops

3.2 Snow storage

The storage of precipitation in form of snow affects the seasonal distribution of discharge; in spring it also may influence the proportions of direct runoff, interflow and groundwater runoff. Therefore, water storage in the snow cover is important in water balance models.

In LARSIM, the modelling of the snow cover is carried out separately for every land use class of each subbasin. The subarea ground elevation is estimated as the mean of the upper and lower elevation channel within the subbasin. In LARSIM, the following subprocesses described in the subsequent Sections describe the snow storage process:

- Accumulation of snow (Section 3.2.1)
- Potential snow melt (Sections 3.2.2 and 3.2.3)
- Calculation of snow temperature (Section 3.2.4)
- Evaporation from melt water (Section 3.2.5)
- Compaction of snow cover because of increasing retention of liquid water (Section 3.2.6)

3.2.1 Snow accumulation

The first problem is to decide, whether precipitation for a particular area is solid or liquid. Corresponding to results of SFB81 (1980), it is assumed that precipitation falls as snow if the air temperature is smaller than a threshold temperature in the particular area:

$$\begin{array}{ll} \textit{snow precipitation} & \textit{if } T_L <= T_{Grenz} \\ \textit{rain precipitation} & \textit{if } T_L > T_{Grenz} \end{array} \tag{3.3}$$

T_L [°C] measured air temperature 2 m above ground

T_{Grenz} [°C] threshold for air temperature (2 m above ground), below which precipitation falls as snow

Because precipitation is formed in high altitudes, it is possible that precipitation falls as snow even if the air temperature is positive near the ground (see Fig. 3.2). Thus, the threshold temperature for snow often ranges between 0°C and +2°C (BRAUN 1985: 31). In LARSIM, the user can select a threshold temperature. If there is no other information, a value of +1°C is recommended.

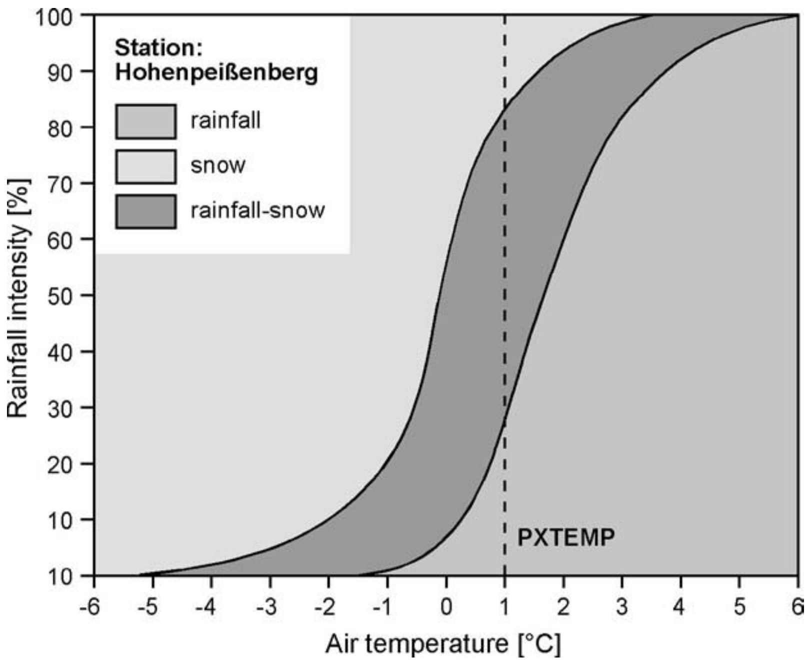

Fig. 3.2 Precipitation in form of rain, snow or sleet depending on near-surface temperature for the station Hohenpeißenberg (from SFB81 1980)

It has been tested, how a variable instead of constant air temperature threshold values influence results. An upper limit was defined above which precipitation would occur as 100% rain, and a lower limit, below which only snow would fall. Between these temperatures the proportion of rain and snow parts were defined by a linear function. This test did not improve results for catchment areas and therefore has not been used in the model. Furthermore, different assumptions specific for different types of land use did not lead to an improvement of the snow model.

3.2.2 Potential snowmelt according to the simplified method of Knauf

The potential snowmelt rate, i.e. the portion of melting snow can be simulated in LARSIM by two methods, the simplified and the extended method of KNAUF (1980).

In the simplified method the potential snow melt rate, i.e. the percentage of snow that changes from solid to liquid state, is described by a simplified modelling of the heat balance of a snow cover. This method takes into account the following input parameters for potential snow melt calculation:

- turbulent flow of sensible heat
- heat supply through rain
- flux of ground heat

The potential snowmelt rate calculates to:

$$i_p = \frac{1}{r_S} \cdot (a_0 + a_1 \cdot v) \cdot T_L + 0.01255 \cdot i_N \cdot T_N + c_B \tag{3.4}$$

i_p	[mm/h]	potential snow melt rate
r_S	[Wh/kg]	specific melting energy of snow (= 92.6 Wh/kg)
a_0	[W/(m^2·°C)]	constant in heat transfer coefficient, according to Knauf ranging from 1 W/(m^2·°C) to 7 W/(m^2·°C). LARSIM uses the average value 4.0 W/(m^2·°C)
a_1	[J/(m^3·°C)]	constant in heat transfer coefficient, according to Knauf ranging from 0.8 J/(m^3·°C) to 2.5 J/(m^3·°C). LARSIM uses the average value 1.6 J/(m^3·°C)
v	[m/s]	wind speed (average per hour, measured 10 m above ground)
T_L	[°C]	air temperature (average per hour, measured 2 m above ground), modified here: $T_L = T_L - T_{Grenz}$
i_N	[mm/h]	rain intensity (average per hour)
T_N	[°C]	rain temperature (average per hour), here: $T_N = T_L$
c_B	[mm/h]	melt rate due to flow of ground heat, according to Knauf ranging from 0.1 mm/h to 1.0 mm/h. LARSIM uses a value of 0.1 mm/h

3.2.3 Potential snowmelt according to the extended method of Knauf

The extended Knauf method models the temperature conditions in the snow cover in more detail and considers the following terms:

- Net radiation
- Turbulent flow of sensible heat
- Turbulent flow of latent heat
- Temperature increase by rain
- Flux of ground heat

The potential snowmelt rate calculates to:

$$i_p = \frac{1}{r_S} \cdot \left\{ \varepsilon \cdot Q_S + (a_0 + a_1 \cdot v) \cdot \left[(T_L - T_S) + \beta \cdot (e_L - e_S) \right] + i_N \cdot T_N \right\} + i_B \tag{3.5}$$

i_p	[mm/h]	potential snow melt rate
r_S	[Wh/kg]	specific melting energy of snow (= 92.6 Wh/kg)
ε	[-]	absorption coefficient, after Knauf between 0.02 and 0.6
Q_s	[Wh/(m²·h)]	global radiation
a_0	[W/(m²·°C)]	constant in heat transfer coefficient, according to Knauf ranging from 0.5 W/(m²·°C) to 3.5 W/(m²·°C). LARSIM uses the average value 2.0 W/(m²·°C)
a_1	[J/(m³·°C)]	constant in heat transfer coefficient, according to Knauf ranging from 0.8 J/(m³·°C) to 2.5 J/(m³·°C). LARSIM uses the average value 1.6 J/(m³·°C)
v	[m/s]	wind speed (average per hour, measured 10 m above ground)
T_L	[°C]	air temperature (average per hour, measured 10 m above ground), modified here: $T_L = T_L - T_{Grenz}$
T_S	[°C]	snow temperature (hourly mean values)
β	[K/mbar]	reciprocal value of the psychrometric constant over ice and snow (= 1.76 K/mbar)
e_L	[mbar]	vapour pressure of air
e_S	[mbar]	vapour pressure of snow cover at 0°C
i_N	[mm/h]	rain intensity (average per hour)
T_N	[°C]	rain temperature (average per hour), here: $T_N = T_L$
i_B	[mm/h]	melt rate due to flow of ground heat, according to Knauf ranging from 0.1 mm/h to 1.0 mm/h. LARSIM uses a value of 0.1 mm/h

According to Knauf, Q_s is the net radiation. This seems to be an error because it should be the global radiation, after multiplication with the absorption coefficient the short wave net radiation results. Because long wave radiation components compensate each other to a great extent with regard to the total balance, long wave radiation components are neglected for the calculation of net radiation.

The loss of global radiation by vegetation is considered depending on the monthly leaf area index. These losses amount to about 30% for coniferous forest, and between 1.5 and 3% for deciduous forest depending on the month.

Tests have been made to consider the application of the different albedo values to calculate the (short wave) net radiation instead of the empirical absorption coefficient ε in dependence from new or old snow. Even in combination with the reduction of the global radiation by vegetation the values of the short wave net radiation were overestimated, so that the simulated snowmelt amounts were too high . Therefore this procedure was not implemented.

3.2.4 Calculation of snow temperature (cold content of the snow cover)

To consider the cold content stored in the snow cover the snow cover temperature is calculated for each time interval.

At negative snow temperature the snow cover has a cold content, which must be consumed by energy input, before snowmelt can occur. The potential snowmelt is therefore set to zero in case of negative snow temperatures.

The snow temperature is calculated using the energy balance of the snow cover. The net energy input in the snow cover is calculated by the following formula KNAUF (1980):

$$W = \varepsilon \cdot Q_S + (a_0 + a_1 \cdot v) \cdot \left[(T_L - T_S) + \beta \cdot (e_L - e_S)\right] + i_N \cdot T_N + i_B \tag{3.6}$$

W	[Wh/(m^2· h)]	energy gain of the snow cover
ε	[-]	absorption coefficient, between 0.02 and 0.6
Q_s	[Wh/(m^2·h)]	global radiation
T_S	[°C]	snow temperature (hourly mean values)
β	[K/mbar]	reciprocal value of the psychrometric constant over ice and snow (= 1.76 K/mbar)
e_L	[mbar]	vapour pressure of air
i_N	[mm/h]	rain intensity (average per hour)
T_N	[°C]	rain temperature (average per hour), here: $T_N = T_L$
i_B	[mm/h]	melt rate due to flow of ground heat, according to Knauf ranging from 0.1 mm/h to 1.0 mm/h. LARSIM uses a value of 0.1 mm/h

Changes of snow temperature for a calculation time interval are:

$$\Delta Ts = W / (m \cdot cw) \tag{3.7}$$

ΔTs	[°C]	temperature change in the snow cover
W	[J]	net energy input in the snow cover
m	[kg]	mass of the snow cover
cw	[J/(kg·K)]	specific heat of the snow cover

and:

$$cw = cw_{Eis} \cdot A_{fl} + cw_{Wasser} \cdot \left(1 - A_{fl}\right) \tag{3.8}$$

cw	[J/(kg·K)]	specific heat of the snow cover
cw_{Eis}	[J/(kg·K)]	specific heat of ice (2.106 J/(kg·K))
A_{fl}	[-]	portion of fluid water of the water equivalent of the snow cover
cw_{Wasser}	[J/(kg·K)]	specific heat of water (4.182 J/(kg·K))

3.2.5 Evaporation of melt water

Evaporation can have a considerable influence on a snow cover under special meteorological conditions. Such conditions prevail for instance in mountainous areas of more than 3 500 m.a.s.l. in California and Nevada, where very dry air and strong sun radiation exist simultaneously. Under such conditions, 50% to 80% of the snow cover may be affected by evaporation in springtime (BEATY 1975).

Because such conditions do not exist for longer time periods in lower regions (BRAUN 1985: 35), evaporation from snow is of rather small importance for the long-term water balance of the snow cover (DVWK 1996: 72). LEMMLÄ AND KUUSITO (1974) found a mean daily evaporation of snow of about 0.3 mm in 107 days for an investigation area of 60 m.a.s.l. in Finland. ZINGG (1951) derived similar values for an investigation area of about 2 500 m.a.s.l. in the Swiss Alps, RACHNER (1987) found daily mean values of 0.05 mm for January/February to 0.2 mm for March/April for the north-German plains.

Because evaporation from snow cover may play a role also in middle-European mountainous regions during cloud-free weather situations in spring, this process can be simulated by the procedure in LARSIM since Release 73 described below.

The potential snowmelt mainly takes place at the snow/atmosphere interface. Melt water can evaporate from here. For the calculation of evaporation from melt water the following formula is used (KNAUF 1980):

$$V = \frac{-1}{r_V} \cdot (a_0 + a_1 \cdot v) \cdot \beta \cdot (e_L - 6.1) \tag{3.9}$$

V	[mm/h]	evaporation
r_V	[Wh/kg]	evaporation heat of water at 0°C after BAUMGARTNER (1990)
a_0	[W/(h·°C)]	constant in heat transfer coefficient, according to Knauf ranging from 0.5 W/(h·°C) to 3.5 W/(h·°C) at v = 1 m/s. LARSIM uses the average value 2.0 W/(h·°C)
a_1	[W/(h·°C)]	constant in heat transfer coefficient, according to Knauf ranging from 0.8 W/(h·°C) to 2.5 W/(h·°C) at v = 1 m/s. LARSIM uses the average value 1.6 W/(h·°C)
v	[m/s]	wind speed (average per hour, measured 10 m above ground)
β	[K/mbar]	reciprocal value of the psychrometric constant over ice and snow (= 1.76 K/mbar)
e_L	[mbar]	vapour pressure of air

3.2.6 Compaction of snow and effective snow melt

When snow is loosely packed, the potential snowmelt rate does not add directly to the runoff. Most of the free water from snowmelt and from rain on snow is initially stored within the snow cover and changes the snow structure. The proportion of liquid water in the snow cover increases at the cost of the frozen part. By this metamorphosis, the compactness of the snow pack rises.

The snow cover stores water until a critical value of compactness is exceeded. The following release of water from the snow pack is called effective snowmelt. To determine the effective snowmelt, it is therefore necessary to calculate the concentration of liquid water in the snow cover.

LARSIM uses the simplified snow-compaction method according to Bertle (described by KNAUF 1980: 110-124) for this purpose. This method makes the assumption that the snow cover is isothermal at 0°C. Basis for the computation of the compactness of the snow pack is an empirical correlation between the decrease of the initial snow depth and the amount of the supplied free water, which is described by the following equation:

$$P_H = 147.4 - 0.474 \cdot P_W \tag{3.10}$$

P_H	[%]	snow depth as percentage of the initial depth
P_W	[%]	total accumulated water equivalent as percentage of the initial frozen water equivalent

Additionally an extended assumption has been implemented, in which the snow cover is calculated after the following formula:

$$P_H = c1 - c2 \cdot P_W \tag{3.11}$$

there is:

$$c1 = 100 \cdot (D_{GS} - D_{NS})/(D_{GS} \cdot R_{max}/100) \tag{3.12}$$

and:

$$c2 = c1/100 - 1 \tag{3.13}$$

D_{GS} [kg/m^3] maximal snow density (420 kg/m^3)

D_{NS} [kg/m^3] density of new snow (130 kg/m^3)

R_{max} [%] maximal retention of liquid water (standard value in LARSIM: 30%, other values can be applied)

With this correlation, the potential snowmelt intensity and the measured rainfall, a water content - snow depth calculation can be made. The boundary value for the compactness of the dry snow pack (amount of frozen water in the snow cover) is specified according to the following equation:

$$PT_{max} = 0.678 \cdot (PT_0 + 0.474 \cdot PD_{krit}) \tag{3.14}$$

PT_{max} [%] upper limit for the density of dry snow in a wet snow cover

PT_0 [%] density of dry snow before begin of compaction

PD_{krit} [%] threshold of the snow pack density, required for the begin of water release from the snow cover. According to KNAUF (1980: 113), the values range from 40% to 45%. LARSIM uses 42%

If the calculated compactness of snow reaches the threshold value PD_{krit}, further liquid water from potential snow melts and/or rainfall is released from the snow cover as effective snow melt.

Besides the approaches for snow modelling described here, further snowmelt models of varying complexity were implemented in an earlier version of FGMOD by BREMICKER AND LUDWIG (1990).

3.3 Soil storage

The soil storage (of water = soil water model) has a decisive influence on the water balance, because it can store water, which stems from rain and snow melt, and subsequently provides the water for runoff and evapotranspiration. In the absence of soil storage (e.g., in lakes or on sealed areas) a considerably larger percentage of precipitation becomes part of the runoff (Section 3.4).

In the soil storage, precipitation is divided into several runoff components (direct runoff, interflow and groundwater runoff). Consequently, the soil plays a vital role as control and distribution system in the formation of discharge (LEIBUNDGUT AND UHLENBROOK 1997).

In LARSIM the soil storage can be modelled by methods of different complexity. For simulations based on daily time intervals, the method with three runoff components described in Section 3.3.1 seems to be sufficient. For simulations with shorter time intervals, as for instance flood simulations or very detailed investigations, a soil storage module with four runoff components as described in Section 3.3.2 may be useful. Section 3.3.3 contains the description of a method in LARSIM, which uses an intermediate complexity.

3.3.1 Soil storage with three runoff components

To simulate the soil storage, the *Xinanjiang-Model* was applied, which was developed by R.J. Zhao (ZHAO 1977, ZHAO et al. 1980). Here, it is used in a modified form (DÜMENIL AND TODINI 1992, DKZR 1994: 79-82), for a better consideration of the draining of the soil water storage. In the Xinanjiang-Model, the soil water content is calculated by the following water balance equation, taking into account the precipitation supply (including snow melt), the withdrawal of water through evapotranspiration as well as the runoff formation (Eq. 3.15 and Fig. 3.3):

$$W_0(t+1) = W_0(t) + P(t) - E_{ai}(t) - QS_D(t) - QS_I(t) - QS_G(t) \tag{3.15}$$

$W_0(t)$	[mm]	amount of water in the soil storage at the time t
$P(t)$	[mm]	water from precipitation and snow melt
$E_{ai}(t)$	[mm]	current evapotranspiration (Eq. 3.2)
$QS_D(t)$	[mm]	runoff formation on saturated areas (Eqs. 3.17 and 3.18) towards direct runoff storage (Section 3.1.6)
$QS_I(t)$	[mm]	water release from the soil storage through lateral drainage (Eq. 3.19) towards interflow storage (Section 3.1.6)
$QS_G(t)$	[mm]	water release from the soil storage through vertical percolation (Eq. 3.20) towards groundwater storage (Section 3.1.6)

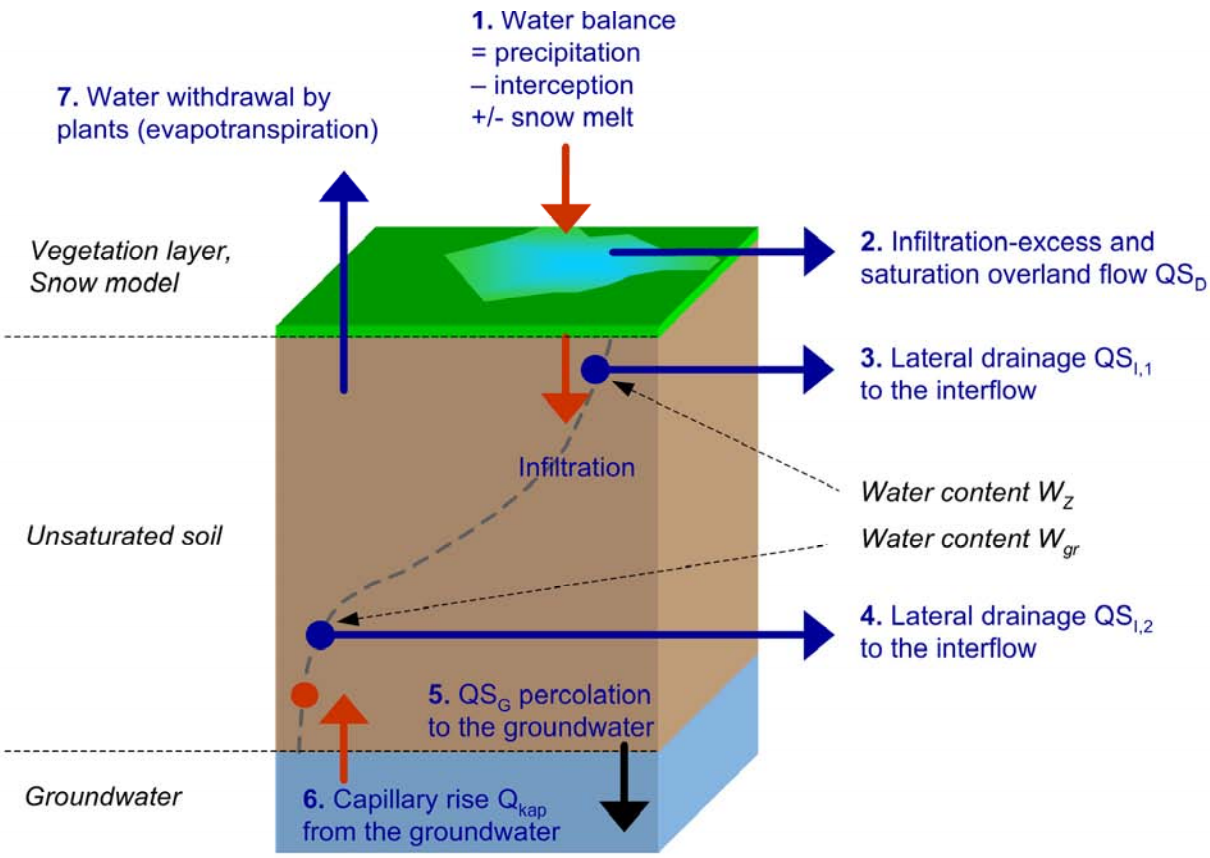

Fig. 3.3 Scheme of the soil water balance model in LARSIM

The Xinanjiang-Model in the version introduced here takes into account that a larger part of precipitation and snow melt discharges near the surface, if the proportion of the saturated surface parts increase or precipitation intensity rises.

One fundamental idea of this method is the assumption that the integration of the local soil water storage compartments across the observed catchment, results in an overall capacity of the soil water storage. The portion of saturated areas within the total catchment area *s/S* is considered as a function of the average saturation of the catchment's area and a parameter b.

This relationship is called *soil-moisture – saturated-areas function (SMSA - function)*:

$$\frac{s}{S} = 1 - \left(1 - \frac{W_0}{W_m}\right)^b \tag{3.16}$$

s/S	[%]	portion of saturated areas in the catchment area
W_0	[mm]	current amount of water in soil storage
W_m	[mm]	maximum amount of water in soil storage
b	[-]	parameter of the SMSA-function (regionalisation of parameter b see Section 3.3.1)

The dependency of the SMSA-function on the value of b is shown in Figure 3.4: according to Eq. 3.16, for relatively small values of b (e.g., b = 0.1) larger portions of saturated areas do not form in the catchment until the soil water storage is almost full; relatively large values of b (e.g. b > 1.0) result in larger portions of saturated areas within the catchment, even if the soil water storage is rather low. There are various approaches for the regionalisation of the parameter b, which are partly described in Section 4.2.

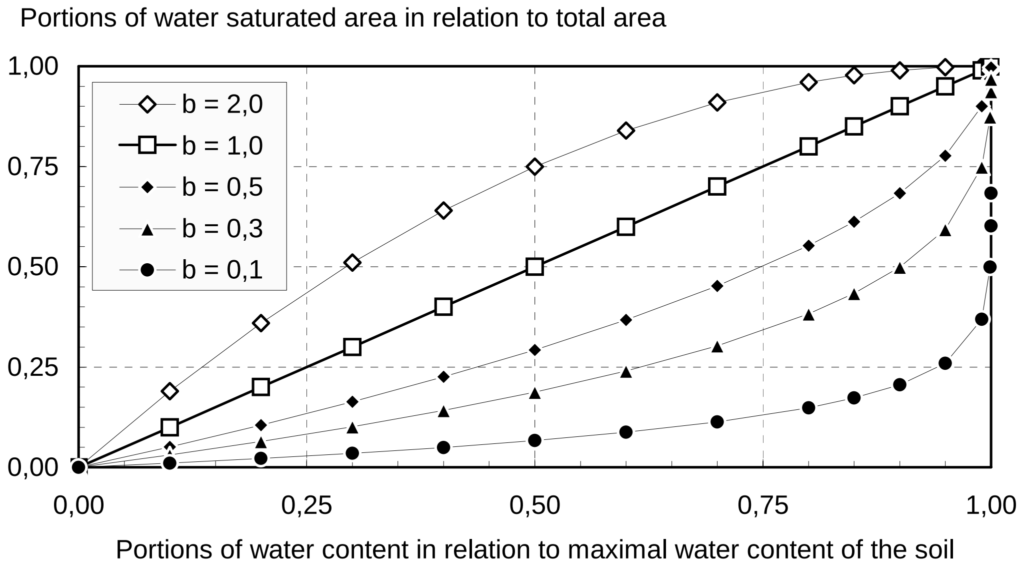

Fig. 3.4 Effects of parameter b on the SMSA-function

The runoff from saturated areas depending on soil storage is calculated as follows:

$$QS_D = P - (W_m - W_0) \tag{3.17}$$

for

$$\left(\left(1 - \frac{W_0}{W_m} \right)^{\frac{1}{b+1}} - \frac{P}{(1+b)W_m} \right) \leq 0 \text{ and } P + W_0 > W_m$$

respectively:

$$QS_D = P - (W_m - W_0) + W_m \left(\left(1 - \frac{W_0}{W_m} \right)^{\frac{1}{b+1}} - \left(\frac{P}{(b+1) W_m} \right) \right)^{b+1} \tag{3.18}$$

for

$$\left(\left(1 - \frac{W_0}{W_m} \right)^{\frac{1}{b+1}} - \frac{P}{(1+b) W_m} \right) > 0$$

QS_D	[mm]	runoff formation from saturated areas ("surface runoff")
P	[mm]	precipitation
W_0	[mm]	amount of water in soil storage at the beginning of the computation time interval
W_m	[mm]	maximum water amount of soil storage
b	[-]	parameter of the SMSA-function (regionalisation of parameter b see Section 3.3.1)

The water release of the soil storage through lateral drainage is calculated according to DKRZ (1994):

$$QS_I = D_{min} \frac{W_0}{W_m} \Delta t \quad for \quad W_B < W_0 < W_Z$$

respectively:

$$QS_I = \left(D_{min} \frac{W_0}{W_m} + (D_{max} - D_{min}) \left(\frac{W_0 - W_Z}{W_m - W_Z} \right)^c \right) \Delta t \quad for \quad W_0 \geq W_Z \tag{3.19}$$

respectively:

$$QS_I = 0 \quad for \quad W_0 \leq W_B$$

QS_I	[mm]	water release from the soil storage through lateral drainage ("drainage loss") to interflow storage (Section 3.1.6)
D_{min}	[mm/h]	drainage (depletion) of the soil storage at filling level W_Z, possible calibration parameter within LARSIM
W_0	[mm]	water amount of soil storage at the beginning of the computation time interval
W_m	[mm]	maximum water amount of soil storage

Δt	[d]	computation time interval
D_{max}	[mm/h]	maximum drainage (depletion) of the soil storage at filling level W_m, possible calibration parameter in LARSIM
W_Z	[mm]	threshold value for water content of the medium depth soil storage, possible calibration parameter in LARSIM
W_B	[mm]	threshold value for water content of the deep soil storage In LARSIM: $W_B = 0.05 \cdot W_m$ (according to DKRZ 1994: 82)
c	[-]	parameter, in LARSIM: c = 1.5 (DKRZ 1994: 82)

It must be noted, that in the calibration of LARSIM the parameters D_{min} and D_{max} are not varied directly, but the dimensionless factors r_dmin and r_dmax contained in the equations:

$D_{min} = 0.001008 \cdot r\_dmin \cdot t$ resp. $D_{max} = 0.1008 \cdot r\_dmax \cdot t.$

In LARSIM, the threshold value W_B for the water content of deep soil storage as well as the parameter c are determined according to assumptions in the climate model REMO (see DKRZ 1994), to prepare the intended coupling of the hydrological and the climate model.

The water release of the soil storage through vertical percolation is calculated according to DKRZ (1994):

$$QS_G = 0 \quad for \quad W_0 \leq W_B$$

respectively: (3.20)

$$QS_G = \beta (W_0 - W_B) \Delta t \quad for \quad W_0 > W_B$$

QS_G	[mm]	water release from soil storage through vertical percolation (“percolation loss”) within the computation time interval to the groundwater storage (Section 3.1.6)
W_0	[mm]	water amount of soil storage at beginning of the computation time interval
W_B	[mm]	threshold value for water content of the deep soil storage. In LARSIM: $W_B = 0.05 \cdot W_m$ (according to DKRZ 1994: 82)
β	[1/d]	drainage index of the deep soil storage, calibration parameter in LARSIM
Δt	[d]	computation time interval

By coupling the soil storage and groundwater storage model in LARSIM, it was possible to account for the effects of a capillary rise from groundwater to the soil storage. Such a capillary rise is possible, if the total hydraulic potential above the groundwater surface sinks due to changes of the matrix potential originating from evaporation losses at the soil surface (SCHEFFER AND SCHACHTSCHABEL 1984: 167).

In LARSIM, capillary rise is modelled using highly simplified assumptions, because the necessary system data for a detailed calculation (e.g. distribution of pore size) are generally not available for large areas. The equation used in LARSIM is:

$$Q_{kap} = \frac{W_{gr} - W_0}{w_{gr}} \cdot QMAX_{kap} \quad for \quad W_0 < W_{gr}$$

and: (3.21)

$$Q_{kap} = 0 \quad for \quad W_0 \geq W_{gr}$$

Q_{kap}	[mm/d]	capillary rise from groundwater storage to soil water storage
W_{gr}	[mm]	threshold value for the water content of soil storage. If water content falls below that value, capillary rise from the groundwater begins (in LARSIM: $W_{gr} = 0.1 \cdot W_m$)
W_0	[mm]	water amount of soil storage at beginning of the computation time interval
$QMAX_{kap}$	[mm/d]	maximum capillary rise (for entirely depleted soil storage)

In an example BENECKE (1996: 393) states, that the capillary rise is roughly 2 mm/d for a clay soil and about 5 mm/d for a fine sand soil, assuming a water table depth of 60 cm.

3.3.2 Extended soil water model with four runoff components

The Xinanjiang approach as described in Section 3.3.1 lumps overland flow and fast subsurface runoff (e.g. lateral macropore flow, lateral flow in highly permeable layers near the surface etc.) to so called direct runoff. It does not explicitly describe the infiltration process on a physical basis. Thus, it is not well suited to investigate the effects of changes in the infiltration properties of soils.

Moreover, it is difficult to accurately describe flash-flood events in small watersheds, which may comprise a considerable proportion of real overland flow, with only one lumped direct runoff component.

To overcome these limitations, the soil water model was extended by an infiltration module, which allows to discriminate between fast subsurface runoff on one hand and infiltration-excess as well as saturation overland flow on the other hand. Consequently a fourth runoff component was also included to describe the process of runoff concentration (Fig. 3.5).

The extension was fit into the existing soil water model of LARSIM. However, care was taken to introduce only a few new parameters with a clear physical meaning (LFU 2004). The resulting extension of the soil water model is schematically depicted in Figure 3.5.

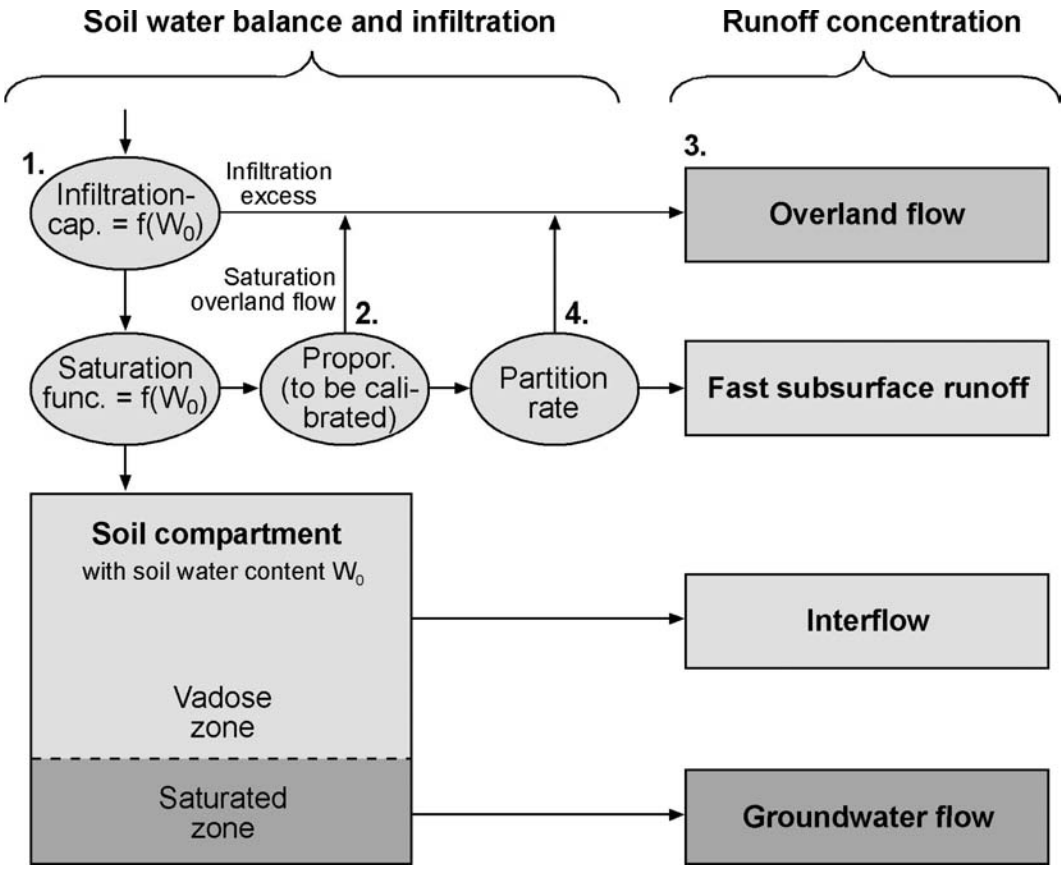

Fig. 3.5 Model concept of the extended soil water model (LFU 2004, modified)

For the model extension, the following soil water balance equation results:

$$W_0(t+1) = W_0(t) + P(t) - E_{ai}(t) - QS_{D2}(t) - QS_D(t) - QS_I(t) - QS_G(t) \tag{3.22}$$

$QS_D(t)$ [mm] water released from the soil to the storage for fast subsurface runoff

$QS_{D2}(t)$ [mm] water released from the soil to the storage for overland flow (infiltration-excess and saturation overland flow)

The following changes in the process description of the soil water balance and runoff concentration result from the extension (numbers correspond to Fig. 3.5):

1. If the rate of water input to the soil (rain + snow melt) exceeds the actual infiltration capacity of the soil, the excess water is directly routed to the storage for overland flow as infiltration-excess overland flow (Horton overland flow).
2. The remainder of the water input reaches the soil storage. The SMSA-function (see above) produces additional direct runoff. This direct runoff is further divided into saturation overland flow and fast subsurface runoff by a land-use specific factor (0.0 to 1.0).
3. A fourth storage component to describe runoff concentration of overland flow is introduced. This component comprises infiltration-excess and saturation overland flow.
4. The partition rate offers an alternate way to partition direct runoff into overland flow and fast subsurface runoff which will be described in section 3.3.3.

The procedures to simulate the formation of interflow and base flow remain unchanged (Section 3.3.1).

The infiltration module

The actual infiltration capacity of the soil is calculated for each subarea and its specific land uses in analogy to Horton's exponential infiltration model (HORTON 1939):

$$I = I_{min} + \left(I_{max} - I_{min}\right) \cdot exp\left(-b_{inf} \cdot \frac{W_0 - W_b}{W_m - W_b}\right) \tag{3.23}$$

I	[mm/d]	actual infiltration capacity
I_{min}	[mm/d]	minimal infiltration capacity
I_{max}	[mm/d]	maximal infiltration capacity ($W_0 = W_m$)
b_{inf}	[-]	decay factor of the infiltration function
W_0	[mm]	actual soil water content (at the start of the calculation interval)
W_m	[mm]	maximum soil water storage capacity
W_b	[mm]	soil water content at the wilting point

To be consistent with the units normally used in LARSIM, infiltration capacities are expressed in mm/d, though mm/h is a more widely used unit.

The relation between the model's actual soil water content, its maximum water storage capacity and the water content at the wilting point is used as a surrogate for the time after the onset of rainfall in Horton's original model. Note that after a long dry spell, when W_0 approaches its minimum of W_b, I approaches I_{max}. On the other hand, with rainwater infiltrating into the soil column and W approaching W_{max}, I asymptotically approaches I_{min}.

The decay factor b_{inf} determines how fast I approaches I_{min} as demonstrated in Figure 3.6. Its value can be derived from infiltration experiments, just as in Horton's original approach.

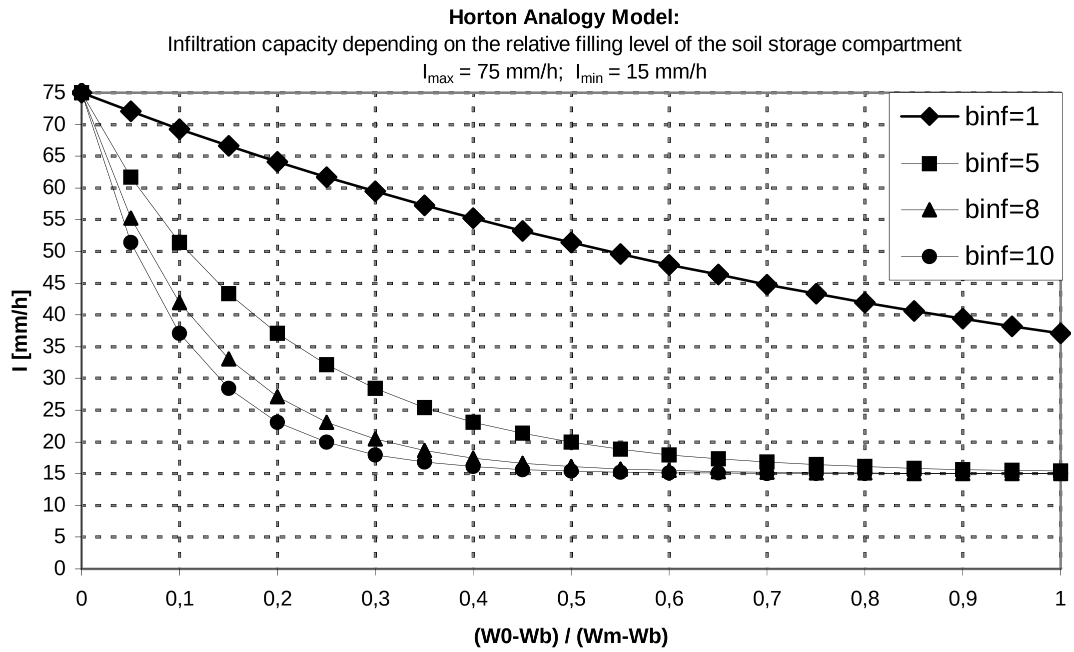

Fig. 3.6 Dependency of the infiltration capacity in the extended soil storage model on the relative soil water content and the decay factor b_{inf}

The parameters W_{max} and W_b are derived from soil classification maps, whereas I_{max} and I_{min} are calibration factors which can be derived from small-scale infiltration experiments (e.g. JURY et al. 1991).

It is important to note that the infiltration process is modelled separately for each land-use class within a subarea. I_{max} and I_{min} are land-use specific parameters (see below). It is thus possible to discriminate between different land-use classes by their infiltration behaviour.

So-called "numerical infiltration experiments" were performed to demonstrate the behaviour of the new soil water module. To simplify the calculations, the water loss from soil due to evaporation and drainage to the three other runoff components was neglected. A calculation time interval of 15 minutes was used.

Figure 3.7 shows selected results of these "numerical infiltration experiments". It can be seen that the resulting curves are very similar to the results of actual infiltration experiments (see e.g. GERLINGER 1997,ZIMMERLING AND SCHMIDT 2002; Section 6.3). Depending on the soil moisture conditions at the start of the experiment, the infiltration capacity is either exceeded immediately or is reached in the progress of the applied constant rain rates. After reaching the infiltration capacity, the infiltration rate drops exponentially, and asymptotically reaches its minimum (I_{min}).

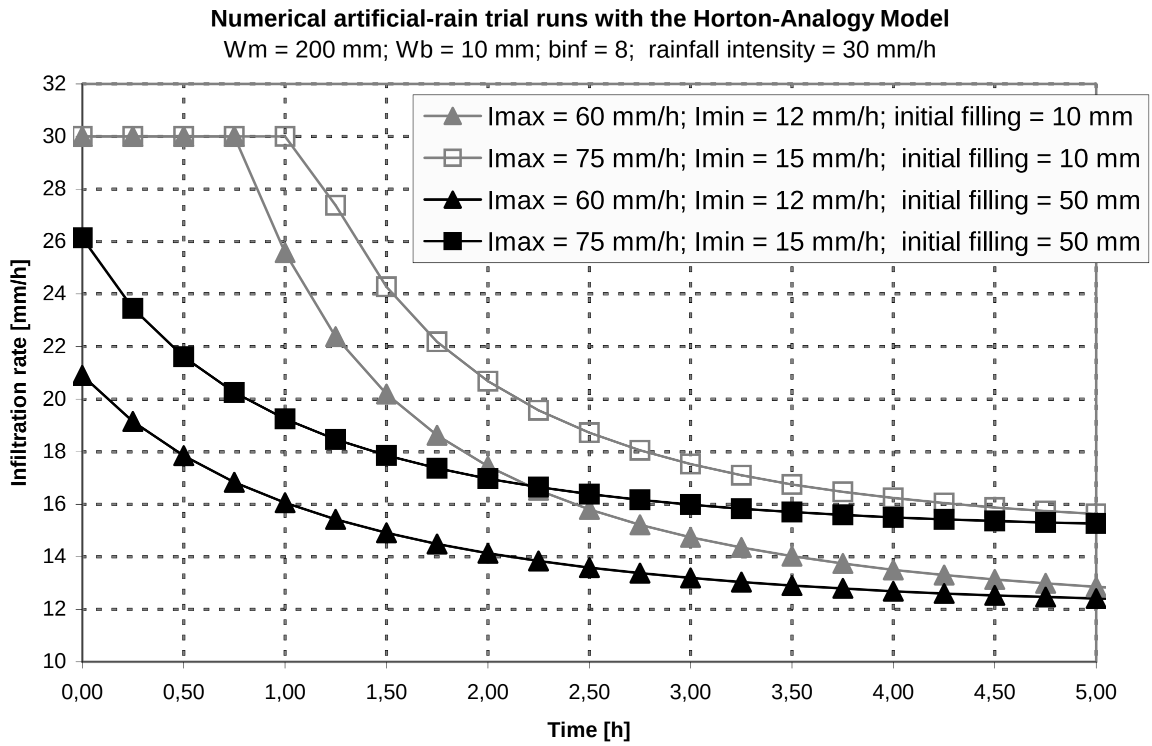

Fig. 3.7 Calculated infiltration rates of "numerical infiltration experiments" with different start values and parameters

Definition of parameter values

The infiltration behaviour of soils (i.e. I_{min} and I_{max}) is mainly influenced by soil type and texture as well as land use. The infiltration properties are extremely variable in space.

LARSIM system data sets contain information on land use and the plant available field capacity of soils, which is used to parameterise the water storage capacity of soils. At the present state of development, LARSIM does not contain additional information on soil type or soil texture.

Given these restrictions, the parameters of the extended soil water model are defined as follows:

- Land-use specific relative values for maximal and minimal infiltration rates ($I_{max, rel}$ and $I_{min, rel}$) are defined within the model's land-use system data set (LANU.PAR).
- A calibration parameter (INF) is introduced. This parameter defines the overall mean of I_{max} of a certain area within the model (in general sub-catchments as defined by discharge gauges).
- Multiplying INF with $I_{max, rel}$ and $I_{min, rel}$, calculates the actual land-use specific values of I_{max} and I_{min} of this area within the model.
- The decay factor of the infiltration curve (b_{inf}) can also be defined as a calibration factor for defined areas.

This means, the information in LANU.PAR primarily defines the relation between I_{min} and I_{max} and further the relative differences in the infiltration properties of different land use classes. The important influence of the soil texture must be defined by the calibration parameter INF for the defined area of the total catchment under investigation.

Proposals for parameter values for $I_{max, rel}$ and $I_{min, rel}$, which were estimated from different literature sources, can be found in Table 3.4 (see e.g. JURY et al. 1991, SEMMEL AND HORN 1995, GERLINGER 1997, IHW 2000, WEILER 2001, BRONSTERT et al. 2001). As a first approximation it is assumed that these values show no interannual variation.

Realistic values for the calibration factor INF are in the range of 30 to 300 mm/h (720 to 7 200 mm/d). However, no upper limit has been introduced into the model, in order to be able to deactivate the infiltration module by use of very high values.

The parameter b_{inf} is primarily an index for soil properties. Its variability is rather low. The "numerical infiltration experiments" showed, that a constant value of 8.0 could be used as a rough estimate for b_{inf}. With this value similar infiltration curves result as have been observed in real infiltration experiments (e.g. GERLINGER 1997, ZIMMERLING and SCHMIDT 2002).

For future developments it seems advisable to incorporate additional information about soil classes (i.e. soil type, texture etc.) in the system data set of LARSIM. Such information might help to considerably improve the physical description of the infiltration process within the setting of the extended soil water model presented here.

Tab. 3.4 Relative values specific for different land use classes for the maximal and minimal infiltration rate (the maximal and minimal infiltration rate I_{min} and I_{max} results from multiplication with the calibration parameter INF)

Land use	$I_{max, rel}$ [-]	$I_{min, rel}$ [-]
Sealed *	0.00	0.00
Fields (conventional)	0.75	0.15
Viniculture	0.75	0.15
Intensive orchards	1.00	0.20
Fallow (overgrown)	1.00	0.20
Unsealed, no vegetation	0.75	0.15
Intensive pasture	1.00	0.20
Wetlands	1.00	0.20
Extensive pasture	1.00	0.20
Sparsely populated forest	1.25	0.25
Coniferous forest	1.25	0.25
Deciduous forest	1.25	0.25
Mixed forest	1.25	0.25
Water	0.00	0.00

* impermeable parts of land uses

Saturation overland flow

Within the framework of the extended soil water model the SMSA-function represents the tendency of soils, to produce larger portions of direct runoff due to an increase of the soil's water content. This direct runoff may either be saturation overland flow or fast subsurface runoff (e.g. macro pores, highly permeable layers).

Thus, within the context of the extended soil water model the term "soil-moisture – saturation-area – function" (SMSA-function) should rather be called "soil-moisture – direct-runoff – function".

The direct runoff, as defined by the SMSA-function, is further divided into saturation overland flow and fast subsurface runoff by a land-use specific factor (see 2. in Fig. 3.5). This constant factor, with values between 0.0 and 1.0, can be defined separately for each land-use class within the system data set of LARSIM. As a first approximation, it is reasonable to set this factor equal to zero for all land-use classes except for wetlands, for which 1.0 would be a reasonable estimation.

For future tasks with other purposes and extended information available, an improved estimation of the land-use specific factors may be achieved.

Storage for overland flow

The newly defined storage for overland flow can be seen as a fourth, extremely fast reacting runoff component, which is fed by infiltration-excess and saturation overland flow.

It is represented by a single linear reservoir. Its retention characteristics are represented by a calibration parameter (EQ_{D2}) for the retention constant in analogy to the same procedure for the storages of the other runoff components. EQ_{D2} is calibrated for a defined area (e.g. area between gauges, see Section 3.1.6).

The calibration of the parameter should be based on floods caused by high intensity rainfall events.

Special land surfaces

In the extended soil storage model, the precipitation, which falls on paved areas, is separated into overland flow and fast subsurface runoff. The portion of runoff, which contributes to overland flow, can be defined in the land use system data set of LARSIM.

3.3.3 The fourth runoff component without extension of the soil storage model

In the calibration of continuous runoff models for the whole runoff spectrum, the use of a fourth runoff component allows better simulation results of flood events, especially because recession limbs of floods can be simulated better by separation of flood runoff in two components of different velocity.

Because infiltration capacity is to some extent specific for single flood evens (e.g. as a consequence of soil treatment) and the calibration value of the portion specific for land use classes independently of the runoff amount, another procedure than the extended soil storage model can be used for conventional calibration.

In this procedure neither infiltration excess (1. in Fig. 3.5) nor saturation overland flow (2. in Fig. 3.5) are calculated. The infiltration capacity is set to a very high value and the value specific for land use to zero. A constant separation rate (3. in Fig. 3.5) is used for the separation of runoff resulting from the SMSA-function in a slower direct runoff (i.e. the quick runoff in Fig. 3.5) and a fast direct runoff (i.e. the surface runoff in Fig. 3.5).

This separation rate with the dimension mm/h is a threshold value above which runoff contributes to the quick direct runoff. Consequence is, that the proportion of the quick direct runoff increases during the rise of a flood wave. The retention constant of the quick direct runoff can be fitted to the flood peak and the retention constant of the slower direct runoff to the recession part of the flood wave.

3.4 Model components for special surfaces

3.4.1 Model components for a water surface

For the water surfaces, defined within a system data set, LARSIM does not simulate snow. LARSIM assumes ice-free water surfaces, which would instantly melt snow. Snow precipitation on water surfaces is directly led to direct runoff storage (Section 3.6).

Since LARSIM version July 1999, evaporation from water surfaces (lakes and streams) is calculated according to the relationship of PENMAN (1948), cited in DVWK (1996):

$$E_w = \frac{\Delta \cdot \frac{R_{NE}}{L} \cdot f(v) \cdot (e_s - e)}{\Delta + \gamma} \tag{3.24}$$

E_w	[mm/d]	evaporation of water
Δ	[hPa/°C]	rise of the saturation vapour pressure curve
R_{NE}	[W/m^2]	net radiation for water surfaces, see Section 3.1.5
L	[Wd/(m^2·mm)]	latent heat for the evaporation of 1 mm water per day (= 28.5 Wd/(m^2·mm) for 15°C water temperature)
$f(v)$	[-]	wind function of Dalton term, according to DVWK (1996) for Neckar and Rhine region: 0.13 + 0.094 · wind speed [m/s] measured 2 m above ground
e_s	[hPa]	saturation vapour pressure at present air temperature measured 2 m above ground
e	[hPa]	water vapour pressure measured 2 m above ground
γ	[hPa/°C]	psychrometric constant (= 0.66 for temperatures in °C)

Land uses in LARSIM do not distinguish between water surfaces of lakes or streams. Therefore, LARSIM subtracts the water evaporated from water surfaces from a model channel at the outlet of a model element to simulate the total water loss from the water surfaces within a model element.

Since typically available land use data sets do not include smaller streams, LARSIM offers an option to include the water surfaces of the stream network defined in the system data set. This calculation option identifies water surfaces of the stream sections registered in the system data set, which have a bed width larger than 5 m.

Subsequently, the larger value, either the one stemming from the land use data set or the one calculated using the stream subsection data, is assigned to each model element as the actual percentage of water surfaces within the entire element. This procedure prevents the double inclusion of broad streams and the omitting of lake surfaces.

To assure that the calculation methods mentioned above are assigned to the water surfaces, the keyword "Wasser" has to be defined in the LARSIM system file for the corresponding land use class. If another keyword (e.g. "water") was applied, the snow modelling would also be performed for water areas.

3.4.2 Consideration of water temperature for evaporation from free water surfaces

The calculation of evaporation from the surfaces of lakes and rivers after PENMAN (1948) is a combination of the energy balance equation with an aerodynamic method, which is derived from the Bowen ratio (DVWK 1996). It considers aerodynamic processes during turbulent mass transport, as well as the short- and long-wave radiation budget. The Penman-method considers the water temperature in a strongly simplified way.

In case of larger rivers and lakes, heat storage and temperature inflows can lead to considerable deviations of temperatures, so that the Penman equation is not exact enough (DVWK 1996: 30).

In such cases, the influence of water temperature on evaporation must be calculated explicitly. If water temperature is known by measurements or a water temperature model, the calculation of the short- and long-wave radiation budget must be neglected, because these energy fluxes are already contained in the water temperature (see Section 3.9). The calculation procedure is thus simplified to an aerodynamic term with the following basic equation:

$$E_w = f(v) \cdot \left(e_{s(T_{Wasser})} - e_{a(T_{Luft})}\right) \tag{3.25}$$

E_w	[mm/d]	evaporation of water
$f(v)$	[-]	wind function, after ATV (1998) for larger rivers: 0.21 + 0.103 · wind speed [m/s] 2 m above ground
$e_{s(TWasser)}$	[hPa]	saturation vapour pressure on the water surface for the given water temperature
$e_{a(TLuft)}$	[hPa]	actual water vapour pressure of air 2 m above ground

According to LAWA (1991) and DVWK (1996: 24) the influence of cooling water inflows on the evaporation of natural rivers and lakes can be quantified by this method.

3.4.3 Hydrological model components for developed areas

In LARSIM, developed areas are divided into different land use classes, for which the vertical water flows are calculated separately. The program internally divides these specific land use portions according to the following scheme:

settlement =	35% sealed, 45% pasture, 20% mixed forest
settlement, dense =	50% sealed, 35% pasture, 15% mixed forest
settlement, light =	30% sealed, 50% pasture, 20% mixed forest
sealed =	100% sealed

For sealed areas, evaporation modelling only takes into account interception and interception losses; there is no calculation of transpiration. The remaining precipitation, which is available for runoff, is fed into the direct runoff. A modelling of the soil water balance or of capillary rise from the groundwater to the soil water compartment does not take place in this case.

3.5 Evapotranspiration

Accounting for the land bound water balance, evapotranspiration represents the water cycles second-most important component after precipitation. For water balance modelling, it is therefore required to describe the processes associated with evapotranspiration as precisely as possible.

To calculate the current evapotranspiration, LARSIM uses the Penman-Monteith method, which was derived by MONTEITH (1979). This method models evapotranspiration under varying meteorological conditions and scales in a large number of test series (e.g. BOUTEN 1995) quite accurately.

In an evaluation by DVWK (1996: 112), the Penman-Monteith method was the only out of 19 evaporation models rated with a high to very high accuracy in computing the actual evaporation. Thus, it was assumed that this evaporation model would be the appropriate choice for mesoscale water balance modelling.

The theoretical background of this method is described in the following sectors:

- Section 3.5.1: Basic equations for calculating evapotranspiration
- Section 3.5.2: Net radiation
- Section 3.5.3: Flow of ground heat
- Section 3.5.4: Aerodynamic resistance
- Section 3.5.5: Surface resistance in consideration of soil moisture

It is possible to calculate potential and actual evapotranspiration with the Penman-Monteith equation. However actual evapotranspiration results from the coupling of soil water content with overall surface resistance.

The equation refers to plants with dry leaf surfaces; if the leaves have wet surfaces (i.e., the interception storage is larger than zero), the interception evaporation is taken into account as well (see Eq. 3.2).

Since it is impossible to directly measure some of the equation variables, the calculation formula of MORECS (Meteorological Office Rainfall and Evaporation Calculation System) of the British Meteorological Office (THOMPSON et al. 1981) was used for parameterisation. Unless mentioned otherwise, the calculation approaches presented in the following paragraphs correspond to the MORECS-scheme.

3.5.1 Basic equation for the calculation of evapotranspiration

The basic equation of the Penman-Monteith method is based on the following correlation (THOMPSON et al. 1981: 15):

$$\lambda E = \frac{\Delta\left(R_{NE} - G\right) + \rho\, c_p \left(e_s - e\right) C/r_a}{\Delta + \gamma\left(1 + r_s/r_a\right)} \tag{3.26}$$

where:

$$C = 1 + \frac{b' \, r_a}{\rho \, c_p} \tag{3.27}$$

and:

$$b' = 4 \, \varepsilon\sigma \left(273.15 + T_{scr}\right)^3 \approx 6 \, \frac{W}{m^2 \cdot K} \tag{3.28}$$

λ	[J/kg]	latent heat of evaporation (= 2 465 000 J/kg)
E	[kg/(m²·s)]	rate of water loss
Δ	[hPa/°C]	slope of saturation vapour pressure curve
R_{NE}	[W/m²]	net radiation for ground surfaces with T_{scr}
G	[W/m²]	flow of ground heat
ρ	[kg/m³]	air density measured 2 m above ground
c_p	[J /(kg·K)]	specific heat capacity at constant pressure (= 1 005 J /(kg·K))
e_s	[hPa]	saturation water vapour pressure at air temperature measured 2 m above the ground, see Eq. 3.48
e	[hPa]	water vapour pressure measured 2 m above ground, see Eq. 3.49
γ	[hPa/°C]	psychrometric constant (= 0.66 for temperatures in °C)
r_s	[s/m]	overall surface resistance
r_a	[s/m]	aerodynamic resistance for heat and water vapour transport
ε	[-]	emissivity of surface
σ	[W/(m²·K⁴)]	Stefan-Boltzmann constant (= $5.67 \cdot 10^{-8}$ W/(m²·K⁴))
T_{scr}	[°C]	measured air temperature 2 m above ground

In LARSIM, the air density ρ, which is a parameter in Eq. 3.26, is calculated according to the correlation of air density and the mixture ratio of water vapour and dry air as described by the German Meteorological Service (DEUTSCHER WETTERDIENST, DWD 1987).

The actual evapotranspiration can be computed using Eq. 3.26:

$$E_a = \frac{E \cdot F_u}{\rho_w} \tag{3.29}$$

E_a	[mm/d]	actual evapotranspiration
E	[kg/(m²·s)]	rate of water loss (Eq. 3.26)
F_u	[s/d]	conversion coefficient from [m/s] to [mm/d] (= $8.64 \cdot 10^7$)
ρ_w	[kg/m³]	water density (= 999.9 kg/m³)

3.5.2 Net radiation

The daily value of net radiation on the ground is calculated by the sum of short and long wave net radiation:

$$R_{NE} = R_{NS} + R_{NL} \tag{3.30}$$

R_{NE} [W/m^2] net radiation on the ground
R_{NS} [W/m^2] short wave net radiation on the ground
R_{NL} [W/m^2] long wave net radiation on the ground

The calculation of the short wave net radiation is based on the measured sunshine duration:

$$R_{NS} = (1-\alpha)\, R_C \tag{3.31}$$

where:

$$R_C = R_A \left(\eta \left(a + \frac{b\,n}{N} \right) + c\,(1-\eta) \right) \tag{3.32}$$

R_{NS} [W/m^2] short wave net radiation on the ground
α [-] albedo (see Table 3.5)
R_C [W/m^2] global radiation on the ground
R_A [Wh/m^2] solar radiation at upper atmospherical limit
a [-] empirical parameter (= 0.24)
b [-] empirical parameter (= 0.55 in summer, 0.50 in winter)
n [h] measured sunshine duration during the day (period of cloudless sky during the day)
N [h] time from sunrise till sunset (see Eq. 3.34)
c [-] empirical parameter (= 0.15)
η [-] (0 for days without direct solar radiation, otherwise 1)

Albedo, which is part of the short wave net radiation calculation, is broken down according to land use classes and seasons. The albedo values used in LARSIM have to be set in a separate file as system data.

Table 3.5 shows the monthly albedo values used for the water balance model Neckar. They were composed on the basis of bibliographical specifications (e.g. THOMPSON et al. 1981, DVWK 1996, RICHTER et al. 1996, MAURER 1997).

Albedo values for land use classes without specifications in literature were estimated. If in the future more accurate albedo data become available, they can easily be included in the LARSIM system data set.

Tab. 3.5 Seasonal albedo values for various land use classes in the water balance model Neckar

Land use	Albedo [%] for short wave radiation											
	Jan.	Feb.	Mar.	Apr.	May	June	July	Aug.	Sep.	Oct.	Nov.	Dec.
Sealed	10	10	10	10	10	10	10	10	10	10	10	10
Fields*	13	13	13	13	16	20	22	18	15	13	13	13
Viniculture	15	15	18	22	22	22	22	22	22	20	17	15
Intensive orchards	15	15	18	22	22	22	22	22	22	20	17	15
Fallow (overgrown)	13	13	13	13	14	15	18	16	14	13	13	13
Unsealed, no vegetation	15	15	15	15	15	15	15	15	15	15	15	15
Intensive pasture	17	17	21	25	25	25	25	25	25	21	19	17
Wetlands	17	17	21	25	25	25	25	25	25	21	19	17
Extensive pasture	17	17	21	25	25	25	25	25	25	21	19	17
Sparsely populated forest	15	15	15	16	18	20	20	18	16	15	15	15
Coniferous forest	12	12	12	12	12	12	12	12	12	12	12	12
Deciduous forest	15	15	15	17	17	17	17	17	17	17	15	15
Mixed forest	14	14	14	15	15	15	15	15	15	15	14	14
Water	16	12	9	7	7	6	7	7	8	11	14	16

*average for miscellaneous crops

The daily value of solar radiation at the upper atmospheric boundary is evaluated in the MORECS scheme according to Eq. 3.33:

$$R_A = SOL\left(N \sin\delta \sin\varphi + \frac{12}{\pi}\cos\delta \cos\varphi\left(\sin\frac{\pi t_1}{12} - \sin\frac{\pi t_2}{12}\right)\right) \tag{3.33}$$

R_A	[Wh/m^2]	solar radiation at the upper atmospheric boundary
SOL	[W/m^2]	solar constant
N	[h]	time from sunrise till sunset (Eq. 3.34)
δ	[rad]	declination of sun = 0.41 cos (2π (d-172) / 365) d = number of day (January 1 = 1)
φ	[rad]	geographical latitude
t_1	[h]	time of sunrise
t_2	[h]	time of sunset

The time of sunrise and sunset as well as the duration of a day is calculated according to THOMPSON et al. (1981: 17):

$$N = t_2 - t_1$$

whereby: (3.34)

$$t_1 = \frac{12}{\pi} \, arc\cos\left(\tan\delta \tan\varphi + \frac{0.0145}{\cos\delta \cos\varphi} \right) \quad and \quad t_2 = 24\,h - t_1$$

N [h] time from sunrise till sunset

t_1 [h] time of sunrise

t_2 [h] time of sunset

δ [rad] declination of sun = 0.41 cos (2π (d-172) / 365), d = number of day (January 1 = 1)

φ [rad] geographical latitude

The long wave net radiation is calculated in the MORECS-approach by the following correlation (THOMPSON et al. 1981: 17-18):

$$R_{NL} = \sigma\, K_{scr}^4 \left(1.28 \left(\frac{e_{scr}}{K_{scr}} \right)^{\frac{1}{7}} - \varepsilon \right) \left(0.2 + 0.8 \frac{n}{N} \right) \tag{3.35}$$

R_{NL} [W/m^2] long wave net radiation on the ground

σ [W/(m^2·K^4)] Stefan-Boltzmann constant (= $5.67 \cdot 10^{-8}$ W/(m^2·K^4))

e_{scr} [hPa] saturation water vapour pressure at air temperature, see Eq. 3.73

K_{scr} [K] measured air temperature (2 m above the ground)

ε [-] emissivity (= 0.95)

n [h] measured sunshine duration during the day (period of cloudless sky during the day)

N [h] time from sunrise till sunset (see Eq. 3.34)

3.5.3 Soil heat flux

Since there are no accurate data of measurements of soil temperature in different depths or of heat capacities of various soil types, it is not possible to calculate the exact soil heat flux. The parameterisation used in MORECS is based on a separate calculation of the soil heat flux for day and night as well as monthly averages of the heat stored in the soil valid for Great Britain.

The soil heat flux during the day can be computed by:

$$G_d = C_r \left(R_{NL} + \frac{(1-\alpha) R_C}{t_2 - t_1} \right) \tag{3.36}$$

G_d [W/m²] soil heat flux during the day

C_r [-] coefficient (0.3 for surfaces without vegetation, 0.2 for surfaces covered with grass; and 0.3 - 0.03·LAI (Table 3.3) for surfaces covered with other vegetation)

R_{NL} [W/m²] net balance of long wave radiation (Eq. 3.35)

α [-] albedo (see Table 3.5)

R_C [W/m²] global radiation on the ground (Eq. 3.32)

t_2 [h] time of sunset

t_1 [h] time of sunrise

The soil heat flux during the night can be calculated by:

$$G_n = \frac{P - (t_2 - t_1) G_d}{2 t_1} \tag{3.37}$$

G_n [W/m²] soil heat flux during the night

P [Wh/m²] average daily heat storage in the ground (tabulated values in MORECS: January until December: -137, -75, 30, 167, 236, 252, 213, 69, -85, -206, -256, -206)

t_2 [h] time of sunset

t_1 [h] time of sunrise

G_d [W/m²] flow of ground heat during the day

3.5.4 Aerodynamic resistance

The aerodynamic resistance for heat and water vapour transport is calculated by using separate approaches for land use classes where the effective population is taller than ten meters and where it is smaller. In doing so, the effective stand height (i.e. the height which effects the aerodynamic resistance) of deciduous forests is reduced for months without fully developed leaves compared to the actual heights.

For stand heights below ten meters and for deciduous forests outside the growing season, the aerodynamic resistance is calculated as follows (THOMPSON et al. 1981: 20):

$$r_a = \frac{6.25}{u_{m,10}} \left(ln\left(\frac{10}{z_0} \right) \right)^2 \tag{3.38}$$

r_a [s/m] aerodynamic resistance for heat and water vapour transport

$u_{m,10}$ [m/s] measured wind speed ten meters above the ground

z_0 [m] roughness length of surface (= 0.1·stand height, optional according to QUAST AND BÖHM (1997): z_0 = 0.021 + 0.163·stand height)

For effective stand heights, which are larger than or equal to ten meters, the aerodynamic resistance is calculated by the following correlation (THOMPSON et al. 1981: 21):

$$r_a = \frac{94}{u_{m,10}} \qquad (3.39)$$

r_a [s/m] aerodynamic resistance for heat and water vapour transport

$u_{m,10}$ [m/s] measured wind speed ten meters above the ground (values of the nearest gauging station)

The values used in LARSIM for the effective stand heights have to be set as system data in a file. Table 3.6 shows the values for the effective stand heights, which were used in the water balance model Neckar.

Tab. 3.6 Seasonal values for effective stand heights in the water balance model Neckar

Land use	Effective stand height [m] (height affecting aerodynamic resistance)											
	Jan.	Feb.	Mar.	Apr.	May	June	July	Aug.	Sep.	Oct.	Nov.	Dec.
Settlement, dense	10	10	10	10	10	10	10	10	10	10	10	10
Settlement, light	5	5	5	5	5	5	5	5	5	5	5	5
Fields*	.05	.05	.05	.20	.40	.60	.60	.40	.20	.10	.05	.05
Viniculture	0.7	0.7	0.7	1.0	1.5	1.8	1.8	1.8	1.8	1.5	1.0	0.7
Intensive orchards	1.0	1.0	1.0	1.5	2.5	3.0	3.0	3.0	3.0	2.5	1.0	1.0
Fallow (overgrown)	.15	.15	.15	.20	.35	.50	.50	.50	.50	.40	.20	.15
Unsealed, no vegetation	.05	.05	.05	.05	.05	.05	.05	.05	.05	.05	.05	.05
Intensive pasture	.15	.15	.15	.15	.15	.15	.15	.15	.15	.15	.15	.15
Wetlands	.15	.15	.15	.15	.15	.15	.15	.15	.15	.15	.15	.15
Extensive pasture	.15	.15	.15	.15	.15	.15	.15	.15	.15	.15	.15	.15
Sparsely populat. forest	1.0	1.0	1.5	1.5	3.5	6.0	6.0	6.0	6.0	3.5	1.5	1.0
Coniferous forest	10	10	10	10	10	10	10	10	10	10	10	10
Deciduous forest	2	2	2	2	6	10	10	10	10	6	2	2
Mixed forest	10	10	10	10	10	10	10	10	10	10	10	10
Water	.05	.05	.05	.05	.05	.05	.05	.05	.05	.05	.05	.05

*average for miscellaneous crops

3.5.5 Surface resistance considering soil moisture

The values for surface resistance used in LARSIM have to be set as system data in a file. For the water balance model Neckar, stomata resistance values were used as shown in Table 3.7. If possible, these values were taken from the data of THOMPSON et al. (1981), or otherwise estimated for non-included land use classes.

Tab. 3.7 Surface and stomata resistance values for several land uses classes

Land use	Daily values for stomata resistance [s/m] assuming sufficient water supply											
	Jan.	Feb.	Mar.	Apr.	May	June	July	Aug.	Sep.	Oct.	Nov.	Dec.
Sealed	(surface resistance 400 all over the year)											
Fields*	32 all over the year											
Viniculture	56 all over the year											
Intensive orchards	56 all over the year											
Fallow (overgrown)	56 all over the year											
Unsealed, no vegetation	80, modified according to Eq. 3.28											
Intensive pasture	64	64	48	40	32	48	48	56	56	56	64	64
Wetlands	32 all over the year											
Extensive pasture	64	64	48	40	32	48	48	56	56	56	64	64
Sparsely populated forest	56 all over the year											
Coniferous forest	56, modified according to Eq. 3.29 and 3.30											
Deciduous forest	64 all over the year											
Mixed forest	60 all over the year											
Water	0 all over the year											

*average for miscellaneous crops

Surface resistance depends not only on stomata resistance, but also on other factors, some of them specific to the type of land use. The most important factors are actual soil moisture as well as the actual length of day and night (yielding different values for stomata resistance). If the ground is not covered with vegetation, the surface resistance is calculated according to (THOMPSON et al. 1981: 29):

$$r_{ss} = 100\,\frac{s}{m} \qquad for \quad F > 20mm$$

$$r_{ss} = \frac{100x_{max}}{x + 0.01x_{max}} \qquad for \quad F \leq 20mm \tag{3.40}$$

r_{ss} [s/m] surface resistance for ground without vegetation
F [mm] field capacity (plant-available water)
x_{max} [mm] maximum filling level of the storage for plant-available soil water (Eq. 3.43)
x [mm] current filling level of the storage for plant-available soil water

To calculate the vegetation's surface resistance, it is initially assumed that the surface resistance is not affected by soil moisture (Table 3.7). For conifers, this uninfluenced surface resistance is corrected due to the impact of air temperature (Eq. 3.41) and the saturation deficit (Eq. 3.42):

$$
\begin{aligned}
r_{sco,conifers} &= 10^4 \frac{s}{m} & T_{scr} &< 5\,°C \\
r_{sco,conifers} &= \frac{1\,750}{(T_{scr}+5)} \frac{s}{m} & -5\,°C < T_{scr} &< 20\,°C \\
r_{sco,conifers} &= 70 \frac{s}{m} & T_{scr} &> 20\,°C
\end{aligned}
\tag{3.41}
$$

r_{sco} [s/m] surface resistance of the plant assuming sufficient water supply
T_{scr} [°C] measured air temperature 2 m above ground

Subsequently, the surface resistance determined according to Eq. 3.41 is modified to take into account the air's saturation deficit with:

$$
\begin{aligned}
r_{sco,\,conifers} &= \frac{r_{sco,conifers}(\delta e = 0)}{(1-0.05\,\delta e)} & \delta e &< 20\ hPa \\
r_{sco,\,conifers} &= 10^4 \frac{s}{m} & \delta e &> 20\ hPa
\end{aligned}
\tag{3.42}
$$

r_{sco} [s/m] surface resistance of the plant assuming sufficient water supply
δe [hPa] saturation vapour pressure deficit of air

To reproduce the influence of soil moisture on the vegetation surface resistance, it is assumed in the MORECS model that this surface resistance increases considerably, if the soil moisture content falls below 60% of the total capacity of the soil. This implicates that the total soil water is split into two storage compartments with the following capacities:

$$Y_{max} = P_y \cdot nFk \tag{3.43}$$

and:

$$X_{max} = (1 - P_y) \cdot nFk$$

Y_{max} [mm] maximum filling of the storage for plant-unavailable soil water

P_y [-] threshold value for the portion of plant-unavailable soil water on field capacity (0.60 in MORECS, in LARSIM: possibility to specify this threshold value with regard to specific regions)

nFk [mm] field capacity (plant-available water)

X_{max} [mm] maximum filling level of the storage for plant-available soil water

The water of the first storage compartment is freely available for plants, whereas the water in the second storage compartment becomes bound more strongly as the storage is drained. The second storage compartment begins to drain, just when the first one is completely empty. The actual filling of the particular storage compartments can be calculated by:

$$x = max\,(W_0 - Y_{max}; 0)$$

and: (3.44)

$$y = min\,(W_0; Y_{max})$$

x [mm] current filling level of the storage for plant-available soil water

W_0 [mm] current filling of the model's soil storage (Eq. 3.15)

Y_{max} [mm] maximum filling of the storage for plant-unavailable soil water

y [mm] current filling of the storage for plant-unavailable soil water

Hence, the influence of soil moisture on the surface resistance is simulated by the following equation:

$$r_{scb} = r_{sco}\left(3.5\left(1 - \frac{y}{y_{max}}\right) + exp\left(0.2\,\frac{y_{max}}{y1}\right)\right) \tag{3.45}$$

r_{scb} [s/m] surface resistance of plants considering the actual soil moisture

r_{sco} [s/m] surface resistance of plants assuming sufficient water supply

Y_{max} [mm] maximum filling of the storage for plant-unavailable soil water

y [mm] current filling of the storage for plant-unavailable soil water

During daytime, the overall surface resistance of land use classes covered with vegetation is composed of the sum of resistance of ground without vegetation and with vegetation (GRANT 1975). Therefore, the surface resistance during the day is represented by:

$$\frac{1}{r_{sT}} = \frac{(1-A)}{r_{scb}} + \frac{A}{r_{ss}} \tag{3.46}$$

where:

$$A = 0.7^{LAI} \tag{3.47}$$

r_{sT}	[s/m]	overall surface resistance during the day (sunrise till sunset)
r_{scb}	[s/m]	surface resistance of plants considering the actual soil moisture
r_{ss}	[s/m]	surface resistance for ground without vegetation
A	[-]	index for uncovered portion of soil surface
LAI	[-]	leaf area index, variable index for the leaf area size depending on type of plant and season (Table 3.3)

During the night, when the stomata are closed, the correlation reads:

$$\frac{1}{r_{sN}} = \frac{LAI}{2\,500} + \frac{1}{r_{ss}} \tag{3.48}$$

r_{sN}	[s/m]	overall surface resistance during the night
LAI	[-]	leaf area index (Table 3.3)
r_{ss}	[s/m]	surface resistance for ground without vegetation

Therefore, the surface resistance of ground covered with vegetation, which is used for the calculation of evaporation on the basis of daily values, is computed by:

$$\frac{1}{r_s} = \frac{N}{24}\frac{1}{r_{sT}} + \left(1 - \frac{N}{24}\right)\frac{1}{r_{sN}} \tag{3.49}$$

r_s	[s/m]	overall surface resistance, 24-hour value
N	[h]	time from sunrise till sunset (Eq. 3.34)
r_{sT}	[s/m]	overall surface resistance during the day (sunrise till sunset)
r_{sN}	[s/m]	overall surface resistance during the night

3.6 Runoff concentration in the catchment

So far, the vertical water transport within the snow-, the vegetation- and the soil-layer was described. It was shown how the water release from the soil storage compartment is computed, separately for direct runoff, interflow and groundwater runoff (Eq. 3.15).

Furthermore, it is necessary to account for the lateral water transport within a catchment area due to these three runoff components. This lateral transport is called runoff concentration. In LARSIM, the lateral transport can be simulated using a variety of different model approaches.

For common applications, the “parallel storage model” as described below simulates the runoff concentration. It is based on the assumption that the runoff components, with water originating from the soil storage model, are added to one of three storage compartments: direct runoff storage, interflow storage, or groundwater storage.

These three storage compartments can be interpreted as upper soil layer, lower soil layer, and groundwater. Each storage compartment is treated as single linear storage. The water release from each unit is always proportional to the filling level of the specific storage compartment:

$$Q_{EL} = \frac{1}{RK_{EL}} \cdot V_{EL} \tag{3.50}$$

Q_{EL}	[m^3/s]	discharge from single linear storage unit
EL	[-]	index: D for direct runoff, I for interflow, G for groundwater
RK_{EL}	[s]	retention constant of single linear storage unit (see Sec. 3.3.2)
V_{EL}	[m^3]	volume (capacity) of single linear storage unit

The groundwater storage therefore shows the highest retention effects, the direct runoff storage the lowest. In LARSIM, the retention constants of each linear storage unit are dependent on an index for the travel times within the subareas (Eq. 4.14). This has been implemented to be able to relate the retention capacity of a catchment to catchment characteristics (form, slope). The discharge from the subareas into the channels equals the sum of the discharge from the three storage compartments:

$$Q_{TGB} = Q_D + Q_I + Q_G \tag{3.51}$$

Q_{TGB}	[m^3/s]	total discharge formed in a subarea
Q_D	[m^3/s]	discharge from the direct runoff storage
Q_I	[m^3/s]	discharge from the interflow storage
Q_G	[m^3/s]	discharge from the groundwater storage

For precipitation on free water surfaces (lakes and rivers) runoff concentration is not considered, the water contributes to the direct runoff component without transformation.

3.7 Channel routing

After the lateral water transport from the subarea to the channels, which was regarded as an area-related process, the water balance model describes the water transport in the channels. LARSIM accounts for the delay by the travel time and the retention in the channels. Other channel-based processes, such as for example an interaction between the channel and the groundwater are ignored in LARSIM.

The calculation of channel routing implemented in LARSIM depends on average geometry and roughness conditions for each channel element, in order to make the independent calibration of area and channel transport parameters possible.

To reduce the data acquisition effort, some simplifying assumptions were made in the hydrological approach used in LARSIM. For instance, it is assumed that the channel geometry of each model element can be described as a double-trapezoid cross-section. The idea behind this is to essentially discern average channel retention characteristics between main bed and flood plains. Furthermore, the discharge – water level relation is assumed to be stationary and uniform.

WILLIAMS (1969) offers a simplified equation for a discharge- or stage-dependent determination of the storage constant:

$$RK_i = \frac{L \cdot A_{n,i}}{3\,600} \cdot \frac{3}{QZ_{i-1} + QZ_i + QA_{i-1}}$$

with n out of: (3.52)

$$Q_n \leq \frac{QZ_{i-1} + QZ_i + QA_{i-1}}{3} \leq Q_{n+1}$$

RK	[h]	storage constant for a channel section
i	[-]	index for the calculation interval
L	[m]	length of a channel section
A	[m^2]	wetted cross-section of a channel profile
n	[-]	index for the water level in a channel profile
QA	[m^3/s]	discharge from a channel section
QZ	[m^3/s]	inflow in a channel section

The wetted cross-section of a channel profile used in Eq. 3.52 is described under the assumption of a stationary uniform discharge according to the equation of (Manning-) Strickler (Eq. 3.53) and unde the assumption of the geometrical characteristics of a double-trapezoid cross-section with different roughness coefficients for main bed and flood plains:

$$Q = A \cdot EK \cdot K_S \cdot \left(\frac{A}{U}\right)^{2/3} \cdot I^{1/2} \qquad (3.53)$$

Q [m³/s] stationary uniform discharge according to Manning-Strickler
A [m²] wetted cross-section of a channel profile
EK [-] possible calibration variable in LARSIM for modification of roughness coefficients
K_S [m$^{1/3}$/s] velocity coefficient according to Strickler
U [m] wetted perimeter of a channel profile
I [-] slope of stream section

The following equation is used for calculating the discharge deformation by such channels, according to FGMOD:

$$QA_i = QZ_i \cdot \left(1 - \frac{RK_i}{TA} \cdot \left(1 - e^{-\frac{TA}{RK_i}}\right)\right) + QZ_{i-1} \cdot \left(\frac{RK_i}{TA} \cdot \left(1 - e^{-\frac{TA}{RK_i}}\right) - e^{-\frac{TA}{RK_i}}\right) + QA_{i-1} \cdot e^{-\frac{TA}{RK_i}} \quad (3.54)$$

QA [m³/s] discharge from a channel section
i [-] index for the calculation time interval
QZ [m³/s] inflow in a channel section
RK [h] storage constant of a channel section
TA [h] calculation time interval

3.8 Lakes, dams, reservoirs and diversions

LARSIM contains extensive options for including river diversions as well as for the simulation of reservoirs and of retention characteristics of lakes.

3.8.1 Retention in lakes and uncontrolled reservoirs

The calculation method for retention in this case is based on the continuity equation in the following form:

$$V_{S(t+1)} = \frac{\Delta t}{2} \cdot \left(QZ_{S(t)} + QZ_{S(t+1)} - QA_{S(t)} - QA_{S(t+1)}\right) + V_{S(t)} \quad (3.55)$$

V_S [m³] storage volume in lake (or reservoir)
QZ_S [m³/s] inflow into lake
QA_S [m³/s] discharge from lake
Δt [s] time of calculation interval

If the volume-discharge characteristic for the lake or the reservoir is given, the hydrograph for the lake's volume and discharge can be calculated from the inflow hydrograph by iteration using the equation above.

With the water balance model, reservoirs or lakes with constant outlet functions and controlled outflow can be simulated. The following data of a lake must be contained in the system data set:

- lake volume function: water level [m.a.s.l], storage volume [1 000 m^3]
- operation rules or uncontrolled water level-discharge function: outflow [m^3/s], water level [m]
- maximal drawdown velocity [cm/day]
- start volume of simulation start [1 000 m^3]

3.8.2 Retention basins with constant outflow

The computation of a reservoir with constant outflow discharge is calculated based on the following data:

- maximum retention volume
- constant discharge (until reservoir is filled)
- in case of overflow: volume-discharge characteristics of the emergency spillway

Using the corresponding conventions within the control file, the discharge from the reservoir is reduced to a constant discharge, as long as the reservoir retention volume has not yet reached its maximum. In extreme cases the retention is calculated according to the method used for retention in lakes or uncontrolled reservoirs.

3.8.3 Controlling reservoir outflow by a downstream gauge

To simulate a reservoir control by a downstream gauge in a moderate distance, the discharge from the catchment between the reservoir and the control gauge has to be available for LARSIM.

In a first simulation run, the initial discharge values between the reservoir and the control gauge are calculated. Subsequently, in a second run the desired regulation can be simulated: the reservoir is controlled in a way, that the release from the reservoir plus the sum of all the discharge from the catchment between the reservoir and the control gauge downstream does not exceed the desired discharge at the control gauge.

This simulates a control mechanism with constant discharge at a gauge downstream of the reservoir. However, it must be considered that such a procedure in practice causes control losses due to the travel time of flood waves, measurement inaccuracies and attenuation in the control capacities. Thus, LARSIM computes an idealized loss-free controlling.

3.8.4 Reservoirs with seasonal outflow

For the simulation of such a reservoir control, LARSIM requires the following characteristics of the storage dam to be set in the system data set:

System data (functions):

- basin volume line: stage [m.a.s.l], storage volume [1 000 m^3]
- characteristics of the emergency spillway channel: stage [m.a.s.l], discharge by the emergency spillway channel [m^3/s]

Operation rules:

- maximum allowable velocity of reservoir (lake) water surface during release of storage [cm/day]
- seasonal process of the operating target hydrograph (target storage volume for each date)
- maximum allowable release volume (discharge for each date)

3.8.5 Diversions and inflows

LARSIM simulates the complete water balance of a catchment area as a closed system. In practice, however, external water diversions or inflows from outside the catchment can play an important role, as for instance in the Neckar catchment as a consequence of the water transfer from Lake Constance into the Neckar basin.

In LARSIM, such water diversions and/or inflows to/from the considered catchment (transboundary transports) or also inside catchment parts can be included at every element within the model.

It is possible to integrate constant in/outlets as well as temporally varying ones. Threshold values for the in/outlet have to be defined and some prepared functions are available in the program to do this. If these are not sufficient, discharge hydrographs may be defined for this task. Inflows stemming from an outflow in the considered system are possible as well as the treatment of diverting branches within the available hydrologic models.

3.9 Water temperature

LARSIM has been extended by specific modules to simulate and forecast the water temperature (HAAG et al. 2006a). These modules are called water temperature model (WTM). The integrated model is called water balance and water temperature model (WBTM). The WBTM can either be used as an offline tool or for operational discharge and water temperature forecasting. It can be operated in different time steps (e.g. hours, days).

Fig. 3.8 shows the general scheme of the WBTM. The water balance simulation, as described in previous sections, is the basis for the subsequent calculation of water temperatures. Accumulation and melting of snow cover, interception and evapotranspiration as well as the soil model are simulated with unchanged modules of the water balance model (WBM) without considering the water temperature.

Water temperature calculations are integrated in the simulation of the three (or four) runoff components (runoff concentration) and the flood routing in channels. In addition to meteorological influences, local sources of heat can also be taken into account. Such sources may include cooling water inputs from thermal power plants or the discharge of sewage treatment plants.

A WBTM-run results in the calculation of discharge and water temperature along the river reaches of the catchment under investigation (HAAG et al. 2005).

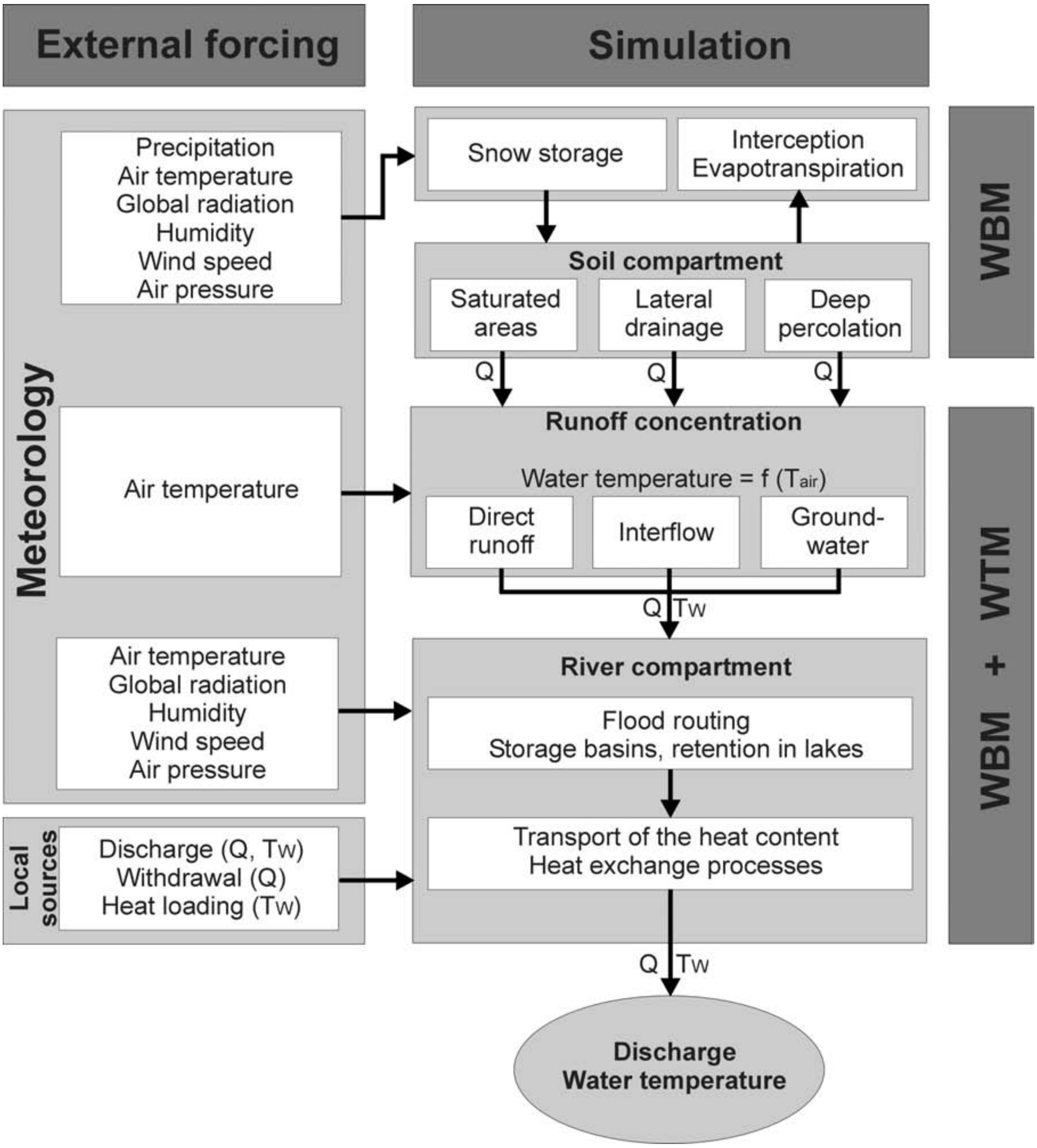

Fig. 3.8 General scheme of the water balance and water temperature model (WBTM)

3.9.1 Physically based simulation of water temperature

The standard calculation of the water temperature with the WTM modules of LARSIM accounts for the relevant processes, which govern the temporal and spatial evolution of water temperature within different compartments of a watershed.

As a starting point, the water temperatures of the three, or possibly four, runoff components (direct runoff, interflow and groundwater runoff) are expressed as linear functions of the actual air temperature:

$$Tw_{GS} = MIN\left\{\begin{array}{c} MAX\left\{\begin{array}{c} Y0TW_{GS} + B1TW_{GS}\cdot\left(T_L - Y0TW_{GS}\right) \\ 0 \end{array}\right\} \\ Tw_{max} \end{array}\right\} \tag{3.56}$$

Tw_{GS}	[°C]	water temperature of runoff component (with GS = D for direct runoff, I for interflow and B for base flow)
$Y0TW_{GS}$	[°C]	calibration parameter of the regression equation
$B1TW_{GS}$	[-]	slope of the regression equation (calibration parameter)
TL	[°C]	actual air temperature
Tw_{max}	[°C]	maximal admissible water temperature for the runoff component

This simple regression equation allows taking into account that the temperature of groundwater is close to the long-term mean of the air temperature. In contrast, direct runoff may be strongly influenced by short-term variations of air temperature, because of its short residence time and its shallow flow path. Interflow is somewhere in between these extremes (e.g. BICKNELL et al. 1996).

Moreover, it is taken into account that the water temperature cannot fall below 0°C and that its maximum is also naturally limited by evaporative cooling (see MOHSENI AND STEFAN 1999).

This simple regression approach gives a rough approximation for the water temperatures of the runoff components. It is sufficiently accurate, since the river water temperature is usually mainly governed by heat exchange with the atmosphere and the riverbed.

The transport of the heat content within the channel subreaches is calculated with the one-dimensional advection-dispersion-equation:

$$\frac{\partial T_W}{\partial t} + u\cdot\frac{\partial T_W}{\partial x} = E_x\cdot\frac{\partial^2 T_W}{\partial x^2} \pm S \tag{3.57}$$

T_W	[°C]	water temperature
u	[m/s]	mean flow velocity
E_x	[m^2/s]	longitudinal dispersion coefficient
S	[°C/s]	source-sink-term

The longitudinal dispersion coefficient (E_x) is estimated by an empirical equation proposed by Fischer (FISCHER et al. 1979, HAAG et al. 2006a).

The source-sink-term (S) considers all relevant heat exchange processes with the atmosphere and the riverbed, which may gradually change the water temperature. This can be viewed as the rate of water temperature change (dT_W/dt). On the other hand, the source-sink-term also takes into account local heat sources, such as cooling water or sewage water discharge.

The rate of temperature change is defined by the sum of the heat exchange processes schematically depicted in Figure 3.9. Within WBTM it is thus expressed as follows:

$$\frac{dT_W}{dt} = \frac{R_K + R_L + H_F + H_L + R_{Sed}}{c_p \cdot \rho_W \cdot h} \tag{3.58}$$

with (for definition of other variables see Fig. 3.9):

c_p [H/(kg·K)] specific heat of water (4.187 J/(kg·K))
ρ_w [kg/m^3] density of water (1 000 kg/m^3)

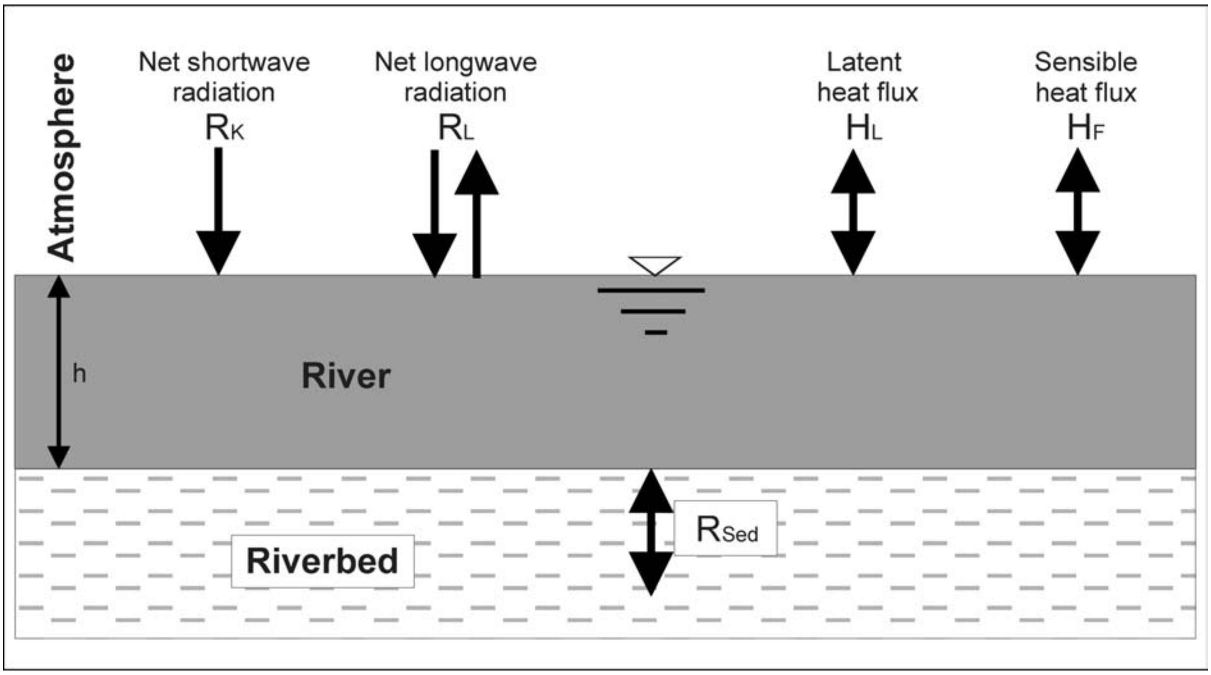

Fig. 3.9 Heat exchange processes considered in the physically based simulation of the water temperature budget

The short-wave radiation balance of the water body (R_K) is determined in the same way as in the calculation scheme for evapotranspiration (Eq. 3.31). The seasonal variation of the albedo of water is taken into account in the system data set. Additionally, a shading factor (F_{schatt}) has been introduced. This calibration factor comprises the shading of the water bodies by riparian vegetation and horizon sheltering.

$$R_K = F_{schatt} \cdot (1-\alpha) \cdot R_C \tag{3.59}$$

F_{schatt} [-] shading factor of the river (0 to 1); depending on horizon sheltering and bank vegetation, possible calibration parameter

The calculation of the long-wave radiation balance includes the thermal radiation of the water body and the long wave atmospheric counter radiation of the atmosphere. Since the water temperature is known, the thermal radiation of the water body can be expressed with the Stefan-Boltzmann law. The calculation of the counter radiation from the atmosphere takes into account the air temperature, air humidity and the percentage of cloud cover. This is achieved by combining the procedures suggested by BRUTSAERT (1975) and by MEIER (2002). Thus, the long-wave radiation balance is expressed as follows:

$$R_L = F_{Ratm} \cdot \sigma \cdot K^4 \cdot \left(\frac{e}{K}\right)^{1/7} \cdot \left(1 + c \cdot \left(1 - \frac{n}{N}\right)^2\right) - \varepsilon \cdot \sigma \cdot (Tw + 273.15)^4 \tag{3.60}$$

F_{Ratm}	[-]	empirical factor (standard: 1.28), possible calibration parameter
K	[K]	air temperature 2 m above ground
e	[hPa]	actual vapour pressure of air 2 m above ground
c	[-]	factor depending on cloud type (mean value = 0.22, MEIER 2002: 91)
Tw	[°C]	actual water temperature
N	[h]	astronomically possible sunshine duration of the current day
n	[h]	actual sunshine duration of the current day

The calculation of evaporation from the water body is also based on the water temperature. Thus, an aerodynamic approach can be used to determine the rate of evaporation or condensation (in contrary to the calculation of terrestrial evapotranspiration; see Section 3.5):

$$E = K_L \cdot (e_{s,Tw} - e) \tag{3.61}$$

E	[mm/d]	rate of evaporation
K_L	[mm/(d hPa)]	turbulent exchange coefficient for water vapour
$e_{s,Tw}$	[hPa]	saturation vapour pressure at the water surface

Within the WBTM the formula proposed by Rinsha and Domschenko (cited in LAWA 1991) is used as a standard to calculate the turbulent exchange coefficient for water vapour. This formula has shown to be reliable, especially in the case of larger rivers such as for instance the Neckar river (HAAG AND WESTRICH 2002). In addition, a windshield factor is introduced. This calibration factor accounts for the fact, that the wind measurements at climate stations are frequently not representative for wind speeds above rivers (see SINOKROT AND STEFAN 1993). Thus, the turbulent exchange coefficient for water vapour is expressed as follows:

$$K_L = 0.211 + 0.103 \cdot v \cdot F_{wind} \tag{3.62}$$

v [m/s] (interpolated) wind speed 10 m above ground

F_{wind} [-] windshield factor (~1; possible calibration parameter)

The flux of latent heat (H_L), as a consequence of evaporation (respectively condensation), is expressed as follows:

$$H_L = -\rho_w \cdot \frac{E \cdot L}{86\,400 \cdot 10^3} \tag{3.63}$$

H_L [W/m^2] flux density for sensible heat

L [J/kg] latent heat of evaporation (LAWA 1991: (2500 – 2.39·Tw·10^3)

For the simulation of the sensible heat flux (H_F) it is assumed, that the turbulent exchange term for temperature is equal to that of water vapour (ARYA 1988). Additionally considering the Bowen-ratio, the turbulent flux of sensible heat can be calculated in analogy to the turbulent flux of latent heat:

$$H_F = -\gamma \cdot \frac{P_{akt}}{1013} \cdot K_L \cdot L \cdot \frac{T_W - T_L}{86\,400 \cdot 10^3} \cdot \rho_w \tag{3.64}$$

γ [hPa/°C] psychrometric constant at normal pressure (0.655 hPa/°C)

T_L [°C] air temperature 2 m above ground

The temperature of the riverbed and the resulting temperature exchange with the water body is simulated by using a simple single-layer sediment-model (DITORO 2001). The heat flux density across the riverbed is driven by the temperature gradient within the sediment close to the boundary. The temperature at the boundary is equal to the water temperature (of the homogenously mixed water body). The heat flux density across the riverbed is thus expressed as follows:

$$R_{sed} = -K_{sed} \cdot \left(T_W - T_{sed}\right) \tag{3.65}$$

K_{sed} [J/(m^2·s·°C)] temperature transfer coefficient at the riverbed

T_{sed} [°C] effective temperature of the river bed (near the boundary)

T_{sed} is called effective riverbed temperature, because it does not correspond to a real measurable temperature in a certain depth of the bed. It is rather the temperature, whose difference to T_w gives a reasonable measure for the temperature gradient near the riverbed.

Therefore, the time series of the effective riverbed temperature T_{sed} have to be simulated. Because no transport term is involved, the following equations are used:

$$\frac{dT_{sed}}{dt} = \frac{K_{sed}}{CZ_{sed}} \cdot \left(T_W - T_{sed}\right)$$

with:

$$CZ_{sed} = cp_{sed} \cdot \rho_{sed} \cdot \Delta z_{sed} \qquad (3.66)$$

$$K_{sed} = \lambda_{sed} \cdot \frac{\Delta z_{sed}}{2}$$

CZ_{sed}	[J/(m^2·°C)]	effective heat capacity of the river bed (calibration parameter)
cp_{sed}	[J/(kg·°C)]	specific heat of the riverbed
ρ_{sed}	[kg/m^3]	bulk density of the riverbed
Δz_{sed}	[m]	effective thickness of the riverbed layer affected by the heat exchange process
λ_{sed}	[J/ (m·s·°C)]	thermal conductivity of the riverbed

The effective heat transfer coefficient K_{sed} is a lumped parameter. Formally it can be expressed as product of the thermal conductivity of the riverbed and one half of the thickness of the riverbed layer affected by the heat exchange process.

Also CZ_{sed} is a lumped parameter, with a formal physical meaning: it can be interpreted as the product of specific heat, bulk density and the thickness of the riverbed layer, which is affected by the heat exchange process.

Although, both parameters (K_{sed} and CZ_{sed}) can be explained in terms of physical properties, theses properties are usually not known. Furthermore, the two parameters may possibly be influenced by radiation reaching the riverbed and to a smaller extent by river geometry.

Thus, despite the physical basis of K_{sed} and CZ_{sed}, they are used as calibration parameters (HAAG et al. 2006a).

The intensity of the heat exchange is primarily controlled by K_{sed}. The parameter CZ_{sed} is mainly governed by the heat storage capacity of the riverbed.

Besides the heat exchange processes along the river, local sources such a cooling water or sewage discharge are also taken into account. This is done by assuming complete mixing of the sewage or cooling water inflow at the point of discharge (HAAG et al. 2006a).

3.9.2 Regression models for the calculation of local water temperatures

The simulation of water temperature with the physically based approach described above generally leads to very good results. However, the calibration procedure can be tedious for small watercourses with small water depths, where shading and wind shielding may vary considerably in time and space.

Therefore, if local heat sources or storage basins do not essentially influence the channel system, local water temperatures can alternatively be calculated with regression models. It must be noted, that these models are only valid for a specific location. They do not give any information on the situation in the river system upstream of this specific location.

The major advantage of the regression models is, that they can be fitted to measured water temperatures automatically by using only air temperatures and discharges as input variables. Thus, the regression models are particularly well suited to formulate boundary conditions for downstream reaches of interest. These, downstream reaches may then be simulated in detail with the physically based approach (HAAG et al. 2006a).

The general form of the multiple, non-linear regression model has been derived on base of the fundamental interdependency between air and water temperature as described by MOHSENI AND STEFAN (1999) and additional theoretical considerations with respect to the influence of discharge, riverbed and diurnal changes of water temperature. Although the general form of the regression model is based on the underlying physical processes (see HAAG et al. 2006a), water temperature can be predicted by using only air temperature and discharge as predictors.

The simple form of the regression model, which does not take discharge into account, can be written as follows:

$$T_{W,i} = \frac{\alpha}{1 + exp\left(\gamma \cdot \left(\beta - \frac{\sum_{j=i-m}^{i} T_{L,j}}{m}\right)\right)} + b_{1TL} \cdot \left(T_{L,i-lag} - \frac{\sum_{j=i-lag-m}^{i-lag} T_{L,j}}{m}\right) \tag{3.67}$$

$T_{W,i}$	[°C]	water temperature for the actual point in time i
$T_{L,i}$	[°C]	air temperature for the actual point in time i
m	[h]	number of hours to average air temperature (calibration parameter)
lag	[h]	time lag of the water temperature (calibration parameter)
α	[-]	calibration parameter
β	[-]	calibration parameter
γ	[-]	calibration parameter
b_{1TL}	[-]	calibration parameter

If discharge is available for the point of interest, the regression model can be improved, by also including these discharge measurements:

$$T_{W,i} = b_{1Q} \cdot log_{10}\left(\frac{Q_i}{MQ}\right) + \frac{\alpha}{1 + exp\left(\gamma \cdot \left(\beta - \frac{\sum_{j=i-m}^{i} T_{L,j}}{m}\right)\right)}$$

$$+ \left(b_{2Q} \cdot log_{10}\left(\frac{Q_i}{MQ}\right) + b_{1TL}\right) \cdot \left(T_{L,i-lag} - \frac{\sum_{j=i-lag-m}^{i-lag} T_{L,j}}{m}\right) \tag{3.68}$$

Q_i [m³/s] discharge for the actual point in time i
MQ [m³/s] long-term mean discharge

4 Data conversion, parameter regionalisation and quality measures

4.1 Conversion of measured meteorological data

4.1.1 Correction of errors in precipitation measurement

Precipitation measurement is subject to biases, which have been under study for hydrometeorological problems for a long time. SEVRUK (1989) gives an overview over these studies. The measurement errors are caused by the design of the measuring instrument on one hand, and by the conditions at the measuring location and meteorological factors on the other hand. The most important errors are:

- wind error (when the precipitation gauge is installed above the ground)
- wetting losses on the measuring device
- evaporation losses

Since precipitation is the decisive factor for water balance modelling, LARSIM contains correction methods for the measurement error of the three factors mentioned above. In addition, a correction factor for the conversion of point-measurements into area values is included. The corrections are implemented according to the equations below:

$$N_G = \left(N_{meas} \cdot K_G\right)$$

$$N_{G,korr} = \left(N_G \cdot F_{wind}\right) + K_{BV} \tag{4.1}$$

N_G [mm] area precipitation for a subarea (i.e., one model element)

N_{meas} [mm] interpolated, area precipitation values calculated by Thiessen polygons or nearest-neighbour method (see Section 3.2.3)

K_G [-] correction factor for converting measured precipitation (point data) into area data, e.g. used for compensation, if gauging stations systematically show higher precipitation as those in the surrounding area

$N_{G,korr}$ [mm] precipitation for a subarea corrected for the measurement error

F_{wind} [-] factor for determining the wind error in the precipitation measurement (Eq. 4.2)

K_{BV} [mm] losses in precipitation measurement due to wetting and evaporation (Table 4.1)

The correction techniques for the measurement errors refer to the Hellmann precipitation gauge without a windbreak with a catchment area of 200 cm² and a measuring height of one meter above the ground. These gauges are used as standard devices by the German Meteorological Service DWD (Deutscher Wetterdienst).

Wind error

When precipitation gauges are installed above the ground, precipitation may partly drift over the device by wind. Consequently, such a gauge collects less precipitation than a gauge installed at ground level.

The amounts of such losses by drift depend on wind speed, but also on the type and structure of the precipitation. Snowflakes or very small rain droplets drift across these devices to a greater extent than precipitation with rather big drops.

In LARSIM, this wind-induced error is corrected according to a technique by SEVRUK (1989). It uses the air temperature as index for the type and texture of the precipitation:

$$\begin{aligned}
F_{wind} &= 1 + (0.550 \cdot v^{1.40}) && \text{for} \quad T_L < 27^\circ C \\
F_{wind} &= 1 + (0.280 \cdot v^{1.30}) && \text{for} \quad T_L \geq 27^\circ C \quad \text{and} \quad < 8^\circ C \\
F_{wind} &= 1 + (0.150 \cdot v^{1.18}) && \text{for} \quad T_L \geq 8^\circ C \quad \text{and} \quad < T_0 \\
F_{wind} &= 1 + (0.015 \cdot v^{1.00}) && \text{for} \quad T_L \geq T_0
\end{aligned} \tag{4.2}$$

F_{wind}	[-]	correction coefficient for wind error
v	[m/s]	wind speed at the height of the precipitation gauges (1 m above ground)
T_L	[°C]	air temperature measured 2 m above ground
T_0	[°C]	threshold value for the air temperature 0°C after SEVRUK (1989) and –2°C in LARSIM

Figure 4.1 shows the relations between air temperature, wind speed and correction coefficients.

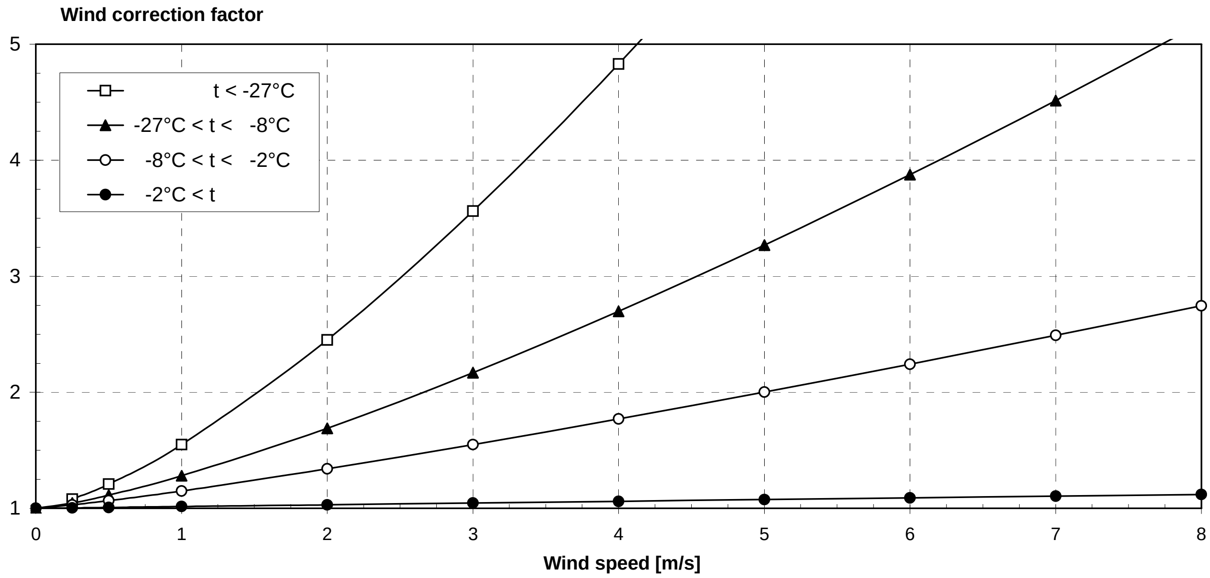

Fig. 4.1 Coefficient for correction of measured precipitation due to wind, air temperature, and wind speed

Measuring errors due to wetting losses and evaporation

Another methodical error in precipitation measurement occurs due to the water losses because of the wetting of the catchment funnel and tank as well as evaporation from the tank. In LARSIM, these losses can be corrected by using the mean monthly error values (Table 4.1), which were calculated by the German Meteorological Service for the lowland of Northern Germany (DWD 1995).

Tab. 4.1 Wetting and evaporation losses in the Hellmann precipitation gauge for the Northern German lowland (DWD 1995)

Wetting and evaporation losses [mm] for	Daily value of precipitation [mm]													
	0.1	0.2	0.3	0.4	0.5	0.6-0.8	0.9-1.2	1.3-1.7	1.8-2.4	2.5-3.4	3.5-4.4	4.5-6.0	6.1-8.9	≥ 9.0
Summer (May - Oct.)	0.07	0.11	0.13	0.15	0.16	0.18	0.20	0.24	0.27	0.31	0.34	0.36	0.41	0.47
Winter (Nov. - April)	0.04	0.06	0.07	0.08	0.09	0.10	0.12	0.14	0.16	0.18	0.20	0.22	0.26	0.30

Alternatively to the above described explicit calculation of the wind drift of precipitation (Eq. 4.2), if necessary in combination with a correction of the wetting and evaporation losses in Tab. 4.1, the systematic measurement errors of Hellmann gauges can also be corrected using the standard correction method of the German Weather Service (DWD 1995). Then the corrected daily value of precipitation is:

$$N_{G,korr} = \left(N_{maes} + b \cdot N_{maes}{}^{\varepsilon}\right) \cdot K_G \tag{4.3}$$

$N_{G,korr}$ [mm] precipitation for a subarea corrected for the measurement error

N_{meas} [mm] interpolated area precipitation values stemming from Thiessen polygons or inverse distance method (see Section 4.1.3)

b [-] correction factor (see Tab. 4.2)

ε [-] correction factor (see Tab. 4.2)

K_G [-] correction factor for converting measured precipitation (point data) into area data, e.g. used for compensation, if gauging stations systematically show higher precipitation as those in the surrounding area

Tab. 4.2 Correction factors for the standard method of the German Weather Service for correction of daily precipitation values of Hellmann gauges

Precipitation type	Relevant air temperature	Coefficient	Coefficient b for a horizontal sheltering of			
		ε	2°	5°	9.5°	16°
			un-sheltered	lightly sheltered	moderately sheltered	heavily sheltered
Rain (summer)	T > + 3.0°C	0.38	0.345	0.310	0.280	0.245
Rain (winter)	T < + 3.0°C	0.46	0.340	0.280	0.240	0.190
Mixed precipitation	-0.7 <T< +3.0°C	0.55	0.535	0.390	0.305	0.185
Snow	T < -0.7°C	0.82	0.720	0.510	0.330	0.210

This method considers factors influencing systematic precipitation errors indirectly using annual variations, air temperature and horizontal sheltering of the rain gauge.

For the application of this correction method in LARSIM for all stations in the investigated area a mean value of horizontal sheltering is to be estimated and entered in LARSIM, because in many cases no specific information about the horizontal sheltering of rain gauges is available.

Because the DWD standard method does not contain an explicit consideration of actually measured wind speeds and can only be used for daily values of precipitation, a correction according to the above-described method of Sevruk can be recommended.

4.1.2 Conversion of dew point temperature and global radiation

In LARSIM, it is possible to optionally use the dew point temperature instead of the relative humidity as input data. The dew point temperature is subsequently converted internally into the relative humidity and into the water vapour pressure, respectively (WEISCHET 1983):

$$RF = \frac{e_s(t_{Taupkt})}{e_s(t_{Luft})} \tag{4.4}$$

$$e_s = 6.1078 \cdot 2.71828^{\left(\frac{17.08085 \cdot t}{234.175 + t}\right)} \tag{4.5}$$

$$e = e_s \cdot RF \tag{4.6}$$

RF [-] relative humidity

e_s [hPa] saturation water vapour pressure for given temperature

t_{Taupkt} [°C] dew point temperature 2 m above ground

t_{Luft}	[°C]	air temperature 2 m above ground
e	[hPa]	water vapour pressure

In case global radiation is used instead of sunshine duration as input parameter, the calculation of the global radiation according to Eq. 3.32 is omitted. However, since sunshine duration is a variable in the calculation of the long wave net radiation according to the MORECS scheme (Eq. 3.35), it is estimated from the measured global radiation according to the simplifying correlation below (DVWK 1996: 26):

$$n = \left(\frac{R_C}{R_A} - a \right) \cdot \frac{N}{b} \tag{4.7}$$

n	[h]	estimated sunshine duration during a day
R_C	[W/m^2]	measured global radiation on the ground
R_A	[W/m^2]	solar radiation at the upper atmosphere boundary (Eq. 3.33)
N	[h]	time from sunrise till sunset (Eq. 3.34)
a	[-]	empirical coefficient (= 0.19)
b	[-]	empirical coefficient, depending on month from 0.53 to 0.57

4.1.3 Transfer of point meteorological data into spatial data

For water balance computation, meteorological time series listed in Table 4.3 are required:

Tab. 4.3 Meteorological time series required by LARSIM

Parameter	Unit	Data properties
Precipitation	mm	Cumulative value per interval
Air temperature	°C	Mean value per interval
Relative humidity (or dew point temperature)	% (°C)	Mean value per interval
Wind speed	m/s	Mean value per interval
Sunshine duration (or global radiation)	hours (W/m^2)	Cumulative value per interval
Air pressure	hPa (=mbar)	Mean value per interval

These meteorological variables can be adopted directly as spatial values from the meteorological model if LARSIM is used in a coupled atmosphere-hydrology model. In contrast, if the water balance model uses measured meteorological data, the values from the weather and precipitation stations, which are only available as point data, have to be transposed to spatial data (subareas).

In this conversion, LARSIM distinguishes between three effects:

- representativeness of the point data for the subarea areas
- consideration of the horizontal distance between gauging station and subarea centres
- consideration of the vertical distance (difference of altitude) between gauging station and the benchmark in the subareas

These techniques, which are used to convert the meteorological data based on point measurements to the average conditions within the subareas, are shown in Table 4.4 and explained in the text below.

Tab. 4.4 Techniques used within LARSIM for the conversion of meteorological data based on point measurements to area values for subareas

Meteorological parameters	**Technique used in LARSIM for conversion of meteorological point measurements to the subareas**		
	Representativeness of point data for the area	Horizontal area-conversion	Vertical area-conversion (altitude dependency)
Precipitation	Possibility of modification of measured data by correction coefficient[1)]	Inverse distance method or Thiessen polygons	Altitude dependency not regarded
Air temperature	Assumption of a representative gauging station	Inverse distance method or Thiessen polygons	Adiabatic gradient: 0.65°C per 100 meters
Relative humidity / dew point temperature	Assumption of a representative gauging station	Inverse distance method or Thiessen polygons	Altitude dependency not regarded
Wind speed	Assumption of a representative gauging station	Inverse distance method or Thiessen polygons	Logarithmic wind profile near the ground [2)]
Sunshine duration / global radiation	Assumption of a representative gauging station	Inverse distance method or Thiessen polygons	Altitude dependency not regarded
Air pressure	Assumption of a representative gauging station	Inverse distance method or Thiessen polygons	Pressure gradient: 12.5 hPa / 100 meters

1) see correction coefficient K_G in Eq. 4.1

2) for conversion of wind speed from 10 m above the ground to wind speed 1 m above the ground

Representativeness of point data for the area

In the conversion of the measured point data of precipitation to the subareas, a correction coefficient K_G (Eq. 4.1) is used: This coefficient serves as a compensation, if the precipitation station used for a certain group of subareas systematically measures higher precipitation than its neighbouring stations. This might be the case when a precipitation station lies on the windward side of a mountain.

In LARSIM, it is assumed that for all the other meteorological parameters the particular gauging stations provide representative values.

Conversion of the point data to the subareas

For the conversion of the meteorological point data to the subareas, it is possible to choose between the following two conversion methods (see LUDWIG 1978, 1982):

- Modified inverse distance method: The computed value of the meteorological parameter for the subarea and the relevant time interval equals the distance-weighted arithmetic mean of the measured values at the stations which lie nearest to the centre of the subarea in the four quadrants.
- Modified Thiessen-polygon method: The computed value of the meteorological parameter for the subarea and the time interval equals the measured value at the station nearest to the centre of mass of the corresponding subarea.

In both conversion methods, the position of the subareas is defined by their centres.

Consideration of altitude dependency for the conversion from point data into spatial data

For the conversion of measured air pressure data into spatial data, LARSIM takes into account the altitude dependency of air pressure following the barometric height formula (e.g., see WEISCHET 1983):

$$p_2 = e^{\left(-\frac{g\cdot(h_2-h_1)}{R(T1+T2)/2}+\log p_1\right)} \tag{4.8}$$

p_1, p_2	[hPa]	air pressure at altitude 1 and altitude 2
g	[m/s^2]	acceleration of gravity (= 9.81 m/s^2)
h_1, h_2	[m]	altitude 1 and altitude 2
R	[J/kg/K]	gas constant (= 287 J/kg/K for air)
T_1, T_2	[K]	air temperature at altitude 1 and altitude 2

For the parameter values, which are representative of the earth's surface, the relationship results in a change of air pressure of about 12.5 hPa per 100 meters. An altitude correction of air pressure is therefore applied when the conversion of the air pressure from the nearest meteorological station to the grid (sub-) area is carried out using the gradient mentioned above. For the parameter "air temperature", a gradient of 0.65 °C per 100 meters (WEISCHET 1983) is used.

With regard to the correction of the wind error in precipitation measurement, a conversion of the wind speed measured 10 m above the ground to the height of the precipitation measurement (i.e., 1 m above the ground) is necessary. Thus, a logarithmic wind profile according to the MORECS scheme for the calculation of evaporation (THOMPSON et al. 1981 and Section 3.1.5) near the ground is assumed. This assumption is a simplification of the real conditions, which is only valid for a neutral atmosphere layering.

In the context of the water balance modelling, this simplified approach was chosen to decrease the number of required model parameters. Hence, the following conversion correlation is used:

$$u_2 = \frac{ln(h_2 / z_0)}{ln(h_1 / z_0)} \cdot u_1 \qquad (4.9)$$

h_1 [m] height 1 above the ground, here: elevation of anemometer (usually 10 m)

h_2 [m] height 2 above the ground, here: elevation of precipitation gauge (usually 1 m)

u_1 [m/s] wind speed at height 1

u_2 [m/s] wind speed at height 2

z_0 [m] roughness length, according to THOMPSON et al. (1981: 20) equal to 0.1 times the stand height, here: z_0 = 0.03 m for pasture

By insertion of these parameters values into the equation, the wind speed one meter above the ground on pasture equals 0.6 times the value measured in ten meters above the ground. Using the correlation given by the DVWK (1996: 85), the same conversion factor of 0.60 applies for hilly or flat terrain with numerous obstacles.

4.2 Regionalisation of hydrological model parameters

The application of hydrological concept models for water balance analysis requires an adjustment of model parameters to the area under investigation, to reproduce the area-specific hydrologic processes as accurately as possible.

This procedure can result in an optimal adaptation of the model parameters for the particular area, but the disadvantage is that the calibrated values are not easily transferable to an area without discharge measurements.

Because of this, it is attempted to keep the number of model parameters, which have to be calibrated, as low as possible. The possibility to deduce model parameters from area characteristics, which should ensure a regional transferability, is called *regionalisation* (BECKER 1992).

LIEBSCHER (1992) gives an overview over international research projects about regionalisation: The United Nations Educational, Scientific and Cultural Organization (UNESCO) for instance has been conducting hydrological research programs since 1965: between 1965 and 1974 it was named International Hydrological Decade (IHD), thereafter International Hydrological Programme (IHP). Among other things, it dealt with hydrological representative and experimental areas, as well as topics from the comparative regional hydrology. A summary of results can be found in FALKEMARK AND CHAPMAN (1989).

In the IHP-projects FRIEND (Flow Regime from Experimental and Network Data) and FRIEND (Flow Regimes from International Experimental and Network Data) aspects of flow regimes were studied comparatively based on an extensive data basis (e.g. ROALD et al. 1989 or DEMUTH 1993).

In the World Climate Programme (WCP) of the World Meteorological Organization (WMO), questions of regionalisation were examined. Furthermore, discharge data collected worldwide are compiled and analysed (WMO 1988b and GRDC 1993). The WCP project GEWEX (Global Energy and Water Cycle Experiment, WMO 1988a) contains substantial research to the improvement of the understanding of processes of the regional and global water and energy cycle.

Further international activities on the field of regionalisation were initiated by the International Council of Scientific Unions (ICSU) and the International Association for Hydrological Sciences (IAHS). A composition of various works on this topic is given for example by DIEKKRÜGER AND RICHTER (1997). Contributions from Germany to "Regionalisation in Hydrology" of the German Research Foundation (DFG, Deutsche Forschungsgemeinschaft) are composed by DFG (1992).

The regionalisation techniques, which are used in LARSIM for parameters of the soil storage, as well as hydrologic storage compartments in the catchment, are described below.

4.2.1 Regionalisation of model parameters for soil storage

The soil storage represents the most sensitive model component in the calibration of LARSIM. Soils can be very heterogeneous due to numerous factors such as geology, geomorphology, climate and land use. Spatial data of the soil conditions are always to a considerable extent a generalization.

In the Xinanjiang model used here, the difficult determination of the soil storage is reflected by the relatively large number of calibration parameters.

For the parameter b of the soil-moisture - saturated-area function (SMSA-function) the following relation for the forest land use part in subareas and as the mean difference in elevation of the tributary streams was determined for the Weser catchment area:

$$b = min\left(\frac{1}{0.0225 + 0.2177 \cdot Forest + 0.0273 \cdot \Delta H}; 0.5 \right) \tag{4.10}$$

b	[-]	parameter in the SMSA-function
Forest	[%]	forest land use part in the subarea
ΔH	[m]	mean elevation difference in main channels of the subareas, based on raster catchments of 13.9 km

For the Weser area it was possible to calibrate the values for the parameter b with a stability index of 0.84 using this correlation equation. The mean elevation difference ΔH in Eq. 4.10 depends on the subareas (grid) size. Because ΔH has considerable less influence on the result than the percentage of forest landuse, the application of Eq. 4.10 should still be valid for grid subareas with edge lengths of 10 to 20 kilometres.

Another regionalisation of the parameter b was developed by ABDULLA (1995) for the Arkansas Red River catchment as a function of the mean annual precipitation and ground characteristics:

$$\sqrt{b} = -3.1014 + 6.4409 \cdot \sqrt{n} - 2.72485 \cdot \sqrt{Fk} \\ - 0.02367 \cdot \sqrt{k_s} - 0.02515 \cdot \sqrt{C} + 0.2736 \cdot \sqrt{I_N} \tag{4.11}$$

b	[-]	parameter in SMSA-function
n	[m³/m³]	total porosity of ground
Fk	[m/m]	field capacity (per depth of ground)
k_s	[mm/d]	saturated hydraulic conductivity
C	[%]	area percentage of SCS ground type C (soils with low infiltration capacity, soils with fine to moderate fine texture or with layers that retains water)
I_N	[mm/d]	mean annual precipitation intensity

In the work of FACKEL (1997) the correlation in Eq. 4.11 was tested for the Weser area and, after modifying the approach by a conversion factor, showed results which were almost as good as the regionalisation according to Eq. 4.10. However, the necessary soil characteristics for the Weser area were not available directly and had to be deduced from other data by relatively complex methods.

Another method for estimation of the SMSA-function parameters was proposed by DÜMENIL AND TODINI (1992) for the climate model ECHAM (DKZR 1994). The correlation used there is:

$$b = max\left(\frac{\sigma_h - \sigma_0}{\sigma_h + \sigma_{max}}; 0.01\right) \tag{4.12}$$

b	[-]	parameter in SMSA-function
σ_h	[m]	standard deviation of ground level elevation in catchment
σ_0	[m]	parameter (= 100 m)
σ_{max}	[m]	1 500 m for ECHAM T21-resolution (≈ 600 km · 600 km); 1 000 m for ECHAM T42-resolution (≈ 300 km · 300 km)

The values for b determined by DÜMENIL AND TODINI (1992: 137) lie in the range from 0.01 to 0.5. But because Eq. 4.12 refers to area resolutions of 90 000 km² up to 360 000 km², this regionalisation is valid for applications in the mesoscale.

4.2.2 Regionalisation of model parameters for runoff concentration

The model for runoff concentration in the subareas requires the determination of the retention constants for the soil storages of direct runoff, interflow and groundwater runoff. It is assumed, according to the procedure in FGMOD (LUDWIG 1978, 1982), that the values for the retention constants are also dependent on travel times in subareas. Subareas with a small travel time index (steep areas, compact shapes) have lower retention values than subareas with large travel time indices (flat areas, elongated shapes).

As an index for subareas, the travel times developed by the U.S. Soil Conservation Service (KIRPICH 1940) are used:

$$T_{IND} = u_F \cdot \left(0.868 \cdot \frac{L^3}{\Delta H}\right)^{0.385} \tag{4.13}$$

T_{IND} [s] index for the travel time in subarea
u_F [s/h] conversion factor hour to second (= 3 600 s/h)
L [km] mean length of main channel in subarea
ΔH [m] mean altitude difference for main channel in subarea

The retention constants for the hydrologic soil storages (single linear storages) results from the travel time index multiplied by a calibration parameter:

$$\begin{aligned} RK_D &= EQ_D \cdot T_{IND} \\ RK_I &= EQ_I \cdot T_{IND} \\ RK_G &= EQ_G \cdot T_{IND} \end{aligned} \tag{4.14}$$

RK_D [s] retention constant of storage for direct runoff
EQ_D [-] calibration parameter for retention constant direct runoff
T_{IND} [s] index for the travel time in subarea
RK_I [s] retention constant of storage for interflow
EQ_I [-] calibration parameter for retention constant interflow
RK_G [s] retention constant for groundwater runoff
EQ_G [-] calibration parameter for retention groundwater runoff

By using this formulation, a significantly smaller variation range of the calibration parameters for different subareas in comparison to the actual model parameters (retention constants) is achieved. In general, calibration parameters for all subareas within a region with uniform runoff character should usually not be further differentiated.

HOLLE AND LUDWIG (1985) determined the following dependency on the subarea size for the calibration parameter of the retention constant of direct runoff:

$$EQ_D = 36 \cdot F_T^{0.385} \tag{4.15}$$

EQ_D [-] calibration parameter for the retention constant direct runoff

F_T [km^2] subarea size

The direct runoff component analysed by HOLLE AND LUDWIG (1985) refers to single-flood river basin models, in which hourly time intervals were mostly used. In water balance models based on daily values, these fast-reacting discharge components are not simulated in detail, but averaged in time. Information about more detailed time-resolution is missing . Thus Eq. 4.15 can be used but must be checked in water balance modelling based on daily time intervals.

Further, the works of SCHWARZE et al. (1997) should be mentioned, in which correlations are shown between the retention constant of the groundwater storage and geological structures. This approach has not been implemented in LARSIM yet, because it was derived for low mountain ranges with palaeozoic and mesozoic bedrock and has not been checked for other catchments.

4.2.3 Regionalisation of channel routing parameters

If no information on actual channel geometries is available, channel width and depth can be calculated according to the downstream hydraulic geometry theory developed by LEOPOLD AND MADDOCK (1953). This theory describes the relations between dependent variables such as width, depth and area as functions of independent variables such as discharge. Exponents and coefficients in these relationships determined by ALLEN et al. (1994) can be used to calculate approximate channel geometries.

Recently, a decisive improvement has been made to this function by KRAUTER (2005) for conditions in Central Europe.

4.2.4 Application of LARSIM for regions outside Central Europe

It is possible to apply LARSIM for catchments outside Central Europe. Examples for this are studies for the Thika-Chania area in Kenya (GATHENYA 1999) as well as tests for Rio Taquarí in Brazil (GERLINGER AND TUCCI 1999). COLLISCHONN AND TUCCI (2001) developed a comparable model on base of LARSIM, which was applied successfully for different investigations in Brasil (TUCCI et al. 2003, COLLISCHONN et al. 2005).

In the applications outside of Europe, the following parameterisations respectively boundary conditions, which are specific for Central European conditions, have to be modified accordingly and their validity has to be verified:

The *correction of the precipitation measurement errors* by wind is only valid for Hellmann precipitation gauges with a measuring height of 1 m above ground. The method for the correction for wetting and evaporation of gauges, which had been developed for Northern Germany (Section 3.2.1) should be checked.

Wind speed measurements are assumed to be made *10 m above ground.* If the measurements are taken at other heights, the factors for the conversion of wind speed have to be adjusted.

The values of the parameters a, b and c for the calculation of the *short wave net radiation* from the measured sunshine duration in Eq. 3.32 are valid for Central Europe. This has no influence on the calculation of the short wave net radiation from the measured global radiation, but the coefficients in Eq. 4.7 have to be adjusted to the particular situation.

The specification of latitude for the calculation of sunrise and sunset (Eq. 3.34) is only assigned correctly by LARSIM if the *specification of the coordinates* for subareas and meteorological stations are declared in northern latitude and eastern length. Other coordinate systems are not supported in the current version.

The *parameterisation of vegetation* (leaf area indices, albedo, stomata resistances, effective stand height) has to be adjusted to the particular conditions.

The *adiabatic gradient* (Section 3.38) and the specifications for the average *flux of ground heat* (parameter P in Eq. 3.37) have to be checked.

The research of GATHENYA (1999) and others mentioned above show, that with an adequate adjustment of the parameterisation it is possible to simulate the water balance of catchments outside Central Europe with LARSIM properly.

4.3 Simulation quality measures

For an objective assessment on simulation quality of a model (comparison of measured and simulated discharges in selected time periods, further called MS-differences) different measures of quality can be applied. An evaluation of such quality measures in precipitation-discharge models is given by AITKEN (1973). In LARSIM the three quality measures are routinely available:

Coefficient of determination according to Bravais-Pearson

$$r^2 = \frac{\left(\sum_{i=1}^{n} \left(Q_{gem,i} - MQ_{gem} \right) \cdot \left(Q_{ber,i} - MQ_{ber} \right) \right)^2}{\sum_{i=1}^{n} \left(Q_{gem,i} - MQ_{gem} \right)^2 \cdot \sum_{i=1}^{n} \left(Q_{ber,i} - MQ_{ber} \right)^2} \qquad (4.16)$$

r^2	[-]	coefficient of determination according to Bravais-Pearson, range: $0 \le r^2 \le 1$
i	[-]	index of calculation time interval
$1, n$	[-]	index for the first / the last calculation time interval
$Q_{gem,i}$	[m^3/s]	daily mean value of measured discharge, interval i
MQ_{gem}	[m^3/s]	average value of measured discharge in total time period
$Q_{ber,i}$	[m^3/s]	daily mean value of calculated discharge, interval i
MQ_{ber}	[m^3/s]	average value of calculated discharge in total tome period

The coefficient of determination describes the share of variance, which can be explained by a regression in relation to the total variance for MS-differences.

Although the coefficient of determination is often used, its application as a quality indicator is problematic, because it does not account for systematic time shifts between measured and calculated discharges (AITKEN 1973: 123).

Model efficiency according to NASH AND SUTCLIFFE (1970)

$$E_Q = \frac{\sum_{i=1}^{n}\left(Q_{gem,i} - MQ_{gem}\right)^2 - \sum_{i=1}^{n}\left(Q_{ber,i} - Q_{gem,i}\right)^2}{\sum_{i=1}^{n}\left(Q_{gem,i} - MQ_{gem}\right)^2} \tag{4.17}$$

EQ	[-]	model efficiency according to NASH AND SUTCLIFFE (1970), range: $0 < E < 1$
i	[-]	index for the calculation time interval
1, n	[-]	index for the first / last calculation time interval
$Q_{ber,i}$	[m^3/s]	daily mean value of calculated discharge, interval i
MQ_{gem}	[m^3/s]	average value of measured discharge in the totally considered time period
$Q_{gem,i}$	[m^3/s]	daily mean value of measured discharge, interval i

In model efficiency, in contrast to the coefficient of determination, deviations between measured and calculated discharges, which are constant throughout the time series, do have an effect on the determined measure of quality.

Model efficiency according to NASH AND SUTCLIFFE (1970) for logarithmic discharge values

The calculation of this quality measure is made according to Eq. 4.17, but logarithmic discharge is used. Thus deviations in the low water region are weighted stronger than in the flood region. The relevant equation is:

$$E_{lnQ} = 1 - \frac{\sum_{i=1}^{n}\left(ln\,Q_{ber,i} - lnQ_{gem}\right)^2}{\sum_{i=1}^{n}\left(ln\,Q_{gem,i} - M\;lnQ_{gem}\right)^2} \tag{4.18}$$

E_{lnQ}	[-]	logarithmic model efficiency according to NASH AND SUTCLIFFE (1970), range: $E_{lnQ} < 1$
i	[-]	index for the calculation time interval
1, n	[-]	index for the first / last calculation time interval
$Q_{ber,i}$	[m^3/s]	daily mean value of calculated discharge, interval i
$MlnQ_{gem}$	[m^3/s]	mean value of logarithmic measured discharge for the considered time period
$Q_{gem,i}$	[m^3/s]	daily mean value of measured discharge, interval i

5 Procedures for operational forecast

On behalf of the Landesanstalt für Umwelt, Messungen und Naturschutz Baden-Württemberg (LUBW, Germany), the water balance model LARSIM has been enhanced for the operational and continuous forecast of discharge and water temperature. The LUBW started the application of LARSIM for the catchment of the Neckar in a daily operational mode in the year 2000, initially for the forecast of low flow.

The operational calculation mode differs from offline simulation runs insofar, as it comprises a combination of simulation and forecast in each run. Therefore the computed period of time can be divided into the period of simulation, where model-parameters are optimized by minimizing the deviation between simulated and measured data, and the period of forecast, which begins with the given date for the start of forecast.

For computing the period of simulation, measured hydrometeorological data received by real-time transmission is used as input. Whereas for the period of forecast, results of numerical weather forecast models are used. The structure of the data for those two periods of time differs in respect to the area reference. The measured data refers to individual meteorological stations, whereas the data of the weather forecast is grid-oriented, so that interpolation techniques within LARSIM are used to assign the meteorological information to the subareas of the model.

The operational calculation mode of LARSIM is designed for a calculation interval of one hour. Different temporal references like Central European Time (CET) for measured hydrometeorological data and the Universal Time (UTC) for the meteorological forecast data are taken into account by the program automatically.

Additionally to the forecast of the discharge, other information like evaporation, soil moisture, snow heights and groundwater regeneration can also be predicted.

The Flood Forecast Centre of the LUBW Baden-Württemberg initiates automated runs of water balance models for the whole area of the federal state once every day during periods of low flow. For the prediction of floods, the models are run every one or two hours (see also Section 6.4).

5.1 Operational aspects

5.1.1 Treatment of missing input values

For an automated operational model application it is vital that gaps in hydrometeorological data input will be automatically identified and filled by using suitable interpolation techniques. In the operational water balance model this is achieved as follows:

Gaps in measured precipitation are compensated with measurements at nearby stations by using the matrix dot method. This procedure allows the determination of the station that will be used to provide measured values depending on the interval.

Gaps in other measured climate data (wind, air temperature, global radiation, relative humidity, air pressure) are compensated by measurements at adjacent stations by using the matrix dot method as well. If no measured data is available at any of the stations, gaps are filled with available "old" numerical weather forecasts. If no "old" weather forecasts are available gaps are filled with the last measured values.

Gaps in predicted precipitation, particularly if the available precipitation forecasts do not cover the period of forecast completely: the resulting gaps are set to the value zero.

Gaps in other predicted climate data, particularly if the available climate data does not cover the selected period of forecast completely: it is possible to extrapolate the existing values into the future by either using the last predicted value for the entire remaining period or by using the last 24 values for data types showing a day-night-transition (e.g. the global radiation).

Gaps in measured discharge data can optionally be substituted by simulated discharges.

5.1.2 Adaptation of the model state for storage components

With LARSIM it is possible to save the state of the storage components of the model at defined points of time. These saved data sets of the current state of the system provide information concerning each subarea. This information includes the current filling of the storage component for base flow and the snow height or information concerning each land use of a subarea like the wetting of the leaf surfaces and the filling of the soil storage component.

These status data sets are created with every run of the model, so that they can be used as input for the following runs. Consequently, a continuous updating of the water balance is guaranteed, even if short forecast simulation runs are intended.

For the operational model run, the period of simulation comprises two days, so that a status data set, which is dated two days before the start of forecast, is used as input.

5.1.3 Operational process procedure

For operational forecasts LARSIM can be used in an automated flow control, which does not require any actions of the user. The program flow in the Flood Forecast Centre of Baden-Württemberg (HVZ) for the automated forecast of discharge is basically the following:

- Setting the internal forecast time to the current system time.
- Automatic import of the latest status data set with the contents of all water storage components which was saved during a former model run and setting the start of the calculation to the date of this latest model state, but at least 2 days before the current start of forecast.
- Automated identification and import of hydrometeorological measurements currently available for the meteorological stations and gauges.
- Creation of a protocol of the current data status for available hydrometeorological time series.
- Import of meteorological forecasts currently available from numerical weather forecast models (e.g. local model of the DWD) for precipitation, global radiation, wind speed, air pressure, air temperature and relative humidity.

- Execution of the water balance model.
- Saving the hydrologic state of all water storage components for the start of forecast.
- Display of the simulated and predicted output values (e.g. discharge forecasts) for the HVZ and automatic distribution of the results via internet and other communication networks.

5.2 Automated model optimization

When computing the operational forecast, differences between simulated and measured discharge (so called "MS-differences") within an analysis time span may occur for different reasons: frequently the differences stem from an insufficient density of meteorological stations, non-representative data or inexact water-level-discharge relationship for gauges. However, model insufficiencies cannot be avoided.

By evaluating the MS-differences it can be checked how the model reproduces the actual hydrologic situation and model parameters can be optimized to improve the quality of the forecast. Therefore the HVZ has included possibilities for an automatic process-oriented model adaptation into LARSIM, which are described in the following.

5.2.1 Use of measured discharge

For the operational forecast, measured discharge at a gauge is used if data is available and of good quality.

To rate the quality of the measured discharge at a gauge, LARSIM analyses a data record with information on the quality of the discharge hydrographs in case of low flow, mean flow and flood. By using this information a situation may arise, where the measured discharge at a gauge is ignored for a model run during a period of low flow, whereas the measured data is taken into account when predicting a flood.

The automated model optimization within LARSIM evaluates MS-differences and subsequently applies different kinds of correction methods depending on the situation. The principle of the automated optimization is shown in Fig. 5.1.

At first it is decided, whether a gauge shall be used for model adaptation in general or not. If this is the case the model evaluates to which range of discharge - either low flood, mean flow or flood - the actual measured discharge belongs to. If the rating curve is assumed to be reliable within the actual range of runoff, a model adaptation is made using the measured discharge data of this gauge. Depending on the range of the runoff the adaptation procedure differs.

5.2.2 Optimization in case of mean and low flow

In case of mean or low flow the MS-differences are generally analysed 48 hours before the start of forecast (NQM-analysis time span), so that the influences of short-term discharge fluctuations are not overestimated. A model adaptation is only initiated if the mean difference between simulated and measured discharge is larger than a preset maximum threshold value (e.g. 5%).

After that, the variation ratio, as a measure for the range of variation of the runoff, is evaluated by computing the ratio of the minimum and the maximum value of observed discharge during the NMQ-analysis time span (Q_{min}/Q_{max}).

If this ratio falls below a preset threshold, it is assumed that the runoff conditions are relatively stationary. If this is not the case, the situation is classified as instationary.

Optimization of the water yield

In case of instationary runoff conditions during a period of low or mean flow, a possible adaptation of water yield is checked. Water yield describes hereby the sum of the effective precipitation and the snow melt (WD in Fig. 5.1). The water yield is optimized if this leads to a lower deviation for the simulated discharge within the NQM-analysis time span. The maximal admissible correction of the water yield is limited by preset minimal and maximal factors.

The correction of the water yield is especially necessary and promising in the following two cases:

- In case of convective rainfall the precipitation in a small area can easily be over- or underestimated in dependence of the position of the meteorological stations. These miscalculations can be compensated to a certain extent by an adaptation of the water yield.
- Also the melting of snow covers can lead to errors in the simulation of discharge if the snow water equivalent is not simulated accurately. Here the optimization of the water yield also leads to an improvement of the results.

Optimization of the storage components for base flow, interflow and direct runoff

The optimization of the water yield is not reasonable if the instationarity of discharge is not caused by precipitation or snowmelt during the period of simulation. This pertains for instance to the falling limb of a hydrograph when the recession of discharge originates from the reduction of the storage components for interflow and direct runoff.

In such periods of instationary flow, the actual water content of those hydrologic storage components is adapted, so that a better simulation of the discharge is achieved. An optimization of the storage components is also carried out when the variation ratio Q_{min}/Q_{max} indicates conditions of stationary flow.

For a further differentiation of this optimization procedure, the minimum portion of base flow from the entire discharge is computed for the given analysis time span.

If the portion of the base flow exceeds a preset threshold value (“$MinQ_B$”, e.g. 90%), the actual conditions are classified as a typical period for low flow.

In this case the contents of the storage components for base flow, interflow and direct runoff are optimized for all subareas belonging to the catchment of the regarded gauge with the same factor at the start of simulation.

It must be noted that despite of using the same factor for all components in this case, it is mainly the storage for base flow that is adapted. However, if the simulated portion of base flow is lower than the preset threshold value $MinQ_B$, it is assumed that there is either a period of mean flow with approximately stationary runoff conditions or that the hydrograph shows a falling limb of a flood wave. Under these circumstances only the two storage components for interflow and direct runoff are adapted.

This procedure prevents that a wrong estimation of the water yield or of the recession properties of the storage components for interflow and direct runoff is compensated to some extent by adaptation of the storage component for base flow.

5.2.3 Optimization in case of floods

In case of floods, the analysis time span normally comprises only the last 6 hours before the start of forecast (HQ-analysis time span), because of the considerably higher hydrologic dynamics in comparison to periods of low or mean flow.

Within LARSIM a flood for a gauge's catchment is defined by at least one value of the measured hydrograph exceeding a given threshold value assigned to flood conditions during the analysis time span.

If a flood is verified, a model adaptation only takes place if the measured data for this range of discharge is classified as reliable and the MS-differences are larger than the given threshold value (MaxAbw).

Instationary conditions are always assumed in flood situations. Therefore the variation ratio Q_{min}/Q_{max} must not be evaluated. In analogy to the optimization of low and mean flow the program first checks, whether an adaptation of the water yield leads to better results during the HQ-analysis time span. In case this check is not meaningful, the contents of the storage components for interflow and direct runoff are adapted. An adaptation of the storage component for base flow is never applied in a flood situation.

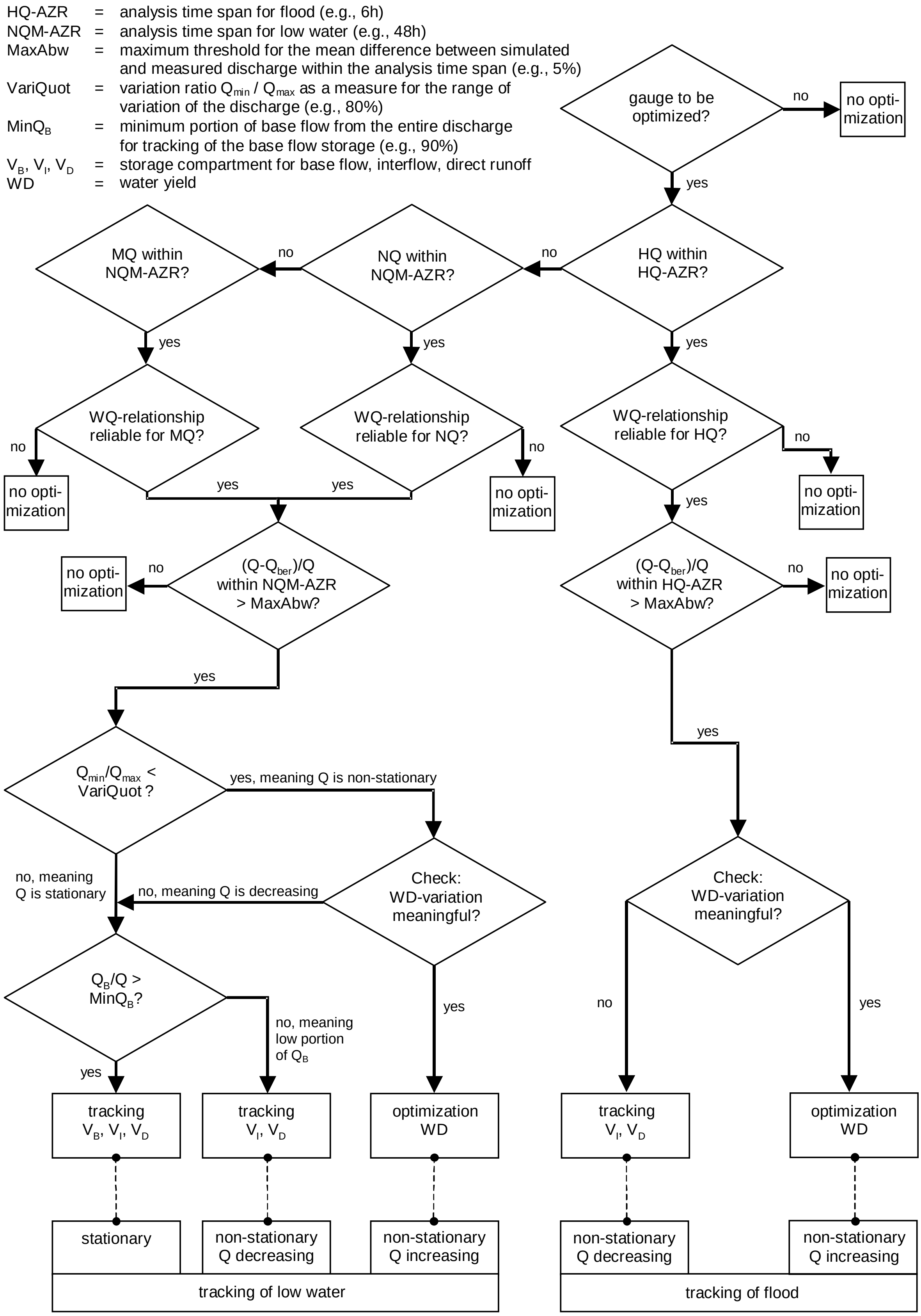

Fig. 5.1 Structure of the automatic model optimization in the operational application of LARSIM (adaptation of snow cover see Section 5.3, water temperature see Section 5.4)

5.2.4 ARIMA-model

In the operational model application the simulated discharge will usually deviate from the measurement at the end of the period of simulation or at the start of the forecast. To adapt the forecasted discharge to the measurement, all predicted values will be corrected by the difference between the simulation at the start of forecast and the last measured value at the same point in time (ARIMA 0-1-0 correction).

In the operational water balance model it can be defined for each gauge, whether an ARIMA-correction is to be applied for a range of discharge or not.

In situations of mean flow or flood an ARIMA-correction is applied, if a measured discharge value is available at the start of the forecast. If no actual discharge measurement exists, a measured value from one time interval earlier is used for the ARIMA 0-1-0 correction. If even for this point of time no measured value is available, the ARIMA-correction will not be applied to this gauge.

For the ARIMA-correction in a period of low flow the model checks first, whether the runoff within the last 24 hours before the start of forecast can be classified as approximately stationary, or if the runoff shows instationarities (e.g. rising discharge at the beginning of precipitation events).

In case of instationary low flow the predicted discharge hydrograph is shifted into the measured discharge at the start of the forecast or into the measured value before as described above. In situations of stationary low flow the forecasted hydrograph is shifted into the 24-hour-mean value of the measurement. By using the 24-hour-mean value the effects of short-term discharge fluctuations (artificial, e.g. due to operation of reservoirs or weirs) can be suppressed and the forecast for low flow can be improved.

For the determination of the valid runoff range the measured discharge is evaluated within the preselected HQ- and NQM-analysis time span, which are also used for the analysis of the plausibility of the measured discharge hydrographs.

If the measured discharge within the period of simulation is classified as plausible for a gauge and an ARIMA-correction is applied, the corrected predicted hydrograph is taken into account for the calculation downstream.

If the measured discharge is not classified as reliable input, a so-called “local ARIMA-correction” is carried out. This does not influence the simulation process downstream of the gauge. Then the correction is only done for the displayed part of the forecasted discharge hydrograph.

ARIMA-corrections, in which the forecasted hydrograph is modified by a constant value over the whole period of forecast, can result in negative and therefore unrealistic discharge values especially in the case of a long theoretical forecast (see Fig. 5.2).

Because of this effect, the above-described ARIMA-correction was extended, so that either a relative (local) or an absolute ARIMA-correction can be made depending on the discharge situation.

If the simulated discharge value at the start of forecast is smaller than the measured discharge at this point of time, the difference is positive and the factor for correction will be the absolute difference between the measured and the simulated value at the start of the forecast.

If the simulated value is larger than the predicted value at the start of the forecast, the difference is negative and therefore a relative correction is applied. With this method the relative difference in percentage is computed and every predicted value is shifted by this relative value in reference to the original predicted value. Fig. 5.2 shows a comparison of a model forecast without correction to the forecast with different correction methods.

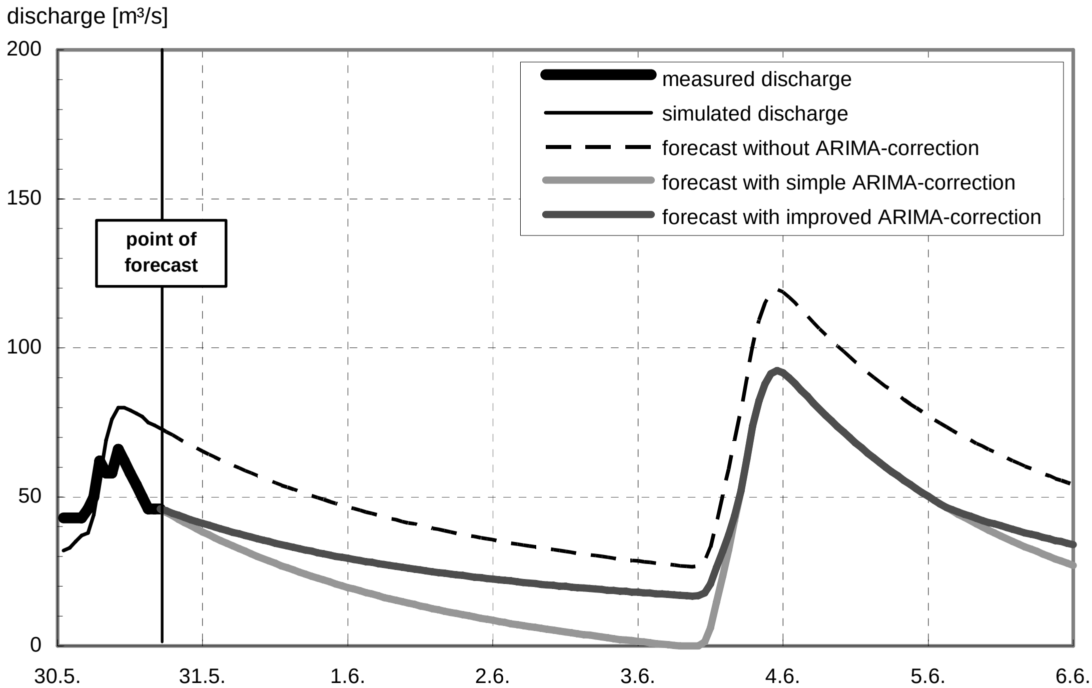

Fig. 5.2 Comparison of runoff forecasts without ARIMA-correction and with different ARIMA-correction methods

5.3 Adaptation of the model snow cover

LARSIM also contains a method for automatic adaptation of simulated and observed snow cover. In this method the temperature threshold value for transition of precipitation from rain to snow is defined in a range of values (of -1°C to + 1°C) specific to different regions, so that the simulated snow cover fits to the observed values as accurately as possible.

Observed values of the snow cover are on one hand produced by surface snow measurements (NSD-measurements of the DWD) and on the other hand by satellite information (NOAH) for snow covered areas and snow-free areas. The relevant adaptation methods have been developed in the DLR-research project InFerno (SCHULZ et al. 2002).

5.4 Operational water temperature forecasting

LARSIM has been enhanced by modules for the simulation and prediction of water temperatures (Section 3.9). Thus it can be used as an operational water balance and water temperature model (WBTM). The WBTM allows the forecast of water temperatures along with discharges (HAAG et al. 2005, 2006).

When LARSIM is used as an operational WBTM, additional operational measurements of water temperature and cooling water input (measurements and predictions) can be considered in the operational scheme. Water and riverbed temperatures are stored in the status data set and can be used as initial conditions for calculations. The operational water temperature measurements can be checked for plausibility within the model. They are only used for further processing if they are considered plausible.

Up to the start of forecast, measured water temperature data is used for the calculation of water temperatures downstream of the measurement locations, analogously to measured discharges. Furthermore, the water temperature measurements are used for an automated adaptation of the model. This simple adaptation is based on the mean deviation between simulated and measured water temperatures during the period of simulation.

With WBTM it is also possible to check for the compliance of water rights regulations, such as upper bounds of water temperatures or evaporation losses due to power plants. The operational WBTM is also used for the online optimisation of cooling water inputs (HAAG et al. 2005, 2006).

The automated WBTM-simulations result in values for measured, simulated and forecasted discharges and water temperatures at specific locations of the river network (e.g. gauges, power plants etc.). These values are automatically visualized and distributed to users.

6 Applications of LARSIM

6.1 Impact of climate change on water balance

6.1.1 General considerations on climate change and hydrologic conditions

According to current predictions in climate research, the large-scale climate in the European region will change generally to higher temperature levels due to anthropogenic influences and in particular due to the increasing CO_2-concentration and other increasing greenhouse gas concentrations in the air.

Climate researchers currently assume that the mean global air temperature will increase by about 1.4 to 5.8 °C in the next 100 years (IPCC 2001). This global warming will have effects on the water cycle. In general, an increase of temperature leads to an intensification of the water cycle, which may result in increased evaporation, changed cloud formation and precipitation characteristics.

The statements derived from global climate models for future climate change to date, mainly refer to large-scale regions such as Europe. Detailed data of the effects on climate and water balance on a regional scale have not been available at regional (e.g. federal state) levels up to now.

In the cooperation project KLIWA (climate change and consequences for water management) of the federal states Baden-Württemberg, Bavaria and the German Meteorological Service, possible consequences of climate change on the water cycle of individual river catchments of the relevant federal states have been assessed (KLIWA 2004).

The consequences are shown and recommendations are developed in terms of a precautionary water management policy. The investigations (which started in 1999) focused first on climate conditions up to now and subsequently on future climate conditions. The examinations were primarily aimed at the description of a possible increase of floods.

The investigation of long time series of historic hydrometeorological measurements provides information about the natural variations observed to date. The results show that the climate conditions in Southern Germany, which have an impact on the entire water balance, have changed noticeably in the past century, especially during the last three decades.

In specific regions the trends found for some of the variables examined exceed the natural (historic) variations derived from long measurement time series (HENNEGRIFF et al. 2006). The results support the explanation that the global and regional climate is human-induced, a basic premise which is generally accepted.

The trends examined to date in the measurement time series of climatological and hydrological parameters cannot be directly extrapolated for the future, as climate processes and their complex interactions are non-linear and may vary over time.

To assess possible climate changes in Southern Germany and their effects on hydrologic conditions for the next decades, regional climate scenarios were developed. As an optimum method has not yet been devised for this purpose, results of three different methods have been investigated.

To achieve comparable results, the KLIWA partners defined conditions for the three different methods that were to a large extent identical: use of measurement data from 1951 to 2000, model verification period from 1971 to 2000, global model ECHAM 4 as model base, IPCC emission scenario B2 and scenario (prediction) period from 2021 to 2050.

The results of the three methods (two statistical downscaling methods and a regional dynamic climate model (REMO)), which (as expected) resulted in a certain range of results, were compared and evaluated (KLIWA 2004, KLIWA 2006).

As a result of this comparison, further evaluations were primarily made on the basis of the results of the Meteo-Research method (ENKE 2003), which is based on a statistical dynamic downscaling using classifications of weather conditions (ENKE AND SPEKAT 1997).

The results of the further development of climate change on the basis of regional climate models can be summarized as follows:

- Warming continues. The air temperature will increase, especially in winter.
- Precipitation will increase in winter.
- An increase in the duration and frequency of west weather conditions (especially west cyclonic conditions), which is important for flood formation in winter, is to be expected.

These changes will have considerable impacts on water balance, especially on the runoff.

6.1.2 Water balance models for Baden-Württemberg

It has been recognized early, that high-resolution (1 km grid) water balance models would be needed in the future for different purposes for the whole area of the federal state of Baden-Württemberg (about 36 000 km^2) (BREMICKER AND LUDWIG 1997, Fig 6.1). Among these purposes are also the investigations of the impact of climate change on the water balance.

Following this strategy, data of regional climate scenarios were used as input data for these models to specify the impact of climate change on the future hydrologic conditions. The high model resolution has been chosen to also use these models for other purposes than climate change investigations such as for instance planning purposes or operational forecast (see Section 6.4).

Organizational structure of the river routing scheme

The water balance models have quadratic grid cells (subareas) of 1 km and the grid is oriented according to the Gauß-Krüger coordinate system. The model representation of the real river network is a simplified model channel network, which was constructed by calculating the intersections of the river network data with the grid cells (subareas resp. model elements) under the condition, that only one river course should be in a grid cell (see Fig. 6.2).

In the few cases, in which a grid cell contains more than one river course, usually the rivers that dispose of a larger catchment is considered in the model. For grid cells, which do not contain a river course in the digital river network, the missing river courses were calculated using a digital elevation model. For each grid cell a main flow direction out of eight possible directions (North, Northwest, West ...) was determined using the digital terrain model.

The simplified tree-like river routing scheme was calculated by computer and if necessary, corrected by hand to reach a good approximation on the real catchment and model channel network.

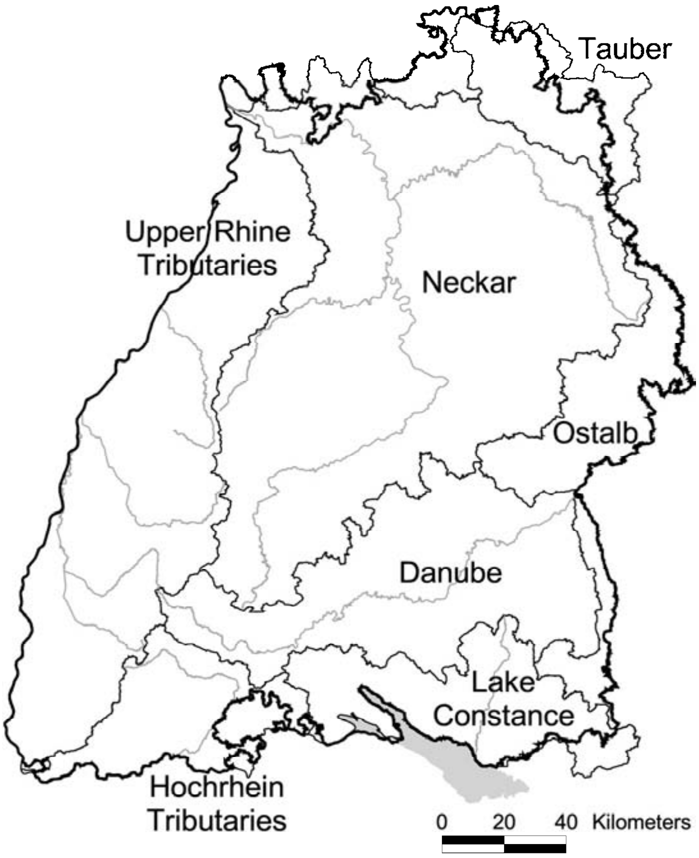

Fig. 6.1 Water balance models in Baden-Württemberg (LARSIM models)

Fig. 6.2 Example for the digital river network (left) **and the river routing scheme of the model** (right) (grid size 1x1 km)

Evaluation of channel data

The necessary river channel data have been derived as follows:

- The length of a channel subreach in a grid cell is equal to the relevant length in the digital river network. If digital channel network data are not available, they are derived from digital terrain models. In this case, the length of the channel subreach in this grid cell is equal to the distance between the centre of the actual grid cell and the centre of the next grid cell downstream.
- The slope of the channel subreaches is equal to the idealized thalweg slope by dividing the height differences between the channel inflow and outflow points by the length of the river for each grid cell.
- The channel geometry is approximated by a double-trapezoidal cross section to discern retention characteristics of main bed and flood plains. For the channels where no profile data were available for the main bed, the cross sections were estimated by use of the morphologic method of LEOPOLD AND MADDOCK (1953) and ZELLER (1965). The necessary values for the bed forming discharge HQ_2 were derived from a correlation function between statistical flood peak values for gauges (LFU 1999a) and catchment size.
- In case of unavailable profile data for the flood plains, their width is estimated according to the main bed width (these data could be improved by meanwhile existing digital terrain models and/or hydraulic models). For the inclination of the side slopes, values of 1.5 (for the main bed) and 5 (for the flood plains) have been assumed.
- Each subchannel has three different roughness coefficients (main bed, flood plain left and right). The roughness coefficients (after Manning-Strickler) for the main bed and the floodplains of the channel subreaches were first set to average values of 30 $m^{1/3}/s$ for the main bed and 20 $m^{1/3}/s$ for the flood plains and adjusted during model calibration where required.
- For several rivers with existing hydraulic models the channel geometry data is replaced by the dV/dQ relations derived from the hydraulic models to improve the flood-routing calculation.

Acquisition of area data

The area data for the water balance models were derived as follows:

- Land use data are based on a classification of satellite data (Landsat TM) with 16 land use classes (30 m grid). The proportions of the land use classes were calculated for each model grid cell. Table 6.1 contains the land use classes for the Neckar catchment and their proportions as an example.
- The lowest and highest surface elevation within each grid cell has been calculated on the basis of a digital terrain model (30 m grid).
- The effective field capacity of soils to a depth of 1 m is used as input value for the soil moisture submodel calculation. Their values with a range from 50 to 250 mm were derived from digital maps for 9 classes of effective field capacity. The effective field capacity has been evaluated for each land use class for the relevant grid cell subareas.

For greater settlement areas data were not available and for these grid cells it was assumed that relevant parameters are equal to the values from the next upstream available neighbour cell.

Tab. 6.1 Considered land use classes and their portions in the grid cells of the Neckar water balance model

Land use classes		Portion per grid cell		
		Mean	Min.	Max.
1	Settlement, dense	2.3%	0%	76%
2	Settlement, light	5.8%	0%	75%
3	Heavily sealed areas (industry etc.)	0.9%	0%	76%
4	Fields	24.1%	0%	100%
5	Viniculture	2.1%	0%	76%
6	Intensive orchards	0.2%	0%	6%
7	Fallow (overgrown)	3.6%	0%	40%
8	Unsealed, no vegetation	0.3%	0%	42%
9	Intensive pasture	14.7%	0%	84%
10	Wetlands	0.04%	0%	32%
11	Extensive pasture	0.5%	0%	43%
12	Sparsely populated forest	7.1%	0%	85%
13	Coniferous forest	19.0%	0%	100%
14	Deciduous forest	5.4%	0%	78%
15	Mixed forest	13.7%	0%	93%
16	Water	0.3%	0%	31%

Data for water transfer

In Baden-Württemberg a considerable amount of the catchments, especially the Neckar catchment, are fed by water transfer from outside the catchment for water supply purposes.

For the Neckar model the measured balances for water transfer were included for 46 subcatchments defined by discharge gauges.

6.1.3 Model calibration and verification

Model calibration

The water balance models for Baden-Württemberg were calibrated with daily data from 1988 to 1991. To eliminate effects of start values for hydrologic conditions, simulations were started a year in advance, at the beginning of 1987.

For the water balance models seven model parameters have been calibrated:

- Calculation of area meteorological data from point data
  - Correction factor K_G for point-area precipitation (see Section 4.1.1)
- Soil storage (see Section 3.3)
  - Drainage index β for the deep soil storage
  - Factor D_{min} for the drainage index for the intermediate soil storage
  - Form b parameter of the soil-moisture – saturation-area function
- Lateral water transport (see Section 3.6)
  - Parameter EQB for the retention constant groundwater storage
  - Parameter EQI for the retention constant interflow
  - Parameter EQD for the retention constant direct runoff

The values of calibration parameters were set equal for all grid cell subareas within the subareas confined by gauges, because there is no additional information that would allow a more differentiated determination within the gauge-controlled subareas. Nevertheless, the grid cells within gauge-controlled areas have different hydrologic properties based on the different system parameters, which is grid-cell specific information (e.g. the elevation conditions in Eq. 4.13).

For the processes of interception, evapotranspiration, snow cover processes, flood-routing in model channels, the parameters were not calibrated but taken from literature (see Section 3).

The calibration aimed predominately at a good approximation of discharges at gauges especially in the low and mean flow spectrum. As an example for the calibration results Fig. 6.3 shows the measured and simulated discharges for the gauge Rockenau/Neckar (calibration time period). The location of the gauge Rockenau can be seen in Fig. 8.8.

The simulation quality is described by different statistical quality-of-fit measures such as the model efficiency (see Section 4.3). An example of the achieved quality measures in the Neckar catchment is provided by Fig 6.6, which shows the logarithmic model efficiency lnQ of the gauges in the Neckar catchment resulting from calibration versus the catchment size. The diagram shows that a good simulation quality could be reached (quality measures between 0.80 and 0.90), especially for gauges with catchment sizes of some hundred km².

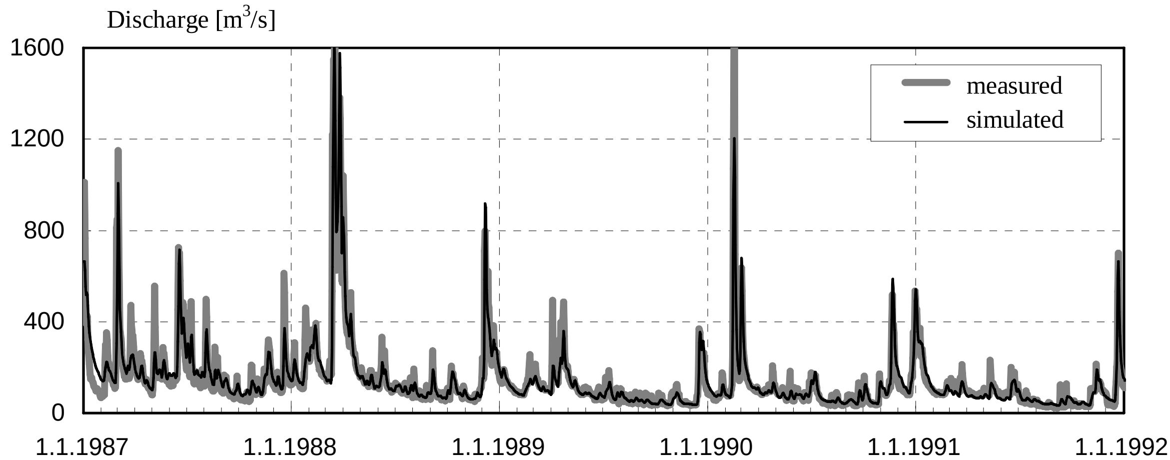

Fig. 6.3 Measured and simulated discharges for gauge Rockenau/Neckar (catchment area 12 676 km²)**, calibration time period**

Model verification

Model verification is a realistic test of the model reliability in which calibration parameters and other model parameters are used to simulate the hydrologic processes with hydrometeorologic data of a time period different from the calibration time period.

For the verification, the simulation time period has been extended until the end of the year 1996 and the simulation quality has been checked for the time period of 1992 to 1996. Examples of the simulated and measured discharges for this model verification for gauges with different catchment sizes are shown in Fig. 6.4 and 6.5.

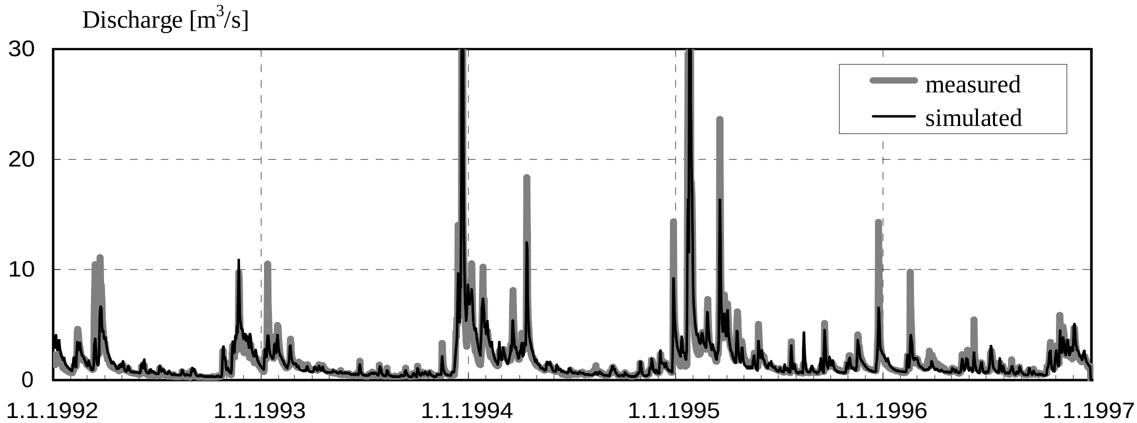

Fig. 6.4 Measured and simulated discharge for the gauge Mosbach/Elz (156 km²)**, verification time period**

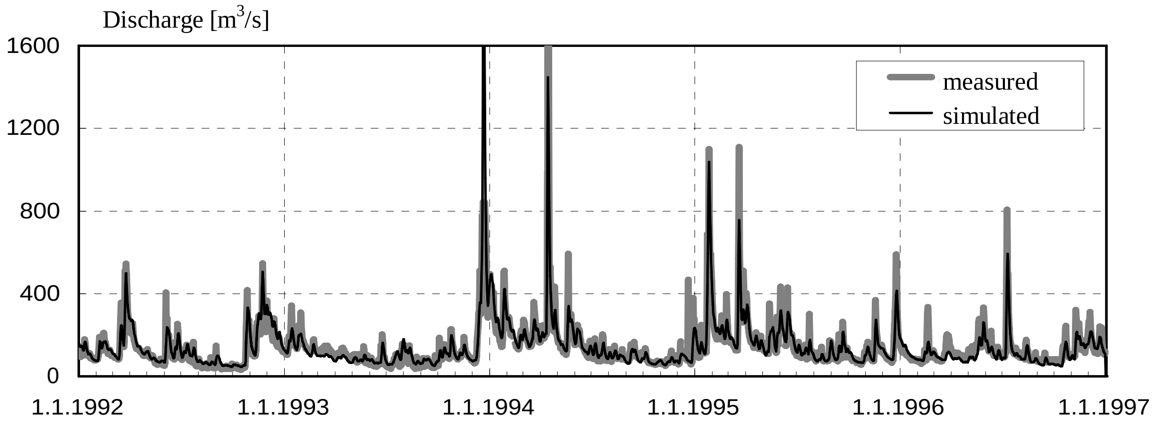

Fig. 6.5 Measured and simulated discharge for the gauge Rockenau/Neckar (12 676 km²)**, verification time period**

The model efficiency lnQ in Fig. 6.6 shows, that a good simulation quality is also achieved in the verification time period, especially for gauges with catchment sizes of several hundred km². Nevertheless, the simulation quality in the verification time period is slightly lower than in the calibration time period. It should be noted, that the model does not necessarily cause this.

The other water balance models with LARSIM in Baden-Württemberg show similar results.

Model calibration and verification indicated that LARSIM is a quite reliable model, if it is used thoroughly and based on relatively reliable data.

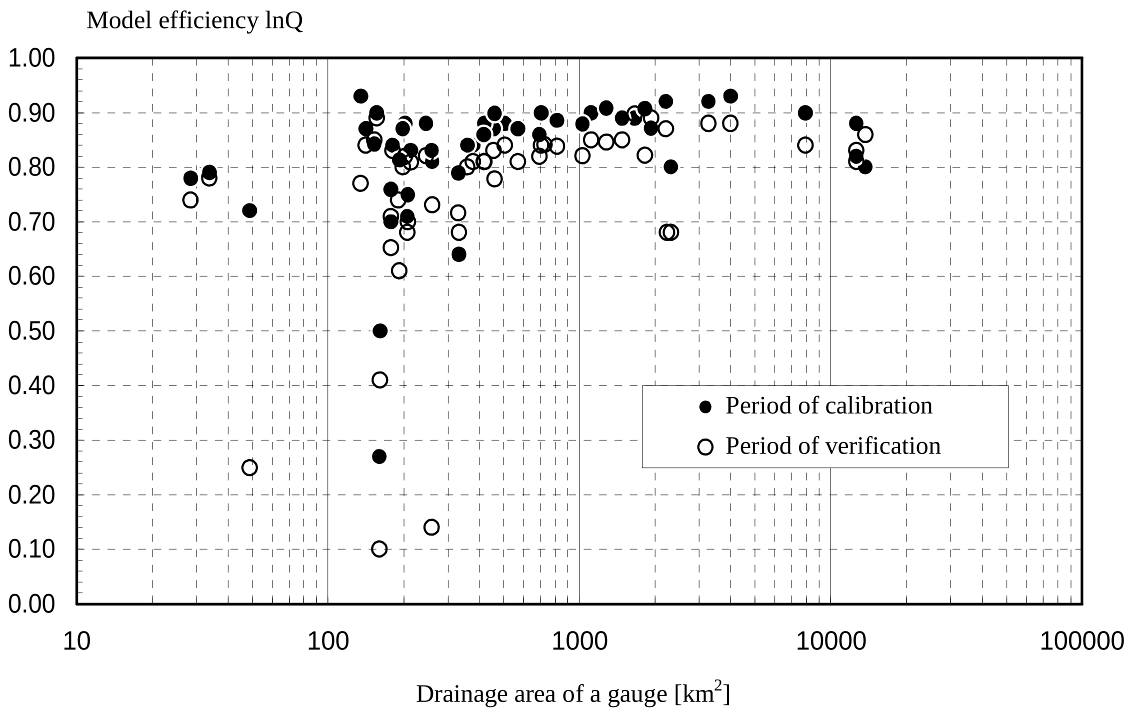

Fig. 6.6 Quality measure for simulated discharges for gauges in the Neckar catchment for the calibration and verification time periods (model efficiency lnQ)

The model results can be further improved. Some aspects, which should be considered in future developments, are discussed below:

- Gauges with smaller catchments show lower quality measures. This could be caused by regional influences (e.g. karst influences).
- Further, in smaller catchments the (more or less accidental) position of precipitation stations (e.g. windward or leeward exposition) may play a role. Also local convection cells can produce systematic problems due to point measurements of precipitation, which in some cases are not representative for the catchment area. If greater catchment sizes are considered, these influences diminish.
- Higher flood peaks could frequently not be simulated properly, because in the climate change simulations the model was calibrated with data on a daily time step.
- In hydrologic situations with snow cover, there are information deficits like influences of precipitation falling as snow/rain. Wind-produced measurement errors are not clearly discernable.

Nevertheless, it can be seen, that the model verification produced good simulation results especially for low and mean flow. It should be noted, that highly different hydrological situations such as the relatively dry year 1989 (mean discharge at gauge Rockenau about 107 m^3/s) or the relatively wet year 1988 (mean discharge at gauge Rockenau about 210 m^3/s) are plausibly simulated by the model. Furthermore, very different situations like snowmelt in spring and dry periods in late summer were successfully simulated.

The good simulation of interannual hydrologic processes can also be seen in the regime curves in Fig. 6.7. For each month, the mean discharges of the measured discharges and of the simulated discharges, using measured climate data as model input, are calculated separately and displayed over the month of the year.

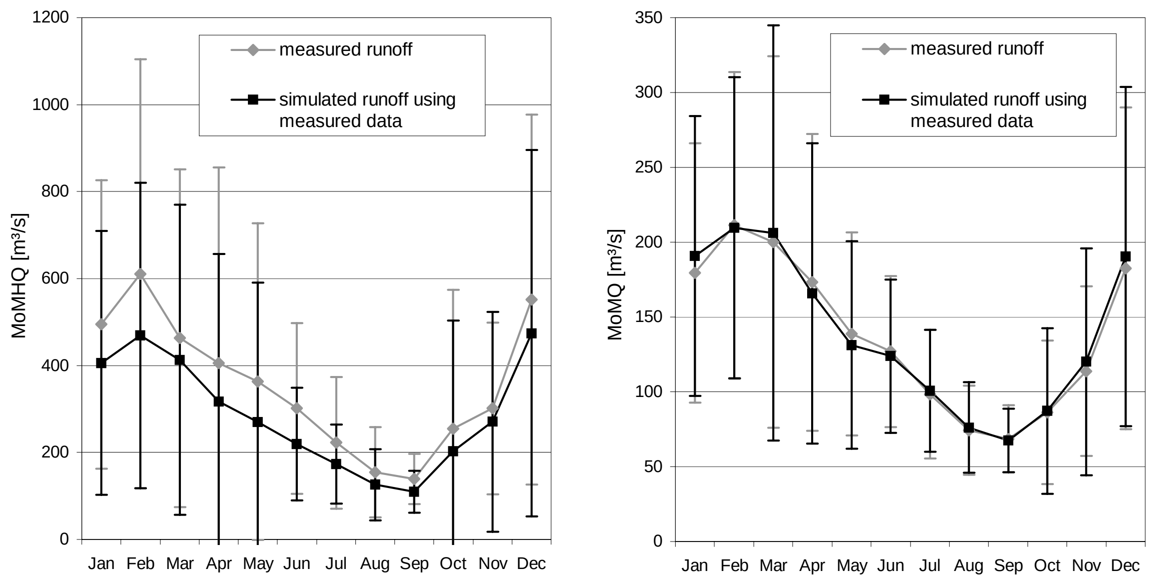

Fig. 6.7 Mean monthly flood values MoMHQ and mean monthly mean flow MoMQ (including standard deviation)**, measured data and simulated data using measured climate data, time period 1971-2000** (gauge Rockenau/Neckar)

In Fig. 6.7, the time period 1971-2000 has been selected, because it was used in the KLIWA-project as reference time period for the current state of the climate. Fig. 6.7 shows, that because of the use of daily calculation time steps, the simulated MoMHQ lies slightly below the measured values, while the simulated MoMQ corresponds well with measured values. The standard deviations also show a good fit, so that not only mean values but also deviations of simulated and measured values are comparable.

From this results it can be deduced, that in an application in which a climate model and the water balance model are applied consecutively the water balance model will not be the cause of decisive result errors (GERLINGER 2004).

Use of water balance models for climate change

The reliable model results allow the employment of the data of the regional climate scenario of the statistical dynamic downscaling model (ENKE 2003). This data is applicable as input quantity for the water balance models, in order to make statements on the impact of climate change on water balance. Mean monthly and yearly values, runoff duration curves and ranks have been analysed (GERLINGER 2004). As an example for the statistical evaluations of the model results, the regime curves with the mean monthly discharges in a year are shown on the following pages to indicate changes in interannual distribution of discharges.

Especially the effects on low flow and on floods are presented in the next two sections. Therefore, the lowest and highest discharge value in a month were selected and averaged for each month (MoMNQ, MoMHQ) for the regime curves. The results of the water balance models for the current climate state and for the future scenario (2021 to 2050) are shown and the relative changes in discharge for the two different climate scenarios are evaluated.

As an example the results for four gauges (Fig. 6.8) from areas with different hydrologic character from simulation results for 110 gauges in Baden-Württemberg have been selected, to explain regional differences within Baden-Württemberg (KLIWA 2006).

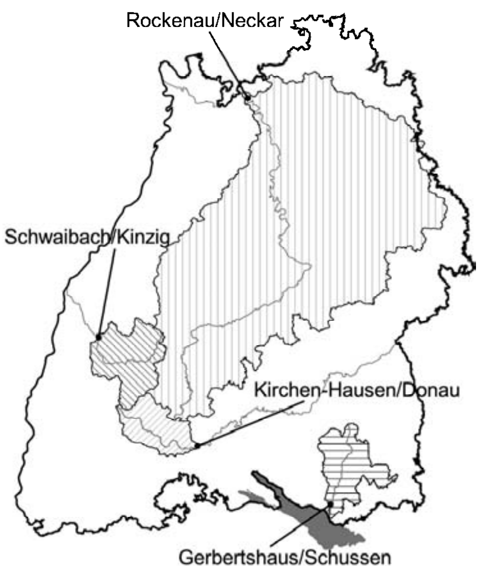

Fig. 6.8 Position of the four gauges and their catchments selected as an example for climate-change influences

6.1.4 Effects of climate change on low flows

The monthly mean low flows (MoMNQ-values) at the selected gauges show an increase of these values over the year (Tab. 6.2, Fig. 6.9). An increase of up to 20% is observed for the two gauges in the catchments of the Neckar and the upper Danube. For the gauges Gerbertshaus and Schwaibach, the relative increases are considerably lower with 4.5% and 7.5% respectively.

The increase of mean yearly low flows is based essentially on a strong increase of low flow values in the winter half-year. Low-flow values are an index of runoff from the slowest soil storage component and thus give information on changing ground water recharge. As ground water recharge occurs mainly in the winter, the increase in the low flow values for the future climate scenario indicates that no decrease in ground water recharge can be expected on the basis of these results for the future.

For the low-flow situation in the summer half-year nearly all gauges show lower values of MoMNQ for the future scenario. The reduction of low flow values for the future scenario reach more than 20% in the critical summer months of July and August in which the lowest discharges occur.

Based on these model results more extreme low flow situations seem to be likely for some parts of Baden-Württemberg for the future climate scenario.

Tab. 6.2 Mean monthly low flow (MoMNQ): relative changes of the current state with respect to the future scenario (LARSIM with climate scenario Meteo-Research as input data, time period 2021 to 2050)

Gauge	Calendar year	Hydrological summer (May - October)	Hydrological winter (November - April)
Rockenau/Neckar	21.6%	2.4%	33.6%
Kirchen-Hausen/Danube	21.7%	- 6.0%	37.1%
Schwaibach/Kinzig	7.5%	- 16.2%	21.2%
Gerbertshaus/Schussen	4.5%	- 6.3%	12.8%

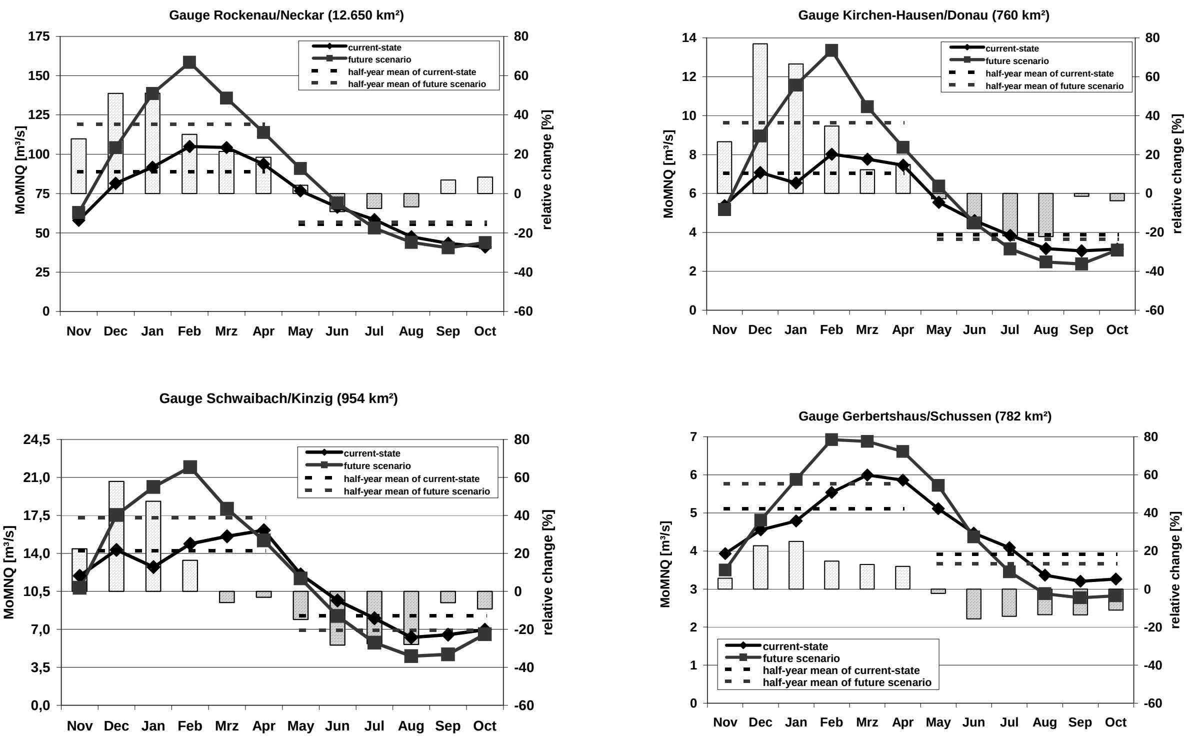

Fig. 6.9 Comparison of mean monthly low flow (MoMNQ) and of their relative changes for current climate state and future scenario 2021-2050 for four gauges in Baden-Württemberg (LARSIM with input data from Meteo-Research model)

6.1.5 Effects of climate change on floods

The mean monthly flood values (MoMHQ) for the year show considerable increases for the future scenario especially for the gauges Kirchen-Hausen in the upper Danube catchment (Tab. 6.3, Fig 6.10). Also the Neckar gauge Rockenau shows a remarkable increase of MoMHQ-values.

The increase with respect to the future scenario is also observed (to a lesser extent) for the gauge Schwaibach. Flood values for gauge Gerbertshaus show only a small increase.

In the summer months June to August decreases of MoMHQ-values result for all of the four gauges in Baden-Württemberg that were selected as an example. Because of this, increases of flood values are caused by increased values in the winter half-year. The MoMHQ-values for the gauges Rockenau and Kirchen-Hausen will increase in winter for the future scenario at a rate of about 40% in single months. Especially January will be up more than 60%. The future increase in flood risk will occur in the month in which in the current climate conditions the highest flood peaks are measured already.

The reason for the regionally differentiated increase of floods is the regionally differentiated increase of precipitation, which is predicted by the Meteo-Research-model (ENKE and SPEKAT 1997), in combination with a higher proportion of rainfall instead of snow due to the higher temperatures in winter for the future scenario.

Tab. 6.3 Mean monthly flood values (MoMHQ): relative changes of the current state with respect to the future scenario (LARSIM with climate scenario Meteo-Research as input data, time period 2021 to 2050)

Gauge	Calendar year	Hydrological summer (May - October)	Hydrological winter (November - April)
Rockenau/Neckar	28.7%	4.5%	38.8%
Kirchen-Hausen/Danube	33.3%	5.1%	44.0%
Schwaibach/Kinzig	21.1%	- 7.0%	34.5%
Gerbertshaus/Schussen	5.0%	- 10.3%	15.8%

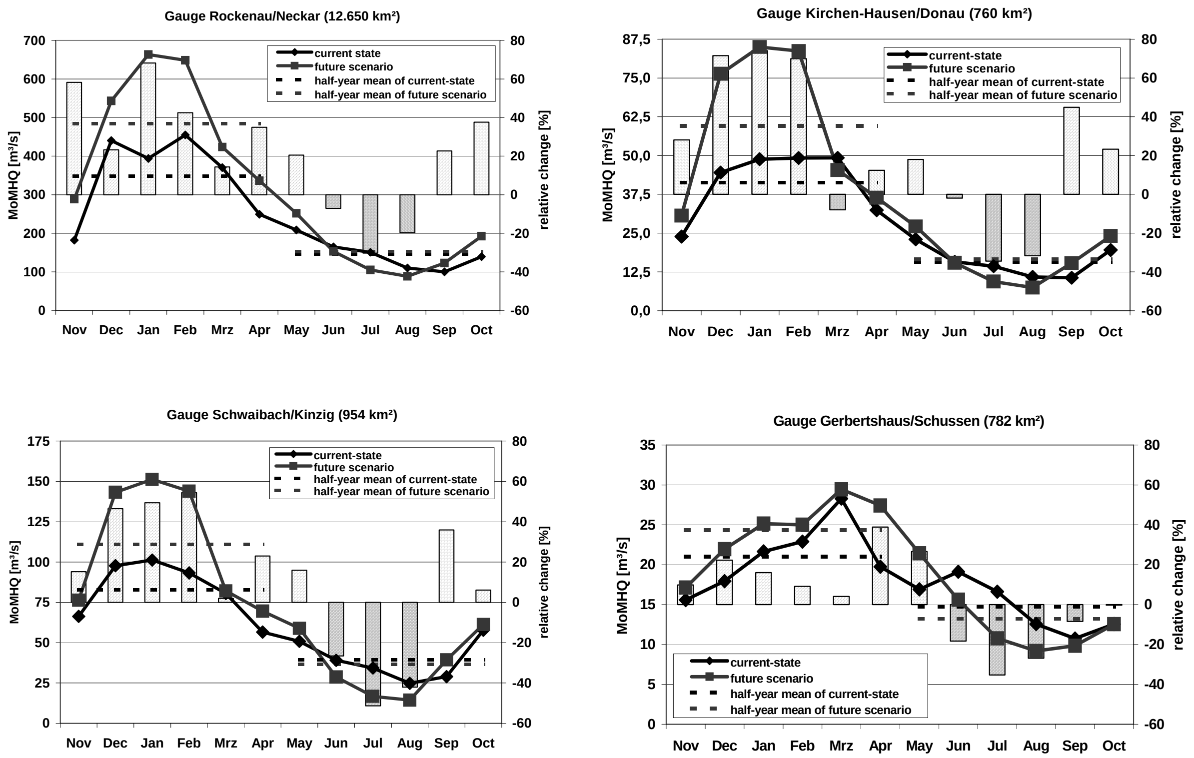

Fig. 6.10 Comparison of mean monthly floods (MoMHQ) and of their relative changes for the current climate state and the future scenario for four gauges in Baden-Württemberg (LARSIM with input data from Meteo-Research model)

6.1.6 Regional change of runoff characteristics in Baden-Württemberg

The changes of low-flow and flood characteristics have been evaluated with the LARSIM simulations not only for the 110 gauges, but also for all model elements in Baden-Württemberg (Fig. 6.11). For the low flow the changes in Fig. 6.11 (left) are visualised for the summer half-year, because in this period the largest changes of the low flow are to be expected. For the floods, the evaluations in Fig. 6.11 (right) refer to the calendar year.

The discussed results are only valid for catchment areas larger than about 1 000 km² as the model chain (global model – regional climate model – water balance model) as well as the model assumptions of the emission scenario and the calculations on a daily time step contain some uncertainties. Because of this, results in Fig. 6.11 should not been interpreted on a grid cell level, but for larger regions in Baden-Württemberg. This leads to the following statements:

- Lower values for the low flow situations in summer are expected in the future especially in the regions of the Black Forest and the northeastern part of Baden-Württemberg (Kocher/Jagst region). Considerable decreases of low flow discharge are to be expected here. In other parts of Baden-Württemberg the expected change of low flow is not significant.
- Floods will especially increase in the regions of the upper Danube and the upper Neckar. Here a decisive increase of floods is to be expected. Smaller increases are to be expected for adjoining areas to the north and the south. Relatively moderate changes are predicted for the eastern part of the federal state (region Bodensee/Alb and Kocher/Jagst-catchments).

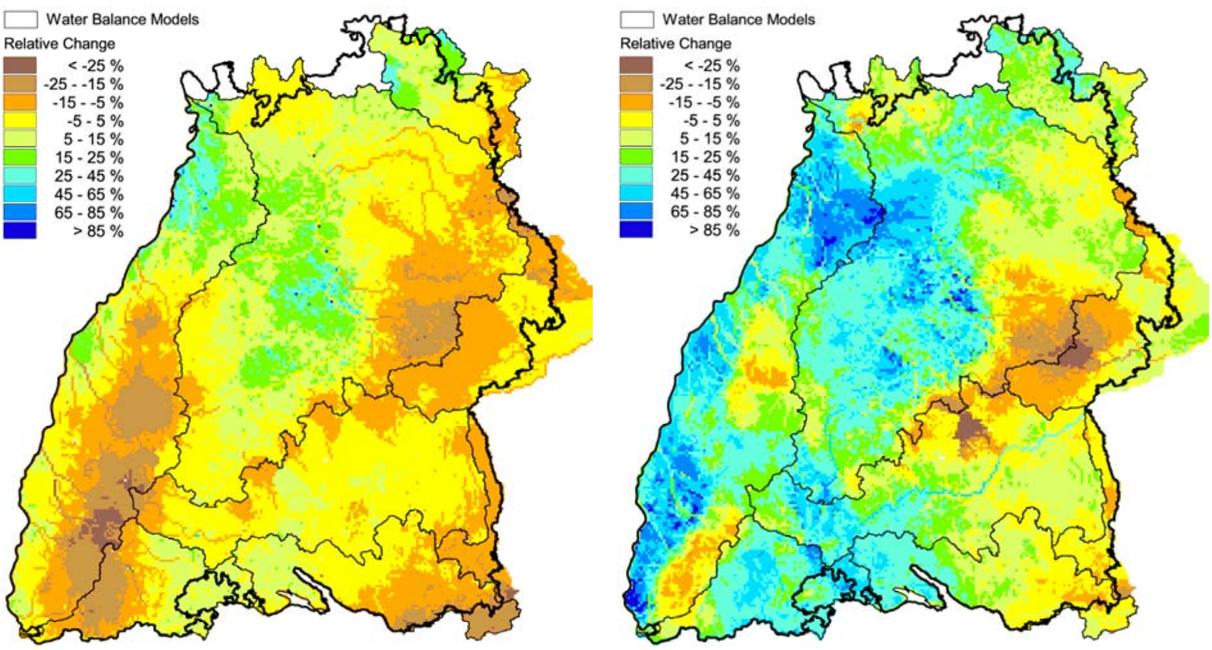

Fig. 6.11 Relative change of the mean monthly low flow in the summer half year (left) **and of the mean monthly floods in the calendar year** (right) **at the model elements** (ratio future climate scenario to current climate scenario) (LfU 2005)

The results show a regionally differentiated increase in floods. This corresponds well with the trend analysis of long time series of historic hydrometeorological measurements in Baden-Württemberg (KLIWA 2004).

The mean and also the extreme floods are expected to increase significantly, although the results are to a certain extent still preliminary. The evaluations of the impact of the climate change on the water balance provided reasons to modify the method previously used to determine design runoff and, as a result of the climate change, to consider a "design assumption climate change" ("Lastfall Klimaänderung", LFU 2005). Increased design runoff has to be taken as the basis for the load case climate change. This is carried out with a supplement ("climate change factor") to the currently valid design value (e.g. HQ_{100}). As the results of the water balance models showed regionally differentiated increases in floods, the climate change factors for the runoffs differ between regions.

This adaptation strategy has been developed as precaution by the water authorities of Baden-Württemberg for the field of flood protection to take into consideration the possible development for the next decades and also the uncertainties. An adaptation of this procedure is included in this design assumption for the case of future improvements of relevant predictions. With the progress of worldwide climate research and improving modelling instruments, the findings to date will inevitably have to be developed further.

6.2 Analysis of runoff for the Baltic Sea catchment

This application aspect has been included here to provide additional information on the origins of LARSIM from the BALTEX research project, which covers the catchment of the Baltic Sea and additionally the Elbe river. The project was carried out by Ludwig Consultant Engineers as a partner of the Max-Plank Institute for Meteorology in Hamburg, Germany (BREMICKER et al. 1997; BREMICKER 1998).

6.2.1 Introduction to the BALTEX application

The major hydrologic task of the Baltic Sea Experiment (BALTEX) was to simulate the water and energy cycle of the Baltic Sea catchment (about 2 Mio. km^2) and to identify relevant hydrologic processes of importance.

In the project BALTIMOS (development and validation of a integrated model system in the Baltic region), which was funded by the German research authorities, a fully integrated model system for the Baltic Sea region was developed (Fig. 6.12). This was done by linking the existing model components REMO for the atmosphere (JACOB 2001), BSIOM for the ocean and the sea ice (LEHMANN 1995) and LARSIM for the hydrology (RICHTER AND EBEL 2003).

In addition, a comprehensive validation of the integrated model for the Baltic Sea and its catchment area has been performed using data from a period of about two decades to show reliable estimates of the water and energy budgets for the Baltic Sea area for present climatic conditions (RICHTER et al. 2004).

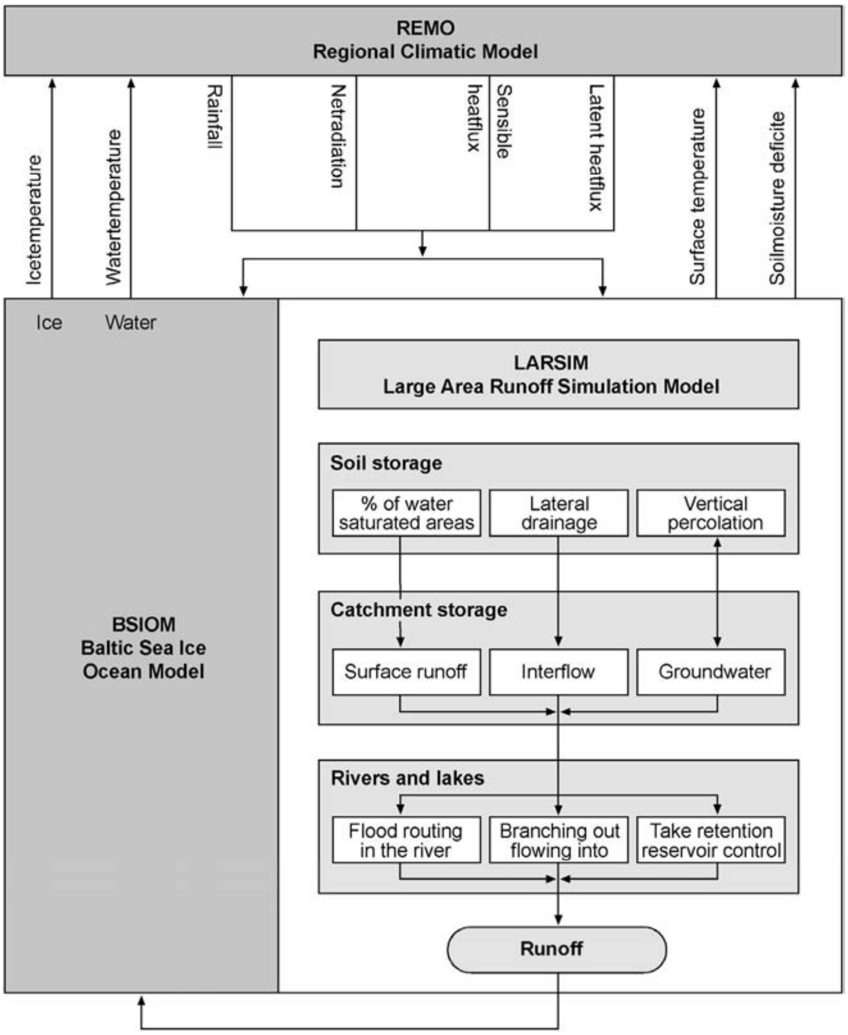

Fig. 6.12 Integrated atmosphere-hydrology-ocean model BALTIMOS

Climate modelling systems have been improved with regard to the hydrological cycle during the last years. Overviews are given by PITMAN et al. (1993), HENDERSON-SELLERS et al. (1995) and VITERBO (1996). A better understanding of the components of the hydrological cycle and the interaction between atmosphere, biosphere and the land phase of the water is described in the SVATS-models (Soil Vegetation Atmospheric Transfer Schemes) (DICKENSON et al. 1986, WIGMOSTA et al. 1994).

An improved hydrological model for describing the infiltration and runoff generation was implemented into the climatic model ECHAM/REMO (DKRZ 1994) by DÜMENIL AND TODINI (1992), see Section 2.1 and 2.2 .

The differentiation of rainfall as infiltration and surface runoff has been coupled to an orographic factor. The climate predicted by REMO at this time included two parameterisations for a short term and a long-term prediction, which was not efficient enough to describe the hydrological cycle on a regional scale. Therefore, REMO has been coupled directly to the water balance model LARSIM to form an integrated model (IM). LARSIM has been developed during the first phase of BALTEX with respect to the climatic model REMO/ECHAM.

The model area of the atmospheric model covers a region between 0 and 30 degrees east and 45 to 75 degrees north with a horizontal grid mesh size of 1/6 degree. The hydrological model area with a catchment area of approximately 1 750 000 km² and the river routing scheme using an identical grid size is shown in Fig. 6.13.

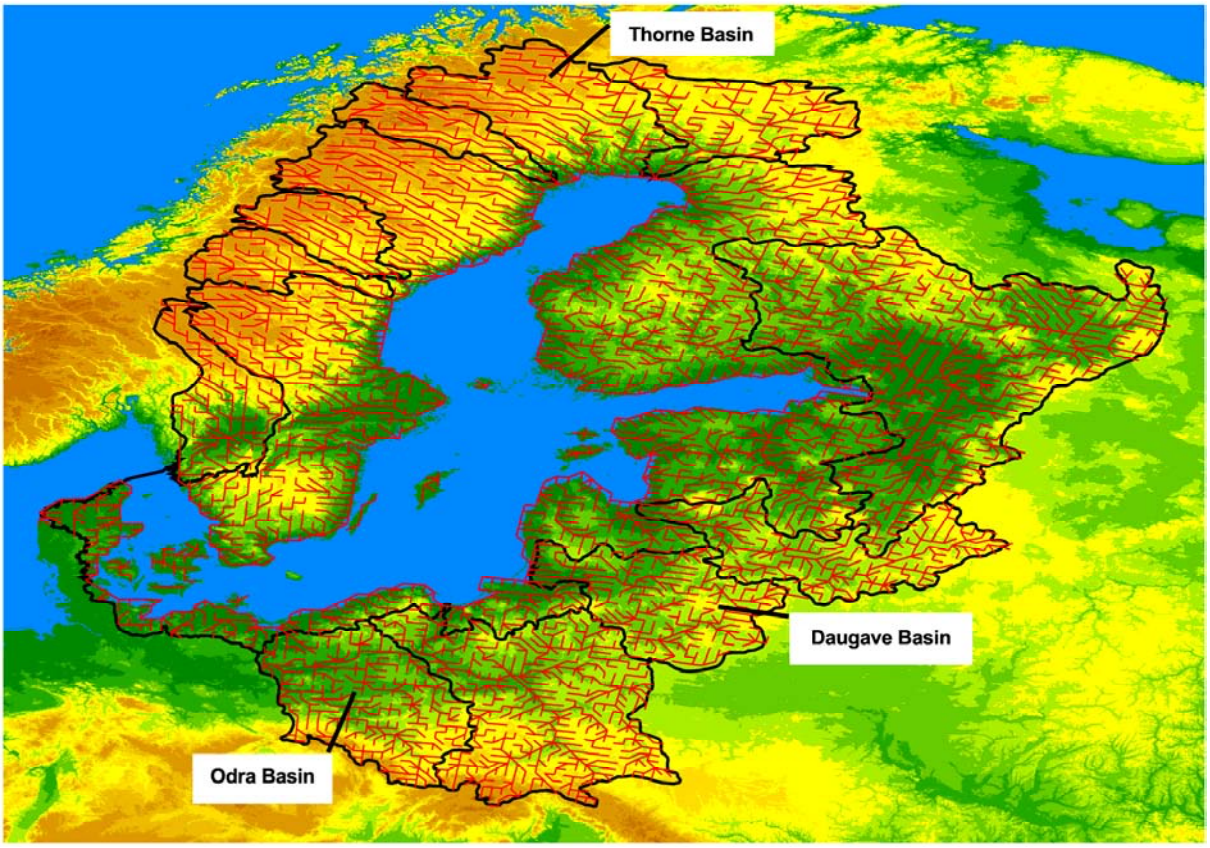

Fig. 6.13 Baltic basin area and river routing scheme of BALTIMOS

Data, which are used to derive the model channel network, are available on a global scale. To calculate the channel length the Digital Chart of the World (DCW 1992) has been used. To evaluate the channel slope, the USGS elevation data base (USGS 1993, 1-km resolution) has been used.

The experiment was carried out in 4 steps:

(1) Calibration and validation of LARSIM as a hydrologic model, covering the whole BALTEX land area and river network.

(2) Estimation of the river runoff from the entire Baltic Sea basin using measured climatic data as an essential additional information for oceanographic models.

(3) Parameterisation of REMO for the hydrological model LARSIM and improved modelling of the terrestrial water regime in a high-resolution atmosphere-hydrological-ocean model.

(4) Determination of the freshwater influence to the entire Baltic Sea basin based on calculated climatic data for a 20-year period within the integrated atmospheric-hydrology-ocean-model for a three-year period.

The calibration and validation (step 1 and 2) were done with measured meteorological input for LARSIM. The results are described in detail in RICHTER AND EBEL (2006). The major result is that the hydrological model LARSIM is able to describe the hydrological processes of the different regions of the Baltic basin and their different hydrological characteristics well. Based on the parameter evaluation of these three representative basins, the model parameters were used for the comparable regions of the entire Baltic basin (step 3). The efforts of calculation runoff with an integrated model (IM) and a non-integrated model system (NIM) are described in Section 6.2.2 (step 4).

6.2.2 Validation of the integrated and non-integrated model

Runoff has been calculated with the integrated (IM) and non-integrated (NIM) model system and subsequently compared to measurements. Using the integrated model should lead to a better understanding of hydrological processes within atmospheric models and improve overall results.

When the calculations were performed with the non-integrated model, the two runoff components of REMO were routed using the LARSIM routing scheme off-line. When using the integrated model, the three model components (atmosphere, hydrology and the ocean model) were joined in a single program to be run together.

In Figure 6.14 the mean monthly runoff for the representative basins Thorne, Daugava and Odra for the period from 1999 to 2001 (for the Daugava only up to 2000) calculated with both model systems has been compared with measurements.

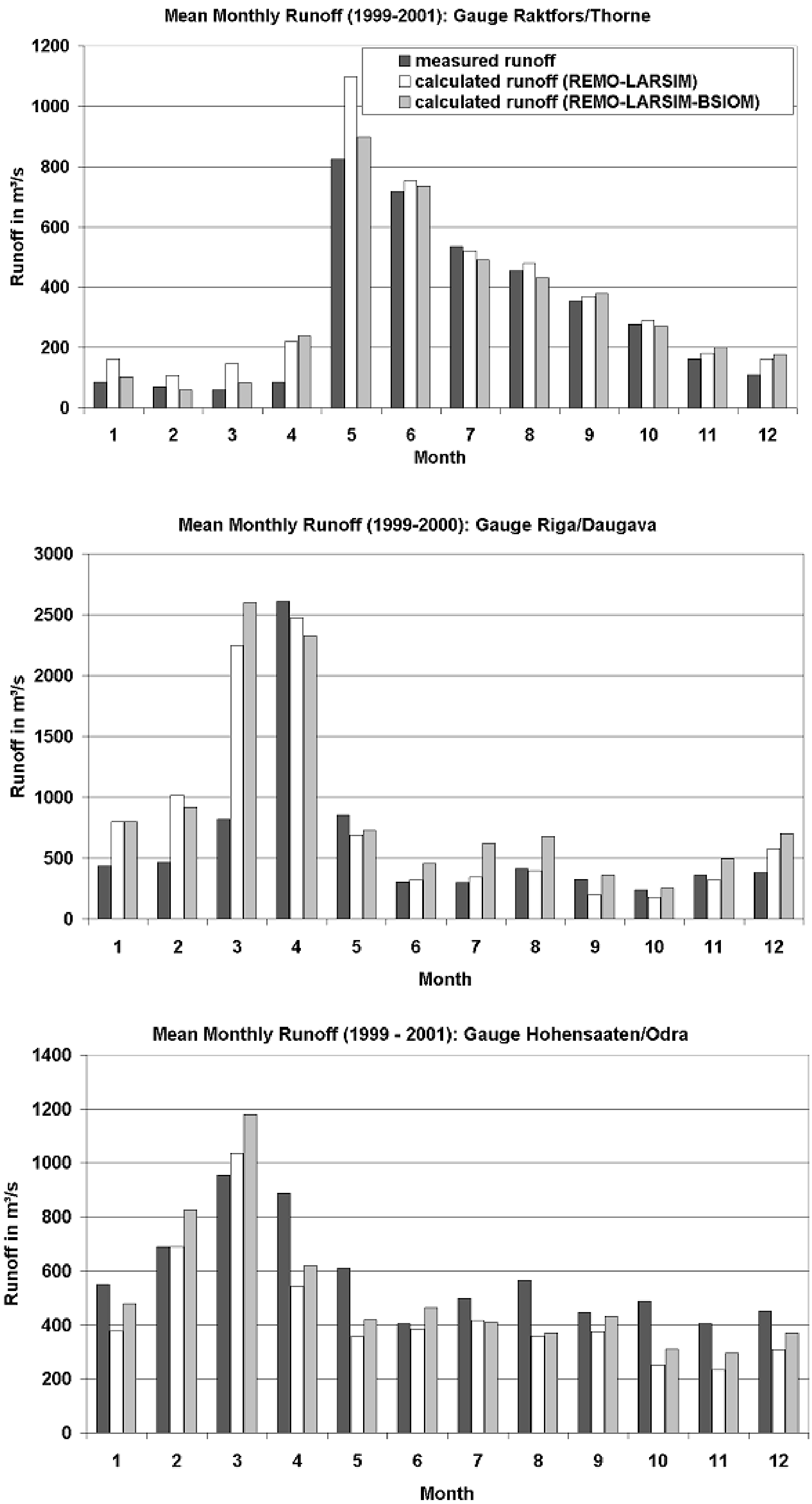

Fig. 6.14 Mean monthly (measured and simulated) **runoff for the integrated and non-integrated model for the three representative basins**

For the gauge Raktfors/Thorne, an overestimation of runoff during January to March and in May using the non-integrated model can be largely reduced with the integrated model. Between June and November there is a good agreement between the mean monthly measured and calculated runoff values with both IM and NIM model runs.

The yearly variation of the mean measured and calculated monthly values is low in both simulations. The mean monthly simulated runoff values are about 10% higher than the measured values.

For the gauge Riga/Daugava runoff values from both simulations are overestimated significantly throughout the months of January to March. During the rest of the year, the runoff measurements and calculated runoff values with both systems are very similar.

During the winter and spring periods, there are small differences between the IM and NIM mean monthly runoff simulation values. In summer, mean monthly runoff simulation values with the IM are higher than those of the NIM, caused by more interaction of the atmosphere and the ground during weather situations which are dominated by ground-heating (convective weather situations).

For Hohensaaten/Odra, the calculated runoff values of both model runs are close to the measured ones for the entire year, with an underestimation for both simulation methods in January and from April through December. For February and March, a slight overestimation of the mean monthly simulated runoff can be seen.

The results for the total measured and calculated mean monthly runoff are shown in Fig. 6.15. Runoff generally is overestimated during winter, with a maximum in March (IM) and April (NIM), and underestimated during summer.

The effect of using the integrated model versus the non-integrated model to simulate runoff is rather small throughout most months of the year, with an exception in spring. There is a delay of one month in the runoff peak for the non-integrated model in spring, which is caused by different interactive processes during the melting period. These are analysed in detail by JACOB AND LORENZ (2006).

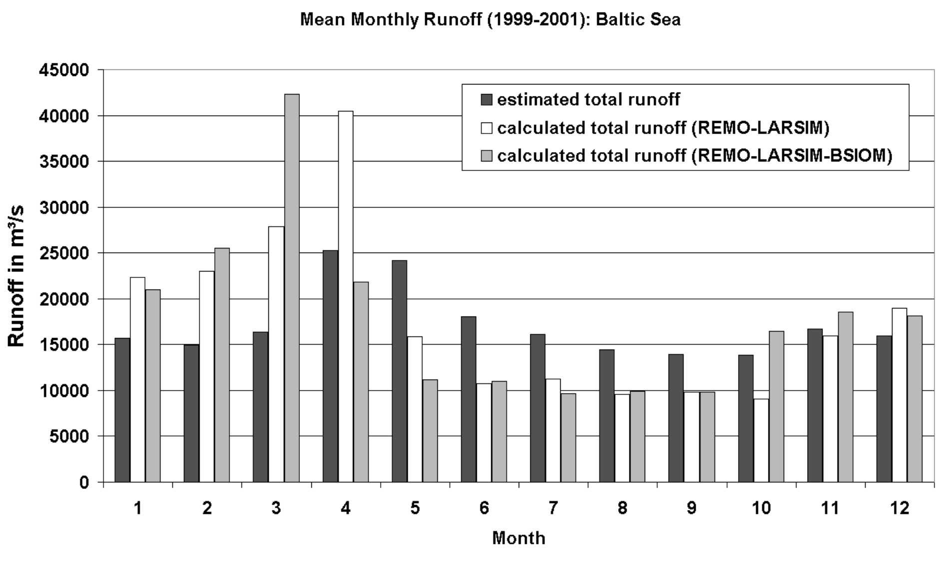

Fig. 6.15 Mean monthly (measured and simulated) **total runoff for the integrated and non-integrated model**

6.2.3 Conclusions and outlook for the BALTIMOS system

The integrated BALTIMOS system has been validated in detail. The model validation shows that LARSIM is able to describe the hydrological processes of the different regions of the Baltic Sea basin and their different hydrological characteristics.

By using the meteorological output of REMO as input for the hydrological model LARSIM the calculated runoff can be used as an integrating indicator for the influence of REMO meteorological data for runoff, without comparing simulated meteorological parameters to measured meteorological parameters in detail. The results show an overestimation of runoff from 10 to 15% over a long-term period (1980 to 2000), caused by an overestimation of precipitation within REMO.

Comparison of the results of the integrated BALTIMOS model system and the non-integrated model for a three-year period show only small differences between mean monthly runoff values with the exception of spring. There is a delay of one month in the runoff peak for the non-integrated model in spring caused by different interactive processes during the melting period.

Looking ahead, it is expected that rainfall simulation will be improved within the atmospheric model. This is a prerequisite for improved results in runoff simulation within integrated models.

6.3 Effects of conservation tillage on storm flow

6.3.1 Introduction

At present, there is a vivid discussion whether carefully directed land-use changes may help to mitigate flood discharges. In particular, it is frequently stated that changing agricultural practice from conventional to conservation tillage may decrease flood discharges in watersheds of variable size.

Conventional tillage involves mouldboard ploughing and harrowing, while conservation tillage is characterized by less soil disturbance, reduced penetration depth without topsoil inversion and higher soil coverage with mulch residues and intercrops (TEBRÜGGE AND DÜRING 1999).

Most small-scale field experiments show, that the infiltration capacity of loess soils is increased by conservation tillage, which is mainly attributed to an increased vertical connectivity of macro pores (GERLINGER 1997, HANGEN et al. 2002).

There is also some experimental evidence that the soil's total water storage capacity may be increased because of less compaction and the additional connection to deeper soil layers (BUCZKO et al. 2003). Moreover, mulch residues and intercrops increase interception losses and evapotranspiration on conservation tillage sites.

Based on this, it has often been concluded that conservation tillage leads to a reduction of infiltration-excess overland flow and consequently to reduced flood discharges in watersheds of variable size (for a discussion see: NIEHOFF 2001).

However, it is difficult to upscale field experiments and predict the effects of tillage conversion on the watershed-scale, because the commonly used conceptual hydrological models cannot be directly parameterised by experimental results (e.g. BRONSTERT 2000).

The primary goal of the case study was to elucidate the effects of tillage conversion on flood discharge for the river Glems, using LARSIM with its enhanced soil water model described in Section 3.3.2. The major results presented below have previously been published by HAAG et al. (2006b).

6.3.2 Modelling approach

LARSIM allows discerning different land-use classes (i.e. fields with conventional and conservation tillage) on a high spatial resolution. The enhanced soil model implementing an infiltration module which allows to explicitly account for the formation of infiltration-excess overland flow (see Section 3.3.2) was used to run tillage scenarios for the agricultural meso-scale watershed of the river Glems in southwest Germany. The model results help to show the influence of tillage conversion on flood discharge in the watershed-scale (HAAG et al. 2006b).

The river Glems drains a catchment area of 195 km^2 near the city of Stuttgart in southwest Germany (Fig. 6.16). The northern part of the densely populated watershed is under intense agricultural use. The soils in this area are dominated by silty Luvisols above loess. At present, 37% of the catchment area (72 km^2) is under tillage. All fields are conventionally managed by mouldboard ploughing and harrowing.

Average air temperatures range between -2°C in January and 16°C in July. The long-term average precipitation is about 750 mm per year. Precipitation is mostly produced by large-scale advective events. Consequently, most floods are caused by long lasting advective rain events (including rain on snow). However, thunderstorms with high rain intensities (> 25 mm/h) may occasionally cause floods during summer (LFU 2004).

Using measured hydrometeorological data as input variables, the model was calibrated using measured discharge at the stream gauge of Talhausen for the years 1997 to 2000. The model was validated for the time period 2001 to 2003. For any single year of the calibration and validation period correlation coefficients of 0.85 to 0.92 and Nash-Sutcliffe coefficients of 0.70 to 0.85 were obtained.

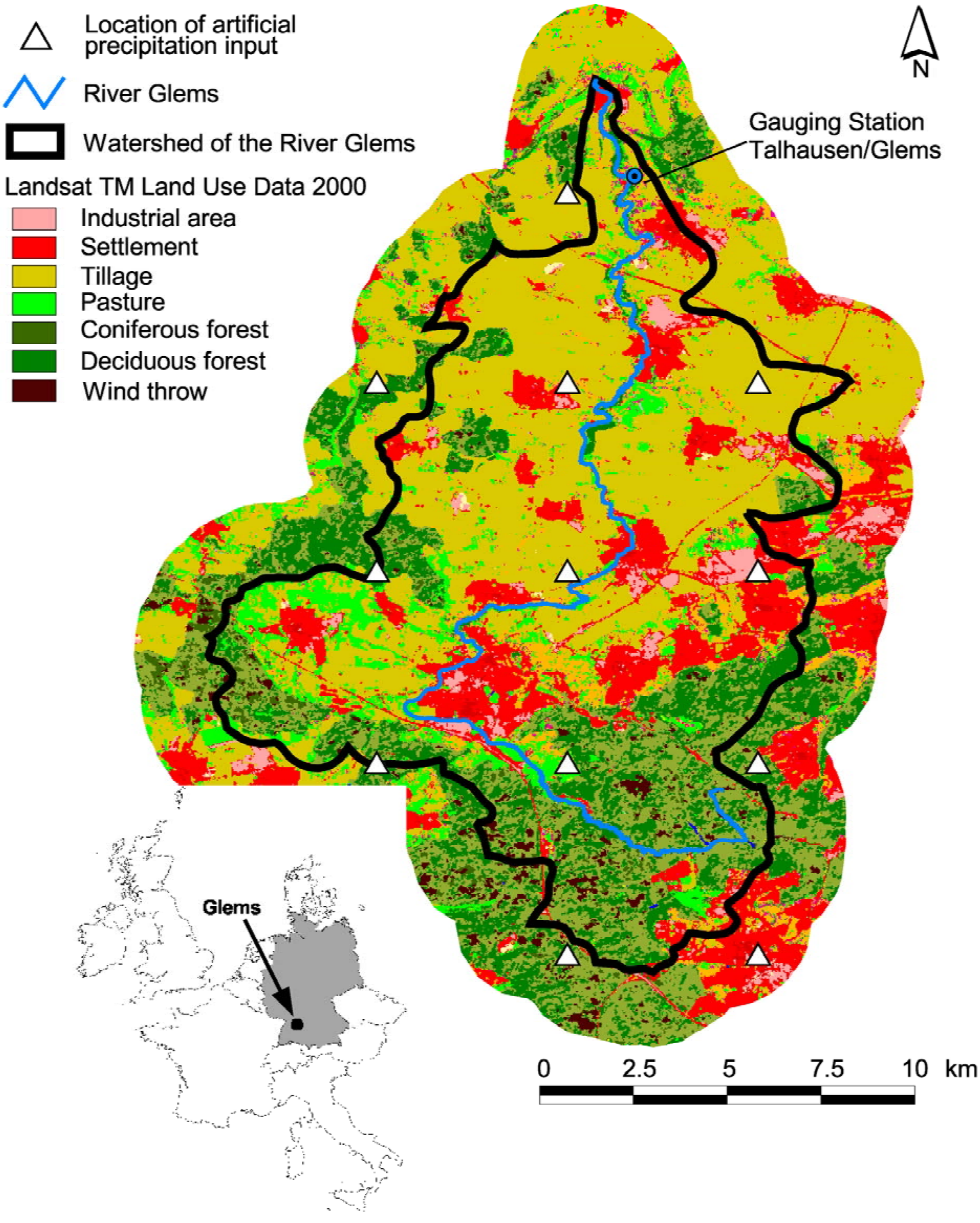

Fig. 6.16 Watershed of the river Glems: Land-use, location of the stream gauge and locations of artificial precipitation input

Measured rain data with a high temporal resolution were only available for seven years (1997 to 2003). Since the present study focuses on major floods, it was necessary to simulate a longer time period. Therefore, in addition to measured data, the model was also run using a 30-year record of artificial precipitation with a high temporal and spatial resolution (Fig. 6.16).

The artificial rain data set had been generated by BÁRDOSSY et al. (2001), applying external-drift-kriging and a simulated-annealing-algorithm (BÁRDOSSY 1998). The artificial data have proven to represent measured precipitation appropriately with respect to intensity and overall amount as well as temporal and spatial distribution and correlation (BÁRDOSSY et al. 2001).

The flood frequency analysis of the simulated 30-year hydrograph matches well with the frequency analysis of the measured long-term discharge record (data not shown). This shows that the calibrated model is also valid for extreme floods with return periods beyond 10 years.

To analyse the effect of tillage conversion, an additional land-use class for conservation tillage has been introduced and ascribed. 10, 20 and 50% of the area originally classified as conventionally tilled arable fields has been ascribed to this new class.

Since there was no further information about the likely location of the conservation tillage sites, a conversion rate of 10, 20 and 50% was assumed for each 1 km grid cell. As discussed above, the major hydrological effects of converting tillage practice from conventional to conservation are changes of the infiltration capacity, the soil water storage capacity, the interception and the evapotranspiration.

Based on the results of a literature review (GERLINGER 1997, LFU 2004), these effects were taken into account by changing land-use specific parameters of the new land-use class as follows: I_{min} and I_{max} were increased by a factor of 1.33 and W_{max} by a factor of 1.05.

Fig. 6.17 demonstrates that the effect of these changes on the modelled infiltration process are very similar to those observed in field experiments. The effects of intercrops and mulching were taken into account by adjusting the leaf area index and the albedo during the winter months, which cause increased interception capacities and evapotranspiration for the newly introduced land-use class of conservation tillage.

According to the local agricultural authorities on 10 to 20% of the farmers would be willing to change their soil management to conservation tillage. Thus, the 50% scenario is primarily used to give an indication of what would theoretically be possible. The three scenarios were driven by the assumed rainfall data described above. They can thus be evaluated by comparison with the above-mentioned long-term validation run, which assumes 0% conservation tillage.

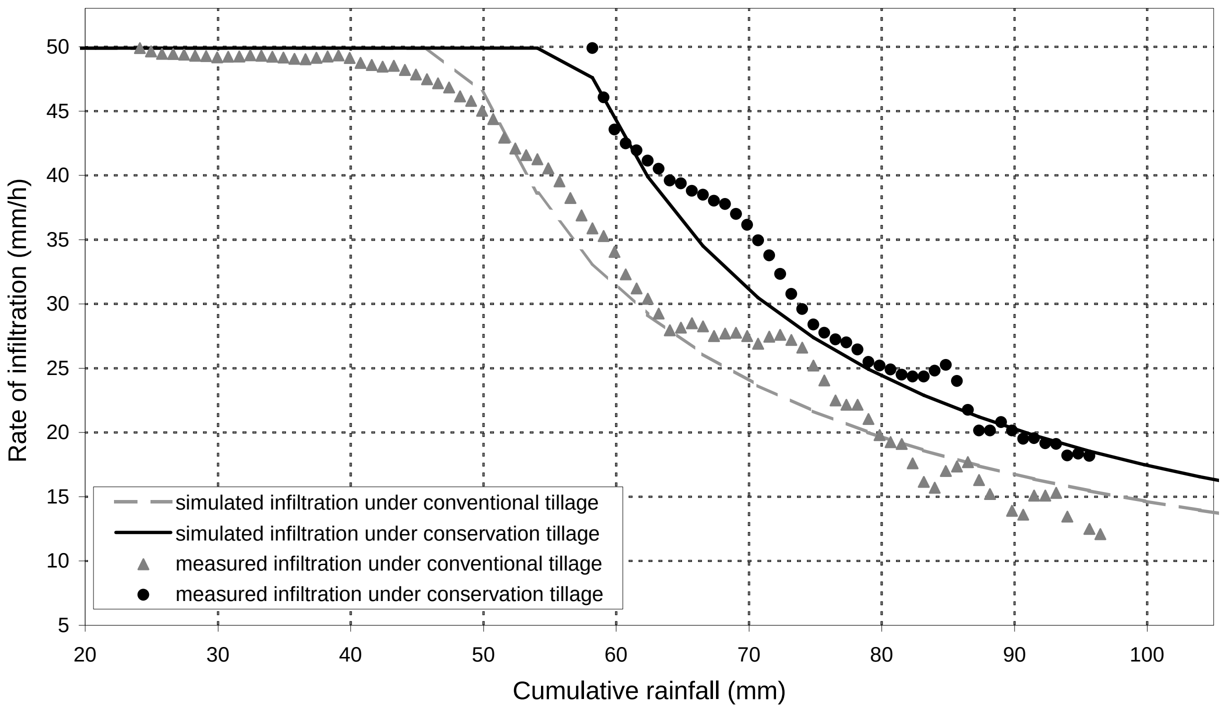

Fig. 6.17 Numerical infiltration experiments with the infiltration module for a model soil under conventional and conservation tillage in comparison to experimental results from GERLINGER (1997)

6.3.3 Results of tillage conversion scenarios

Analysing the simulated effects of conservation tillage showed that generally only events that are produced by intensive rainfall (at least ~ 25 mm/h) exhibit a visible reduction of peak discharge due to tillage conversion.

Such an event is shown in Fig. 6.18(a) for the 0% and the 50% scenario. On the other hand, floods caused by long-lasting advective precipitation, are not decisively influenced by tillage practice, as shown in Fig. 6.18(b).

To further assess these qualitative results, the simulated reduction of peak discharges of the largest yearly floods of the 30-year period, which result from changing the soil management from conventional to conservation tillage on 50% of all arable land were analysed. The frequency distribution of the resulting relative changes is shown in Fig. 6.19.

For 21 out of 30 events, discharge peaks are reduced by less than 1.5%. For the flood exemplified in Fig. 6.18(a), the discharge peak is reduced by 7.9%. The remaining eight events show peak discharge reductions between 20 and 6.5% (Fig. 6.19). As could be expected, the 10 and 20% scenarios show the same pattern with a generally smaller reduction of peak discharges (data not shown).

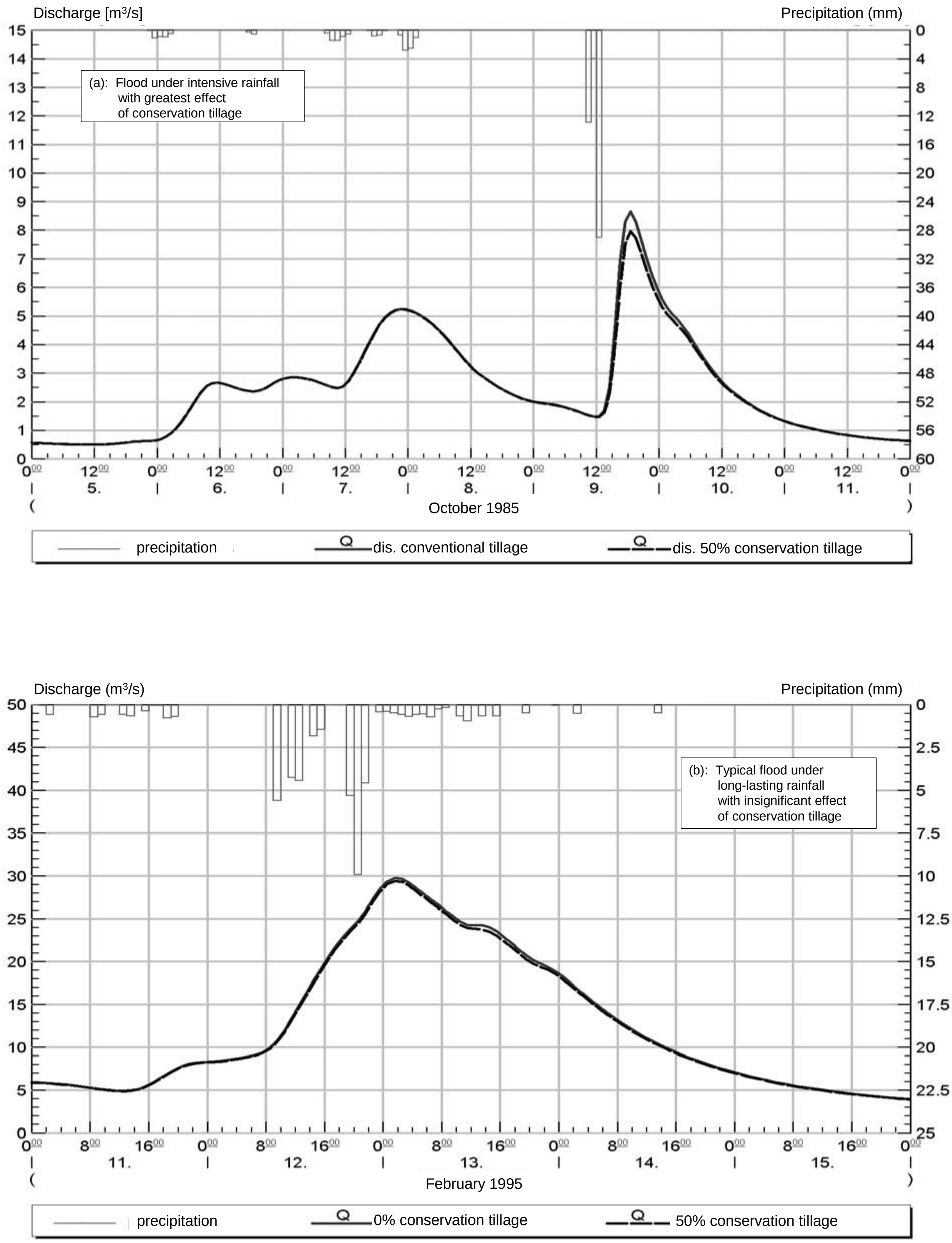

Fig. 6.18 Results of scenarios for the present tillage practice (0% conservation tillage) **and for assuming conservation tillage on 50% of all arable land**

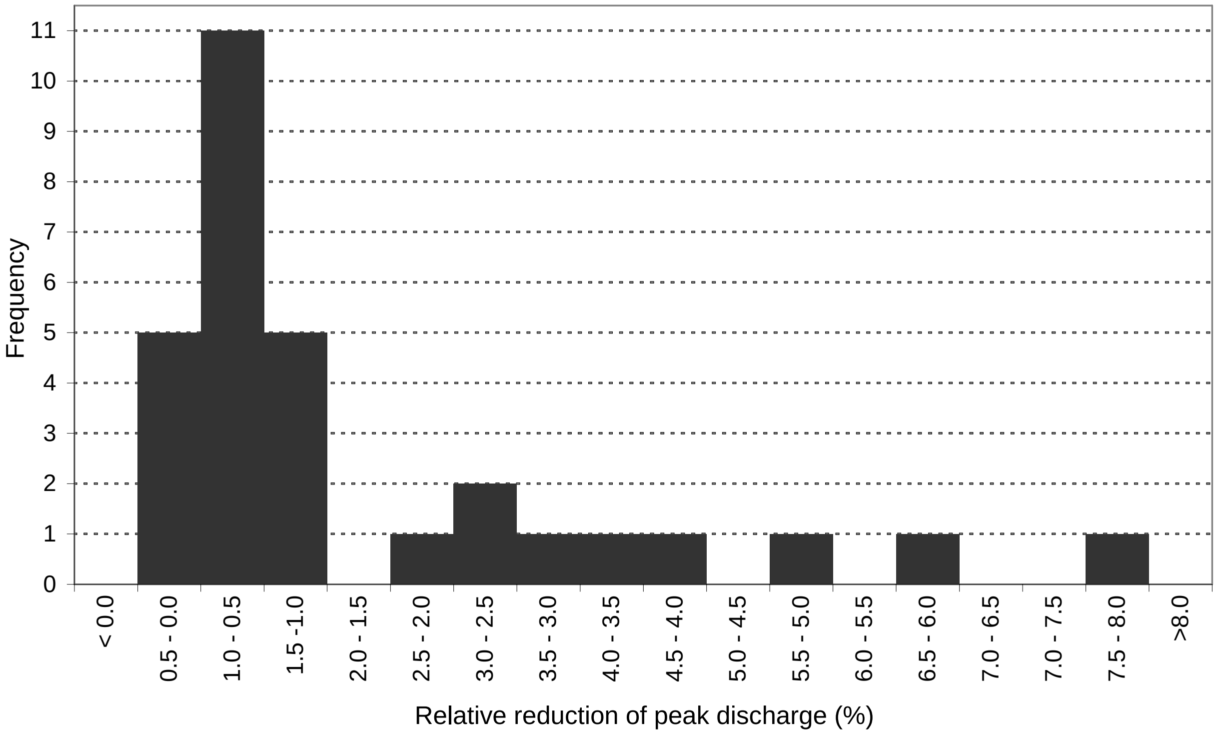

Fig. 6.19 Frequency distribution of the relative reductions of peak discharges of yearly floods, as caused by changing soil management from 0% to 50% conservation tillage within the watershed of the river Glems

Finally, a flood frequency analysis has been made, using the largest flood peaks simulated for each year. For this analysis the Log-Gumbel distribution was chosen out of 14 statistical distributions, because it fitted the data best. The results of the frequency analysis are summarized in Table 6.4.

In general, there is a slight reduction of peak discharge for all return periods, when changing agricultural practice to conservation tillage.

However, the resulting reduction is less than 1%, when assuming that 10 or 20% of all fields are under conservation tillage. Even with an unrealistically high proportion of 50% of conservation tillage, the resulting reduction of flood discharges with return periods between 2 and 100 years would be less than 2%.

Tab. 6.4 Calculated peak discharges of various return periods for assuming 0, 10, 20 and 50% conservation tillage on all arable land, and relative changes as compared to the 0% scenario

Return period (years)	Peak discharge						
	0%-scenario (m3/s)	10%-scenario (m^3/s)	10%-scenario (Δ%)	20%-scenario (m^3/s)	20%-scenario (Δ%)	50%-scenario (m^3/s)	50%-scenario (Δ%)
2	10.12	10.09	-0.3	10.06	-0.6	9.98	-1.4
5	14.89	14.84	-0.3	14.80	-0.6	14.66	-1.5
10	19.23	19.16	-0.4	19.10	-0.7	18.92	-1.6
20	24.58	24.48	-0.4	24.39	-0.8	24.16	-1.7
50	33.76	33.61	-0.4	33.49	-0.8	33.16	-1.8
100	42.82	42.62	-0.5	42.46	-0.8	42.03	-1.8

6.3.4 Discussion and conclusions for tillage conversion scenarios

The characteristics of the precipitation event producing a particular flood are of outstanding importance for the flood mitigating effect of conservation tillage within the 195 km^2 large watershed of the river Glems.

For floods caused by long lasting (advective) rain events with moderate intensities (less than ~ 25 mm/h) fast subsurface runoff processes are the main cause of flood formation, whereas infiltration-excess overland flow on tilled sites is of little importance. Consequently, for this majority of flood events, increasing infiltration capacity by conservation tillage has very little effect on peak discharge.

On the other hand, for a minority of floods, which are caused by very intensive rain events (i.e. thunderstorms), infiltration-excess overland flow on tilled sites plays an appreciable role in flood formation. In these cases, the effect of increasing infiltration capacity by tillage conversion decreases infiltration-excess overland flow and consequently leads to a visible reduction of peak discharge. Using a different model and measured precipitation data, NIEHOFF et al. (2002) obtained similar results for another meso-scale watershed in Germany.

Since the clear majority of major floods at the stream gauge of the river Glems are caused by advective rain events, the resulting flood frequency distribution is barely affected by tillage practice. Even under the extremely optimistic assumption that soil management on 50% of the arable land (i.e. 19% of the watershed area) is changed to conservation tillage, peak discharges with return periods between 2 and 100 years would only be reduced by less than 2%.

For similar climatological conditions, convective rain events and infiltration-excess tend to be more important for flood formation within very small watersheds (BRONSTERT 2000). Hence, tillage conversion is likely to have an overall appreciable flood mitigating effect in such small (about 10 km^2), loess covered, agricultural watersheds.

However, as demonstrated in the study described here and in that of NIEHOFF et al. (2002), the flood mitigating effect of tillage conversion diminishes in the meso-scale (~ 100 km^2).

For large river systems (~ 10 000 km^2 and more) very intensive, convective rain events and infiltration-excess are usually of very little importance for flood formation (BRONSTERT 2000). Consequently, most likely there is no appreciable flood mitigating effect of conservation tillage at the macro-scale.

6.4 Operational LARSIM application in the Flood Forecast Centre of Baden-Württemberg

6.4.1 Model configuration

LARSIM is used in the Flood Forecast Centre of Baden-Württemberg (HVZ) in a daily and automated mode for about 90 gauges for which discharge forecasts are calculated. For this, the water balance models which exist for the whole area of the federal state (see Section 6.1) have been changed to hourly calculation time intervals and have been re-calibrated to allow a more precise simulation of flood discharges. The structure of the models with grid cell sizes of 1x1 km and 16 land use classes has not been changed.

These operational water balance models comprise 7 larger catchment areas and some smaller catchments (see Fig. 6.1). The water temperature for 17 gauges is forecasted additionally for the Neckar catchment. In the operational routine the models produce fully automated new forecasts of discharge and water levels once a day, which are published routinely on the internet.

After the automatic start of the forecast procedure, a simulation for a time period of at least 2 days before the time of the forecast is made using measured data of water level, discharge, precipitation, air temperature, global radiation, wind speed, air moisture and air pressure.

These operationally collected data are derived from the discharge and air measurement network of the federal state of Baden-Württemberg, the ombrometer network, which is served jointly by the federal state and the German Weather Service (DWD), the “Network 2000” of the DWD and the measurement network of the Meteomedia company.

For the subsequent time period of seven days, discharges are forecasted using results of numeric weather forecasts. Until the third forecast day the LME-model (local-model Europe) is used as input of LARSIM, for the following days the GME-model data (global-model Europe) of the DWD is utilised. Alternatively forecasts from other weather services can be used or combined with the forecasts of the DWD.

Additionally a scenario is simulated in which it is assumed that no precipitation exists in the forecast time period. It is used to define the minimal possible discharge for the forecast time period, which is important information for low-flow management.

Routinely the forecast results are published at about 11:00 CET on the internet under www.hvz.baden-wuerttemberg.de. In case of floods, experienced staff is active in the Flood Forecast Centre. In this case, forecasts are produced every hour and the results are presented on the internet more frequently.

The reliability of the forecasted discharges and water levels decreases (depending on the used weather forecasts) with increasing forecast time. Forecasts for smaller catchments (approx. less than 500 km^2) contain additional uncertainties, because the weather models only forecast small-scale precipitation structures approximately.

Therefore the published future discharges and water levels are separated in a time period with reliable values (“forecast”) and in a time period with less reliable forecast values (“estimation”, see Fig. 6.20). The length of the “forecast” time period depends on the discharge state and the catchment size of the gauge.

During floods the “forecast” time period is between 4 and 24 hours depending on catchment size. In low-flow situations the “forecast” time period is up to 120 hours. In the flood case, the No-Rain-Scenario is not calculated and the total forecast time period is shortened (Fig. 6. 21).

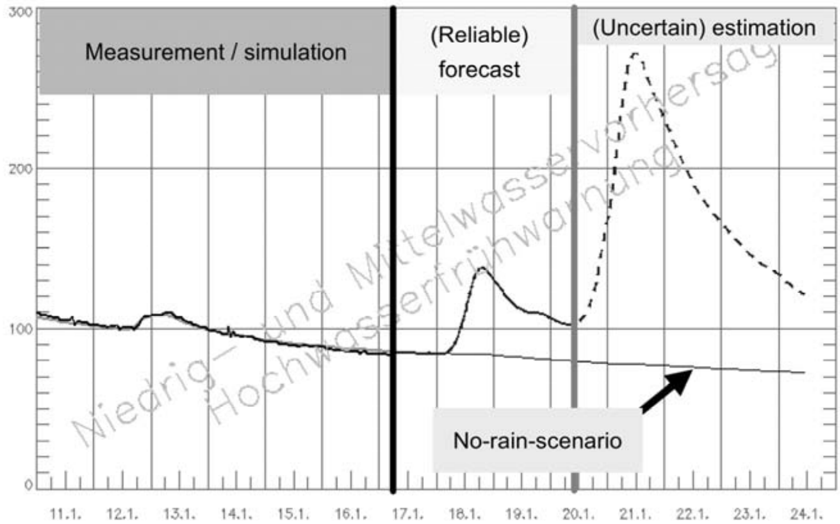

Fig. 6.20 Example of a water level forecast in the routine forecast mode (gauge Schwaibach/Kinzig)

Fig. 6.21 Example for a water level forecast in the flood forecast model (gauge Gundelsheim/Neckar)

6.4.2 Flood forecast and early warning

The operational water balance models are both used for a gauge-oriented flood forecast and early warning.

Intention of the *early flood warning* is to give information at an early stage (several days before a flood) to the water resources authorities, the emergency management authorities and the interested public. Because of the long forecast time period and the uncertainties of the precipitation forecast, the early warning is only an estimation of a probably imminent flood, but it is very likely, that forecasted peak flood values have an uncertainty of some decimetres.

On the other hand, the *flood forecast* should give information shortly before and during a flood situation, which is as exact as possible. In the following table 6.5, the essential differences between early flood warning and flood forecast are summarized.

Tab. 6.5 Properties of early flood warning and flood forecast

	Early flood warning	**Flood forecast**
Publication times	All year, in case of low or mean flow	During a flood situation
Publication time intervals	Once a day	Hourly
Forecast time period	Up to 7 days	4 to 24 hours
Desired quality	Order of size of potential water level increases (e.g. +/- 50 cm)	+/- 10 cm
Possible use	Early planning before a possible flood	Execution of short-term flood relief actions

As Fig. 6.22 shows on the example of the flood from January 2005 for the gauge Stein (Kocher), the operational water balance models can forecast floods in many situations already some days before their occurrence with approximate data of flood peaks or time points.

Stable and therefore reliable early flood warnings are characterized by relatively small changes in the forecasted flood values in different forecasts on different days. Such stable early warnings are mainly possible in case of large-scale precipitation events.

Early flood warnings based on small-scale (convective) precipitation forecasts mostly show great uncertainties in time, peak value, as well as the location of the flood. In these cases, subsequent precipitation forecasts can lead to very deviating flood forecasts especially for smaller catchment areas. In such cases, a useful gauge-oriented early flood warning is not possible at this time.

Recent experiences show, that the operationally produced early flood warnings give relatively useful information for catchments larger than about 1 000 km^2 already several days before the flood (BREMICKER et al. 2006).

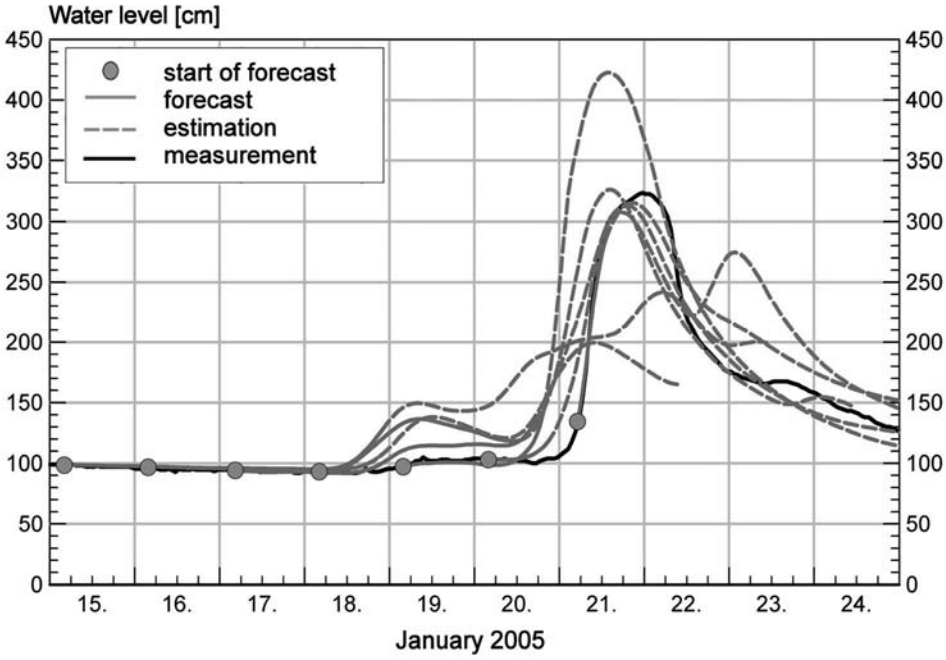

Fig. 6.22 Example for early flood warning for the gauge Stein/Kocher (1 930 km^2)

The early flood warnings thus provide an extended time period of preparation before a flood, which can be used by communities, emergency management and industry to support decisions in situations in which relevant actions are (not yet) urgent or imminent. Examples therefore are:

- early planning of personnel needed for flood defence,
- adaptation of construction sites in the potential flood area,
- removal of goods stored in potential flood areas,
- early removal of sensible or expensive materials from cellars (basements) or lower terrain,
- early preparation of traffic restrictions etc.

Ultimately the potential users themselves must make the interpretation of early flood warnings, because only they can evaluate the relevant information properly with respect to their situation or interests.

During the beginning of a flood, a continuous change from early flood warning to flood forecast takes place in the operational forecast procedure, because forecasts are made more frequently while forecast time periods are shortened (LUCE et al. 2006).

For this reduced forecast time period LARSIM produces reasonable flood-forecast results for smaller catchments as well (see example in Fig. 6.23).

The floods of the last years have shown, that based on flood forecasts a significant reduction of flood damages and improved actions against the effects of floods are possible in many cases. Especially flood damages on houses and infrastructure, as well as production shortages and damages in industry, should be mentioned in this context (HOMAGK 2001).

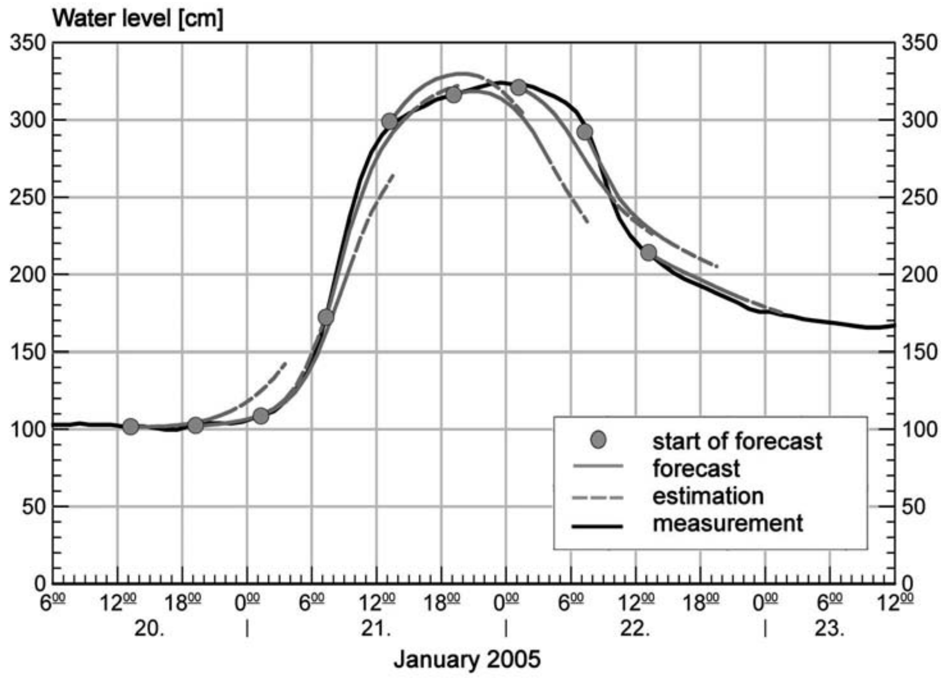

Fig. 6.23 Example for flood forecasts for the gauge Stein/Kocher (1 930 km^2)

6.4.3 Low-flow forecasts

Routine forecasts of discharge and water temperature have considerable importance for the operational low-flow management (ATV-DVWK-ARBEITSGRUPPE NIEDRIGWASSER 2003; HOMAGK 1996).

In dry periods LARSIM can in general produce reliable low flow forecasts for a forecast time period of up to 7 days. Unreliable forecasts of low-flow result especially from meteorological situations with convective cells, when interpretation of area precipitation forecasts may contain considerable errors. In such cases, the so-called worst case-low flow forecast can give information whether in the coming 7 days critical low-flow situations could be reached, assuming no precipitation for this period of time.

Fig. 6.24 shows a forecast from August 2003 for five gauges on the Neckar and the relevant discharges, which were measured later. The measured discharges are drawn as moving averages for a daily time period to suppress short-term fluctuations of anthropogenic origin.

For the three gauges Rottweil, Wendlingen und Plochingen plausible forecasts for the first four days can be produced. At the gauges downstream (Lauffen and Rockenau) the measured discharge rises on the 26.08.2003, without (like on the upper gauges) falling again, probably due to the effect of discharge regulations by weirs of the Neckar. Such artificial operations are not contained in the model, and in this case the model underestimates the actual discharges for the following days.

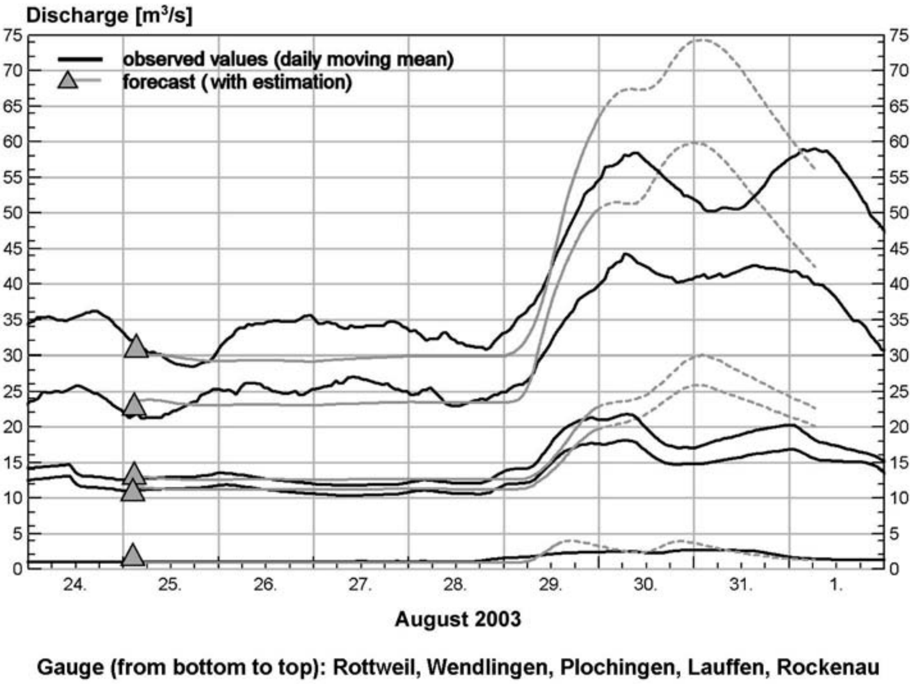

Fig. 6.24 Forecast from August 2003 for five gauges on the Neckar

The runoff increase near the end of the forecast time period as a consequence of precipitation is forecasted for the correct time by the model, but not the correct discharge values. The essential causes for this are principal insecurities of the used middle-range precipitation forecast.

Fig. 6.25 shows a forecast from October 2003 for four gauges on the Neckar tributary Kocher. Here the forecast time point lies within the recession limb of a smaller flood. The model shows, that the more rapid decrease of discharge in the beginning and later the typical recession characteristics of low-flow situations is properly simulated for all gauges.

Fig. 6.26 shows another example for a low-flow forecast for the gauge Lauffen/Neckar. In this case, predicted discharges fall below a value, at which certain water uses have to be stopped. Low-flow forecasts can be used for better planning of irrigation (irrigation before critical low-flow states), the operation of dischargers (eventually intermediate storage), the operation of reservoirs for low flow augmentation and the optimisation of the operation of multi-purpose reservoirs.

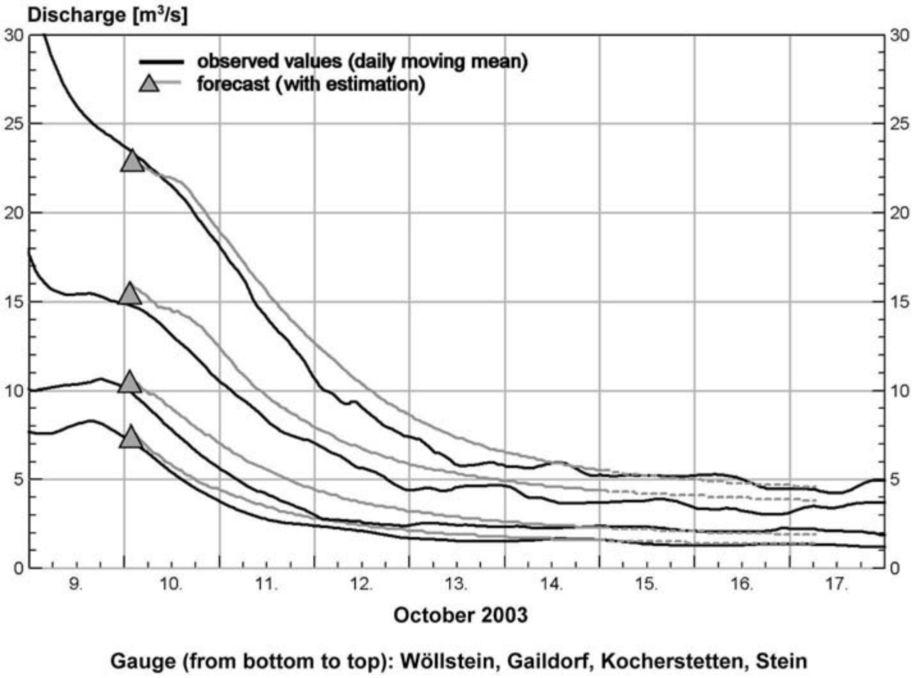

Fig. 6.25 Forecast from October 2003 for four gauges on the Neckar tributary Kocher

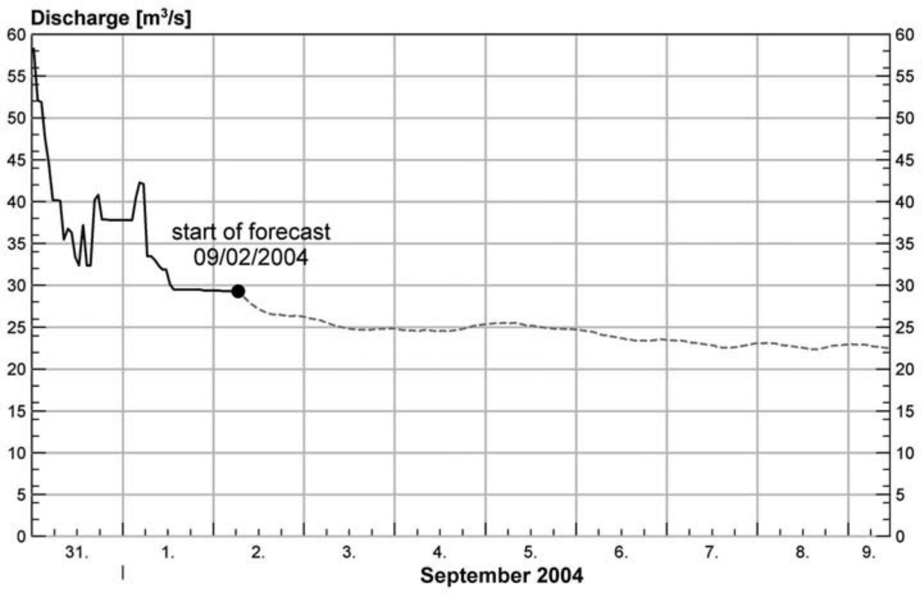

Fig. 6.26 Example of a low-flow forecast for the gauge Lauffen/Neckar

Especially in case of larger rivers, the forecasts can be used for questions of navigation and power production. The loading of ships as well as the provision of alternative means of transport can be planned in time or the operation of thermal power plants can be optimised. The most important users of low-flow forecasts are water authorities, discharger, navigation and energy producers (BREMICKER et al. 2004).

6.4.4 Forecasts of water temperature in the Neckar

Because water temperature is one of the most important water quality parameters and maximal limits for water temperatures are essential factors in the water rights for thermal power plants, operational water temperature forecasts are an important base for decisions in connection with the management of low-flow situations.

In a cooperation project of the federal state of Baden-Württemberg and the Energy Baden-Württemberg AG (EnBW) LARSIM has been extended by modules for simulation and forecast of water temperature. The resulting water-balance and water-temperature model for the Neckar is in operational use at the Flood Forecast Centre of Baden-Württemberg since July 2004.

Fig. 6.27 shows as example results of an operational forecast of water temperature from August 18th 2004 for the gauges Hofen, Gundelsheim and Rockenau on the Neckar. The example shows, that despite high start values and further rising water temperatures an essential limit of 28°C, set by water rights regulations, will not be exceeded.

Fig. 6.28 shows an example of an offline forecast test for the water temperature in the Neckar at the gauge Gundelsheim. Here two forecasts are shown, for which measured data have been used as input and compared with measured water temperature values (forecast time points 01.08.2003 and 05.08.2003). The example shows the high quality of the forecasts, although the daily amplitude is underestimated in most cases.

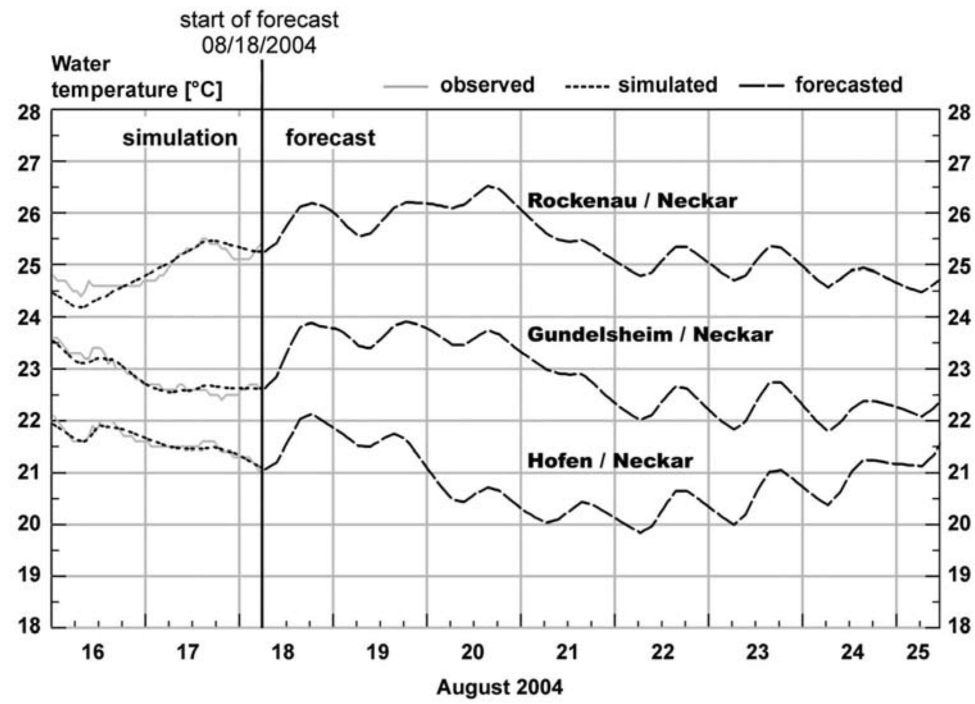

Fig. 6.27 Example of a water temperature forecast for three gauges on the Neckar river

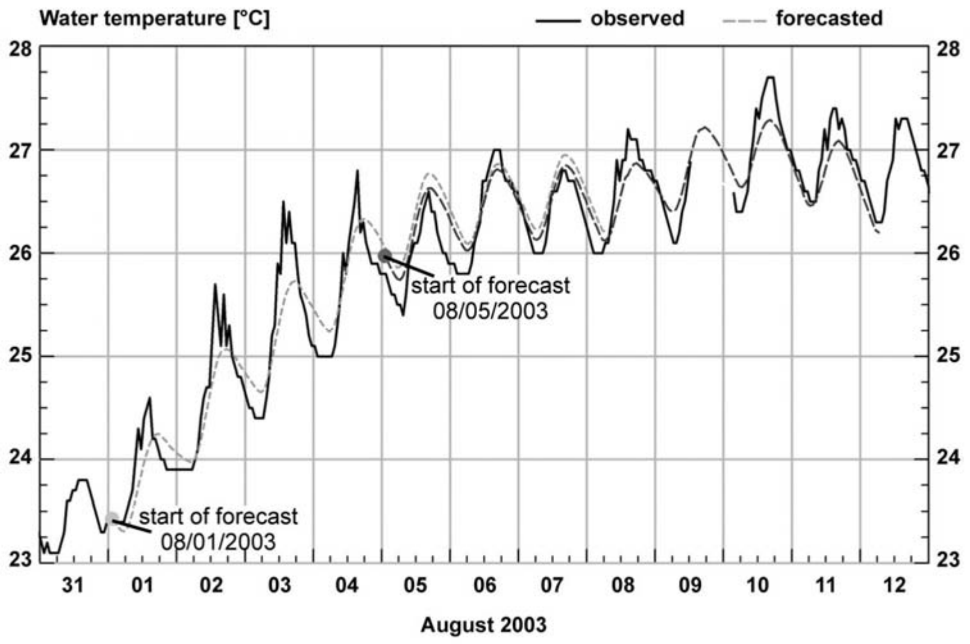

Fig. 6.28 Offline forecast test for the water temperature in the Neckar at the gauge Gundelsheim (forecast time points 01.08.2003 and 05.08.2003)

With daily seven-day forecasts of water temperatures, water authorities and energy producers are warned relatively early before critical temperature situations are reached. On the basis of this information, countermeasures can be executed in time and an optimal operation of thermal power plants can be planned (HAAG et al. 2005).

6.4.5 Description of area distribution of water balance values

The punctual values for discharge, soil water content and other components of the water cycle can be transferred into spatial data (e.g. area distribution of snow cover water content, actual soil water contents, evaporation rates, ground water recharge etc) by the operational water balance models.

This means, that the results of the following variables and their forecasts can be displayed for the whole area of the federal state after each LARSIM simulation (see Fig. 6.29):

- evapotranspiration [mm]
- soil moisture [% or mm]
- ground water recharge [mm]
- snow depth [cm] and snow water equivalent [mm]
- water yield (rain plus snowmelt) [mm]
- runoff formation in the area for groundwater, interflow and direct runoff [m^3/s or mm]

Time resolution of these values can be hours or aggregated values, the area resolution corresponds with the 1x1 km grid cell structure.

Water balance models in this respect are also interfaces to other sciences or fields of interest and can be integrated in interdisciplinary model systems by which interactions between water balance, groundwater, nutrient inflow and water quality can be simulated and forecasted.

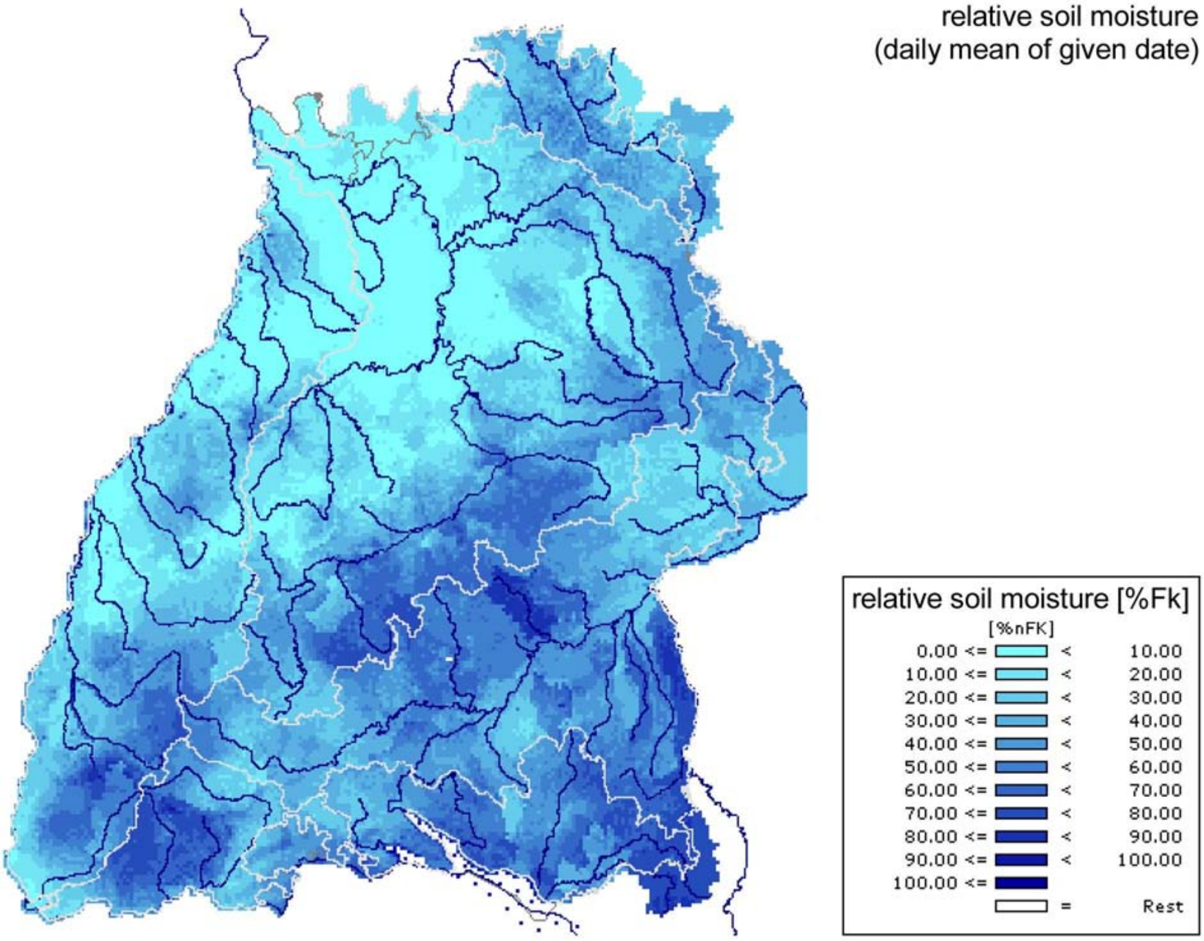

Fig. 6.29 Example of spatial distribution of operationally calculated relative soil moisture for the state of Baden-Württemberg (approx. 36 000 km²)

6.4.6 Future aspects

At this time, the operational application of the water balance model LARSIM is extended to other areas outside Baden-Württemberg. For the water authorities of Rhineland-Palatinate, Hessia, Nordrhein-Westfalen and Bavaria models for several catchments (e.g. Moselle, Lahn, Nahe, Sieg and Iller) are installed.

These models are mostly not oriented on grid-cell structures, but on small subareas (about 2 km²) with real hydrologic boundaries (see Fig. 2.1).

Current developments of LARSIM are aiming at the simulation and forecast of oxygen content of water and also at applications to long-term forecasts for different purposes.

Literature

Abdulla, F.A. (1995): Regionalization of a macroscale hydrological model. Thesis, Department of Civil Engineering, University of Washington, USA.

Aitken, A.P. (1973): Assessing systematic errors in rainfall-runoff models. Journal of Hydrology, 20, pp 121-136.

Allen, P.M., Arnold, J.G. & Byars, B.W. (1994): Downstream channel geometry for use in planning level models. Water Resources Bulletin, 30 (4), pp 663-671.

Arya, S.P. (1988): Introduction to Micrometeorology. International Geophysics Series, 42. Academic Press, San Diego, USA.

ATV (1998): ATV Gewässergütemodell – Handbuch. ATV, Hennef, Germany.

ATV-DVWK-Arbeitsgruppe Niedrigwasser (2003): Anthropogene Einflüsse auf Niedrigwasser. Wasserwirtschaft, 10, pp 32-35.

BALTEX (1994): Scientific plan for the Baltic Sea Experiment. Second Edition. GKSS Research Center, Geesthacht.

BALTEX (1995): Baltic Sea Experiment BALTEX. Initial Implementation Plan. International BALTEX Secretariat at the GKSS Research Center, Publication No. 2, Geesthacht.

Bárdossy, A. (1998): Generating precipitation time series using simulated annealing. Water Resources Research, 34, pp 1737-1744.

Bárdossy, A., Giese, H., Haller, B. & Ruf, J. (2001): Regionalisierte Niederschlagsreihen im 5-Minuten-Zeitraster für Baden-Württemberg. KA – Wasserwirtschaft, Abwasser, Abfall, 48, pp 300-308.

Bauer, Ch. (1999): Bewertung von Maßnahmen der Landnutzungsänderung und Renaturierung am Beispiel eines Mittelgebirgsgewässers mit einem Wasserhaushaltsmodell. Diplomarbeit an der Universität Kaiserslautern, Fachgebiet Wasserbau und Wasserwirtschaft (unpublished).

Baumgartner, A., Liebscher, H. (1990): Lehrbuch der Hydrologie, Band 1: Quantitative Hydrologie. Verlag Gebr. Borntraeger, Berlin – Stuttgart.

Beaty, C.B. (1975): Sublimation or melting: observations from the white mountains, California and Nevada. USA. J. of Glac., 14 (71), pp 275-286.

Becker, A. (1986): Neue Anforderungen und Lösungen bei der großflächigen hydrologischen Modellierung. Wasserwirtschaft – Wassertechnik, 7, pp 150-152.

Becker, A. (1992): Methodische Aspekte der Regionalisierung. In: DFG (1992): Regionalisierung in der Hydrologie. Mitteilung Nr. XI der Senatskommission für Wasserforschung, Deutsche Forschungsgemeinschaft, pp 16-32.

Becker, A. (1995): Problems and progress in macroscale hydrological modelling. In: Feddes, R. A. (ed.): Space and time scale variability and interdependencies in hydrological processes. Intern. Hydr. Series, Cambridge Univers. Press, pp 135-144.

Benecke, P. (1996): Versickerung und Bodenfeuchte. Kapitel 12, pp 380-415. In: Baumgartner & Liebscher (Hrsg.) 1996: Lehrbuch der Hydrologie, Band 1: Allgemeine Hydrologie – Quantitative Hydrologie. Verlag Gebr. Borntraeger, Berlin – Stuttgart, 2. Auflage.

Bicknell, B.R., Imhoff, J.C., Kittle, J.L., Donigian, A.S., Johanson, R.C., Barnwell, T.O. (1996): Hydrological Simulation Program – Fortran. User’s Manual for Release 11. U.S. EPA, Athens.

Bouten, W. (1995): Plant control on evapotranspiration: models and measurement. In: The role of water and the hydrological cycle in global change. NATO ASI Series I, Global Environmental Change, 31, pp 105-133.

Braun, L. N. (1985): Simulation of snowmelt-runoff in lowland and lower alpine regions of Switzerland. Züricher Geographische Schriften, Heft 21, Geographisches Institut der ETH Zürich.

Bremicker, M. (1998): Aufbau eines Wasserhaushaltsmodells für das Weser- und das Ostsee-Einzugsgebiet als Baustein eines Atmosphären-Hydrologie-Modells. Dissertation am Institut für Hydrologie, Albert-Ludwigs-Universität Freiburg.

Bremicker, M. (2000): Das Wasserhaushaltsmodell LARSIM – Modellgrundlagen und Anwendungsbeispiele. Freiburger Schriften zur Hydrologie, Band 11. Institut für Hydrologie, Universität Freiburg.

Bremicker, M., Homagk, P., Ludwig, K. (2004): Operationelle Niedrigwasservorhersage für das Neckareinzugsgebiet. Wasserwirtschaft, 7-8, pp 40-46.

Bremicker, M., Homagk, P., Ludwig, K. (2006): Hochwasserfrühwarnung und Hochwasservorhersage in Baden-Württemberg. Wasserwirtschaft, 7-8, pp 46-50.

Bremicker, M., Ludwig, K. (1990): Einbeziehung des Schneeschmelzprozesses in das Programmsystem FGMOD. Dokumentation. Ingenieurbüro Dr. K. Ludwig, Karlsruhe, im Auftrag des Bayerischen Landesamtes für Wasserwirtschaft (unpublished).

Bremicker, M., Ludwig, K. (1997): Wasserhaushaltsmodelle in Baden-Württemberg – Einsatzmöglichkeiten und Umsetzung. Ingenieurbüro Dr. K. Ludwig, Karlsruhe, im Auftrag der Landesanstalt für Umwelt Baden-Württemberg (unpublished).

Bremicker, M., Ludwig, K., Richter, K.-G. (1997): Effiziente Erstellung mesoskaliger Wasserhaushaltsmodelle. In: PIK Report Nr. 43: Modellierung des Wasser- und Stofftransportes in großen Einzugsgebieten. Zusammenstellung der Beiträge des Workshops am 15.12.1997 in Potsdam. Potsdam Institut für Klimafolgenforschung, pp 23-32.

Bronstert, A. (2000): The possible impacts of environmental changes on flood formation: relevant processes and model requirements. In: European Conference on advances in flood research (ed. by A. Bronstert, C. Bismuth and L. Menzel), pp 183-197. PIK rep. 65, PIK, Potsdam, Germany.

Bronstert, A., Fritsch, U., Katzenmaier, D. (2001): Quantifizierung des Einflusses der Landnutzung und -bedeckung auf den Hochwasserabfluss in Flussgebieten unter Berücksichtung der aktuellen Bodenbearbeitung, des Zustandes der Vegetationsdecke und möglicher Klimaänderungen (Abschlussbericht eines Projektes im Auftrag des Umweltbundesamt, Förderkennzeichen 297 24 508), Potsdam.

Brutsaert, W. (1975): On a derivable formula for long wave radiation from clear skies. Water Resources Research, 11, pp 742-744.

Buczko, U., Hangen, E., Hüttl, R.F., Bens & O., Brunotte, J. (2003): Infiltration and macroporosity of a silt loam soil under two contrasting tillage systems. Landbauforschung Völkenrode, 53(2/3), pp 181-190.

BWK (1998): Wasserbilanzmodelle in der Wasserwirtschaft. Entwurf für das Merkblatt 2/ BWK. Bund der Ingenieure für Wasserwirtschaft, Abfallwirtschaft und Kulturbau e.V., Düsseldorf (unpublished).

Collischonn, W., Tucci, C.E.M. (2001): Hydrologic simulation of large basins (in Portuguese). Brazilian Journal of Water Resources 6(1), pp 15-35.

Collischonn, W., Haas, R., Andreolli, I., Tucci, C.E.M: (2005): Forecasting the river Uruguay using rainfall forecasts from a regional weather-prediction model. Journal of Hydrology, 305, pp 87-98.

Crawford, N.H., Linsley, R.S. (1966): Digital simulation in hydrology: The Stanford Watershed Model IV. Technical report No. 39, Department of Civil Engineering, Stanford University, Palo Alto, California, USA.

DCW (1992): Digital chart of the world, edition 1. Defense Mapping Agency, Fairfax, USA.

Demuth, S. (1993): Untersuchungen zum Niedrigwasser in West-Europa. Freiburger Schriften zur Hydrologie, Band 1. Institut für Hydrologie, Universität Freiburg.

DFG (1992): Regionalisierung in der Hydrologie. Mitteilung Nr. XI der Senatskommission für Wasserforschung, Deutsche Forschungsgemeinschaft.

Dickinson, R. E. (1984): Modelling evapotranspiration for three-dimensional global climate models. In: J.E. Hansen, T. Takahashi (eds.): Climate processes and climate sensitivity. Geophys. Monogr. Ser. 29. AGU, Washington.

Diekkrüger, B., Richter, O. (eds) (1997): Extended abstracts of the International Conference on Regionalisation in Hydrology, 10.-14.3.1997, Braunschweig. Heft 25 der Schriftenreihe Landschaftökologie und Umweltforschung, Institut für Geographie und Geoökologie, Universität Braunschweig.

Disse, M. (1995): Modellierung der Verdunstung und Grundwasserneubildung in ebenen Einzugsgebieten. Mitteilungen des Institutes für Hydrologie und Wasserwirtschaft der Universität Karlsruhe, Heft 53.

DiToro, M. (2001): Sediment flux modeling. John Wiley, New York.

DKRZ (1994): The ECHAM 3 Atmospheric General Ciculation Model. Deutsches Klimarechenzentrum, Technical Report No. 6, Revision 3, July 1994, Hamburg.

Dümenil, L., Todini, E. (1992): A rainfall-runoff scheme for use in the Hamburg climate model. In: Advances In Theoretical Hydrology, A tribute to James Dooge. European Geophysical Society Series on Hydrological Sciences, 1, Elsevier, pp 129-157.

DVWK (1996): Ermittlung der Verdunstung von Land- und Wasserflächen. DVWK-Merkblätter zur Wasserwirtschaft, Heft 238. Deutscher Verband für Wasserwirtschaft und Kulturbau e.V., Bonn.

DWD (1987): Allgemeine Meteorologie. Leitfaden für die Ausbildung im Deutschen Wetterdienst, Nr. 1. Selbstverlag des Deutschen Wetterdienstes, Offenbach a. M., 3. Auflage.

DWD (1995): Ergebnisse methodischer Untersuchungen zur Korrektur des systematischen Messfehlers des Hellmann-Niederschlagsmessers. Berichte des Deutschen Wetterdienstes, Offenbach am Main, Nr. 194.

Dyck, S. (1980): Angewandte Hydrologie, Teil 2: Der Wasserhaushalt der Flussgebiete. VEB Verlag für Bauwesen, Berlin, 2. Auflage.

Ebel, M., Ludwig, K., Richter, K.G. (2000): Mesoskalige Modellierung des Wasserhaushaltes im Rheineinzugsgebiet mit LARSIM. Hydrologie und Wasserbewirtschaftung, 6 (44), pp 308-312.

Enke, W. (2003): Abschlussbericht – Anwendung einer Wetterlagenklassifikation für Süddeutschland auf Kontrolllauf und Szenario eines transienten ECHAM 4 Klimasimulationslaufs (Szenario B2) zur Abschätzung regionaler Klimaänderung für Süddeutschland. Meteo-Research, Berlin, im Auftrag des Arbeitskreis KLIWA (unpublished).

Enke, W., Spekat, A. (1997): Downscaling Climate Model Outputs into Local and Regional Weather Elements by Classification and Regression. Climate Research, 8, pp 195-207.

Fackel, P. (1997): Regionalisierung von Parametern des Wasserhaushaltsmodells LARSIM. Diplomarbeit am Institut für Hydrologie, Albert-Ludwigs-Universität Freiburg (unpublished).

Falkemark, M., Chapman, T. (1989): Comparative hydrology. UNESCO-Press, Paris.

Fischer, H.B., List, E.J., Koh, R.C.Y., Imberger, J., Brooks, N.H. (1979): Mixing in Inland and Coastal Waters. Academic Press, New York.

Gathenya, J. M. (1999): Einsatz von Wasserhaushaltsmodellen zur Wasserbewirtschaftung am Beispiel des Thika-Chania Gebietes in Kenya. Dissertation, Universität Kaiserslautern.

Gerlinger, K. (1997): Erosionsprozesse auf Lößböden: Experimente und Modellierung. Mitteilungen des Instituts für Wasserbau und Kulturtechnik, University Karlsruhe, Heft 194, Karlsruhe, Germany.

Gerlinger, K. (2004): Simulation des Wasserhaushalts im Neckareinzugsgebiet unter Verwendung regionaler Klimaszenarien. In: KLIWA-Berichte Heft 4, pp 87-102. (http:// www.kliwa.de/de/ergebnisse/media/gerlinger.pdf), Arbeitskreis KLIWA.

Gerlinger, K, Tucci, C. (1999): Adaption of the Large Area Runoff Simulation Model LARSIM to the Pantanal region. Abstract in: Workshop on sustainable management of water resources in Brasil. Hannover, 28.-29.9.1999 (unpublished).

Grant, D. (1975): Comparison of evaporation from barley with Penman estimates. Agricultural Meteorology, 15, pp 931-940.

GRDC (1993): Dokumentation bestehender Algorithmen zur Übertragung von Abflusswerten auf Gitternetze. Report No. 2 des Global Runoff Data Centre, Bundesanstalt für Gewässerkunde, Koblenz.

Haag, I., Luce, A., Badde, U. (2005): Ein operationelles Vorhersagemodell für die Wassertemperatur im Neckar. Wasserwirtschaft, 7-8, pp 45-51.

Haag, I., Luce, A., Ludwig, K. (2006a): Entwicklung eines operationellen Wärmemodells für den Neckar zwischen Plochingen und Mannheim. Ingenieurbüro Dr. K. Ludwig, Karlsruhe, im Auftrag der Landesanstalt für Umwelt, Messungen und Naturschutz Baden-Württemberg (unpublished).

Haag, I., Luce, A., Gerlinger, K. (2006b): Effects of conservation tillage on storm flow: a model-based assessment for a mesoscale watershed in Germany. IAHS Publ. 303, IAHS Press, Wallingford, UK, pp 342-350

Haag, I., Westrich, B. (2002): Modellgestützte Optimierung des Einsatzes finanzieller Mittel zur Verbesserung des Sauerstoffhaushalts im Neckar. Wissenschaftlicher Bericht 13/2002 (VA41), Institut für Wasserbau, Universität Stuttgart.

Hangen, E., Buczko, U., Bens, O., Brunotte, J. & Hüttl, R. F. (2002): Infiltration patterns into two soils under conventional and conservational tillage: influence of the spatial distribution of plant root structures and animal activity. Soil and Till. Res., 63, pp 181-186.

Henderson-Sellers, A., Pitman, A., Love, P. K. (1995): The Project for Intercomparison of Land-Surface Parameterisation Schemes (PILPS: Pase 2 and 3). Bull. Am. Meteor. Soc., 94., pp 489-503.

Hennegriff, W., Kolokotronis, V., Weber, H., Bartels, H. (2006): Klimawandel und Hochwasser – Erkenntnisse und Anpassungstrategien beim Hochwasserschutz. Korrespondenz Abwasser (KA), 8, pp. 770-779

Holle, F.-K., Ludwig, K. (1985): Direct runoff retention in catchments. In: Beiträge zur Hydrologie, Sonderheft 5.1, pp 67-78.

Homagk, P. (1996): Hochwasserwarnsystem am Beispiel Baden-Württemberg. Geowissenschaften 14 , Heft 12, pp 539-546.

Homagk, P. (2001): Verlässliche Hochwasservorhersagen zur Vermeidung von Schäden durch rechtzeitige Vorsorgemaßnahmen. Tagungsband zum 2. Forum Katastrophenvorsorge Leipzig, 24.-26.09. 2001, pp 16-28. (www.dkkv.org).

Horton, R.E. (1939): Analysis of runoff-plat experiments with varying infiltration capacity. Transactions, American Geophysical Union, 20, pp 693-711.

Hoyningen-Huene, J. von (1983): Die Interzeption des Niederschlages in landwirtschaftlichen Pflanzenbeständen. In: DVWK Schriften, Heft 57: Einfluss der Landnutzung auf den Gebietswasserhaushalt, pp 1-53.

IPCC (2001): Climate change 2001, Summary for policymakers, Intergovernmental Panel on Climate Change. Cambridge University Press, Cambridge.

IFW (1982): Dokumentation des Programmes FGMOD (Flussgebietsmodell). Institut für Wasserwirtschaft, Hydrologie und landwirtschaftlichen Wasserbau der Universität Hannover (unpublished).

IHW (2000): Die Beurteilung von Einzugsgebieten und ihren Teilflächen nach der Abflussbereitschaft unter Berücksichtigung der landwirtschaftlichen Nutzung – aufgezeigt an drei Einzugsgebieten in Rheinland-Pfalz. Bericht.-Nr. B003, IHW, ETH Zürich.

Jacob, D. (1995): REMO – a model for climate research and weather forecast. In: Conference proceedings of the first study conference on BALTEX, Visby, Sweden. International BALTEX Secretariat, Publication No. 3, p 99.

Jacob, D.(2001): A note to simulation of the Annual and Interannual Variability of the Water Budget over the Baltic Sea Drainage Basin. Meteorology and Atmospheric Physics 77, No 1-4, pp 61-74.

Jury, W.A., Gardner, W.R., Gardner, W.H. (1991): Soil physics, 5th Edition, John Wiley, New York.

Kirpich, Z.P. (1940): Time of concentration of small agricultural watersheds. Civil Engineering 10, Nr. 6.

KLIWA (2004): Klimaveränderung und Folgen für die Wasserwirtschaft – 2. KLIWA-Symposium 03./04.05.2004. KLIWA-Berichte Heft 4. (http://www.kliwa.de/de/ ergebnisse/content0e.html), Arbeitskreis KLIWA.

KLIWA (2006): Regionale Klimaszenarien für Süddeutschland. KLIWA-Berichte Heft 9. (http://www.kliwa.de/de/ergebnisse/content0e.html), Arbeitskreis KLIWA.

Knauf, D. (1980): Die Berechnung des Abflusses aus einer Schneedecke. In: DVWK (Hrsg.) (1980): Analyse und Berechnung oberirdischer Abflüsse. DVWK-Schriften, Heft 46, pp 95-135. Deutscher Verband für Wasserwirtschaft und Kulturbau e.V., Bonn.

Kouwen, N., Soulis, E.D., Pietroniro, A., Donald, J., Harrington, R.A. (1993): Grouped response units for distributed hydrologic modeling. J. of Water Resour. Planning and Management, 119 (3), pp 289-305.

Krauter, G. (2005): Entwicklung eines Ansatzes zur Abschätzung der Geometrie von Fließgewässern. Ingenieurbüro Dr. K. Ludwig, Karlsruhe (unpublished).

LAWA (1991): Grundlagen für die Beurteilung von Kühlwassereinleitungen in Gewässer. Erich Schmidt Verlag, Berlin.

Lehmann, A. (1995): A three-dimensional baroclinic eddy-resolving model of the Baltic Sea, Tellus 47A: pp 1013-1031.

Leibundgut, Ch., Uhlenbrook, S. (1997): Abflussbildung bei Hochwasser. Bd. 5 der Materialien zum Hochwasserschutz am Rhein, herausgegeben vom Ministerium für Umwelt und Forsten, Rheinland-Pfalz.

Lemmlä, R., Kuusito, E. (1974): Evaporation from snow-cover. Hydrol. Sc. Bull. 19 (4), pp 543-548.

Leopold, L.B., Maddock, T. jr. (1953): The hydraulic geometry of stream channels and some physiographic implications. Geological Survey Professional Paper 252, United States Goverment Printing Office, Washington.

LfU (1999a): Hochwasserabfluss-Wahrscheinlichkeiten in Baden-Württemberg. Schriftenreihe Oberirdische Gewässer, Gewässerökologie, Band 54. Landesanstalt für Umweltschutz Baden-Württemberg, Karlsruhe.

LfU (1999b): Das Wasserhaushaltsmodell Neckar. Untersuchung des Ingenieurbüros Dr. K. Ludwig, Karlsruhe, im Auftrag der Landesanstalt für Umweltschutz Baden-Württemberg (unpublished).

LfU (1999c): Wasserhaushaltsmodell für das Einzugsgebiet der Donau bis zur Illermündung. Untersuchung des Ingenieurbüros Dr. K. Ludwig, Karlsruhe, im Auftrag der Landesanstalt für Umweltschutz Baden-Württemberg (unpublished).

LfU (1999d): Weiterentwicklung des Wasserhaushaltsmodells für den Neckar. Untersuchung des Ingenieurbüros Dr. K. Ludwig, Karlsruhe, im Auftrag der Landesanstalt für Umweltschutz Baden-Württemberg (unpublished).

LfU (2004): Analyse der Auswirkungen dezentraler Hochwasserschutzmaßnahmen mit hochauflösenden Wasserhaushaltsmodellen. Untersuchung des Ingenieurbüros Dr. K. Ludwig, Karlsruhe, im Auftrag der Landesanstalt für Umweltschutz Baden-Württemberg (unpublished).

LfU (2005): Leitfaden „Festlegung des Bemessungshochwassers für Anlagen des technischen Hochwasserschutzes“, Karlsruhe. (www.lubw.baden-wuerttemberg.de).

Liebscher, H.-J. (1992): Internationale Aktivitäten auf dem Gebiet der Regionalisierung. In: DFG (1992): Regionalisierung in der Hydrologie. Mitteilung Nr. XI der Senatskommission für Wasserforschung, Deutsche Forschungsgemeinschaft, pp. 63-75.

Luce, A., Haag, I., Bremicker, M. (2006): Einsatz von Wasserhaushaltsmodellen zur kontinuierlichen Abflussvorhersage in Baden-Württemberg. Hydrologie und Wasserbewirtschaftung, Heft 2, pp 58-66.

Ludwig, K. (1978): Systematische Berechnung von Hochwasser-Abflussvorgängen mit Flussgebietsmodellen. In: Mitteilungen des Institutes für Hydrologie, Wasserwirtschaft und landwirtschaftlichen Wasserbau der Technischen Universität Hannover, Nr. 44, pp 263-462.

Ludwig, K. (1982): The Program System FGMOD for Calculation of Runoff Processes in River Basins. Zeitschrift für Kulturtechnik und Flurbereinigung, 23, pp 25-37.

Ludwig, K. (1989): Hochwasservorhersage für große, semiaride Einzugsgebiete am Beispiel des Gelben Flusses. Mitteilungen des Instituts für Wasserwirtschaft, Hydrologie und landwirtschaftlichen Wasserbau der Universität Hannover, Heft 70.

Maurer, T. (1997): Physikalisch begründete zeitkontinuierliche Modellierung des Wassertransports in kleinen ländlichen Einzugsgebieten. Mitteilungen des Institutes für Hydrologie und Wasserwirtschaft der Universität Karlsruhe, Heft 61.

Meier, W.K. (2002): Modellierung der Auswirkungen von Wasserkraftanlagen auf physikalische und chemische Eigenschaften von Bergbächen. Dissertation ETH Zürich, Diss. ETH Nr. 14526, Zürich.

Mohseni, O., Stefan, H.G. (1999): Stream temperature/air temperature relationship: a physical interpretation. Journal of Hydrology, 218, pp 128-141.

Monteith, J.L. (Ed.) (1979): Vegetation and the atmosphere. Academic Press, London.

Nash, J.E., Sutcliffe, J.V. (1970): River flow forecasting through conceptual models. 1. A discussion of principles. Journal of Hydrology, 10, pp 282-290.

Niehoff, D. (2001): Modellierung des Einflusses der Landnutzung auf die Hochwasserentstehung in der Mesoskale. PhD Thesis, Mathematisch-Naturwissenschaftliche Fakultät, Universität Potsdam.

Niehoff, D., Fritsch, U., Bronstert, A. (2002): Land-use impacts on storm-runoff generation: scenarios of land-use change and simulation of hydrological response in a meso-scale catchment in SW-Germany. Journal of Hydrology, 267(1/2), pp 80-93.

Nijssem, B, Lettenmaier, D. P., Liang, X., Wetzel, S. W., Wood, E. F. (1997) Streamflow simulation for continental-scale river basins. Water Resour. Res., 33(4), pp 711-724.

Penman, H.L. (1948): Natural evaporation from open water, bare soil and grass. Proc. Roy. Meteorol. Soc. A, 193, pp 120-145.

Pitman, A.J., Henderson-Sellers, A., Abramopoulos, F., Avissar, R., Bonan, G., Boone, A., Dickinson, R.E., Ek, M., Entekhabi, D., Famiglietti, J., Garratt, J.R., Frech, M., Hahmann, A., Koster, R., Kowalczyk, E., Laval, K., Lean, J., Lee, T.J., Lettenmaier, D., Liang, X., Mahfouf, J-F., Mahrt, L., Milly, P.C.D., Mitchell, K., de Noblet, N., Noilhan, J., Pan, H., Pielke, R., Robock, A., Rosenzweig, C., Schlosser, C.A., Scott, R., Suarez, M., Thompson, S., Verseghy, D., Wetzel, P., Wood, E., Xue, Y., Yang, Z-L & Zhang, L.(1993): Project for Intercomparison of Land-Surface Parameterization Schemes (PILPS). Results from off-line control simulations, GEWEX Report. IGPO Publication Series No. 7.

Plate, E.J. (1992): Skalen in der Hydrologie: Zur Definition von Begriffen. In: DFG (1992): Regionalisierung in der Hydrologie. Mitteilung Nr. X1 der Senatskommission für Wasserforschung, Deutsche Forschungsgemeinschaft, pp 33-44.

Quast, J., Böhm, G. (1997): Ermittlung der realen Evapotranspiration von Niedermoorgebieten unter den hydroklimatischen Bedingungen Nordostdeutschlands am Beispiel des Rhinluchs. Abschlussbericht des BMBF-Verbundvorhaben „Wasserkreislauf“, ZALF, Müncheberg.

Rachner, M. (1987): Verdunstung von der Oberfläche der Schneedecke. Ergebnisse der an der Forschungsstation Harzgerode durchgeführten Messungen. Z. Meteorolog., 37, pp 285-290.

Richter, O., Söndgerath, O., Diekkrüger, B. (1996): Wasser- und Stoffdynamik in Agrarökosystemen. Abschlussbericht SFB 179, Band 1. In: Herrmann, A., Richter, O. (Hrsg.): Landschaftsökologie und Umweltforschung, Heft 24.

Richter, K.-G., Ebel, M. (2003): Analysis of the Water Cycle of the Baltic Area under present and future Conditions. German Climate Research Program (2001-2006), DEKLIM Status Seminar 2003, Bad Münstereifel, 6-8 Oktober 2003: pp 205-206.

Richter, K.-G., Lorenz, P., Ebel, M., Jacob, D.(2004): Analysis of the Water Cycle for the BALTEX Basin wizhin an Integrated Atmospheric Hydrological Ocean Model. Fourth Study Conference on BALTEX, Gudhjem, Bornholn, Denmark 24-28 May 2004, ISSN 1681-6471.

Richter K.-G., Ebel, M. (2006): Analysis of runoff for the Baltic Basin with an integrated Atmospheric-Ocean-Hydrology Model. Advances in Geosciences, 9, pp 1-7.

Roald, L., Nordseth, K., Hassel, K. A. (eds) (1989): FRIENDS in hydrology. IAHS Publ. No. 187. IAHS-Press, Wallingford/UK.

Scheffer, F., Schachtschabel, P. (1984): Lehrbuch der Bodenkunde, 11. Auflage. Ferdinand Enke Verlag Stuttgart.

Schulla, J. (1997): Hydrologische Modellierung von Flussgebieten zur Abschätzung der Folgen von Klimaänderungen. Züricher Geographische Schriften, Heft 69, Geographisches Institut, ETH Zürich.

Schulz, W., Merkel, U., Bach, H., Appel, F., Ludwig, R., Löw, A., Mauser, W. (2002): InFerno – Integration of remote sensing data in operational water balance and flood prediction modelling. Proceedings of the International Conference on Flood Estimation, pp 659-668, March 6-8, 2002, Berne.

Schwarze, R., Dröge, W., Opherden, K. (1997): Regional analysis and modelling of groundwater runoff components from small catchments in solid rock areas. In: Extended Abstracts of the International Conference on Regionalisation in Hydrology, 10.-14.3.1997, Braunschweig. Heft 25 der Schriftenreihe Landschaftökologie und Umweltforschung, Institut für Geographie und Geoökologie, Universität Braunschweig.

Sevruk, B. (1989): Reliability of precipitation measurement. In: Workshop of precipitation measurement, St. Moritz, Dezember 1989.

Semmel, H., Horn, R. (1995): Auswirkungen konventioneller und konservierender Bodenbearbeitung auf das Druckfortpflanzungsverhalten und physikalisch-mechanische Kenngrößen von Ackerböden. In: Kuratorium für Technik und Bauwesen in der Landwirtschaft e.V. (KTBL).

SFB81 (1980): Quantitative Abflussmodelle in einem voralpinen Flusssystem. Schlussbericht für das Teilprojekt B2 im Sonderforschungsbereich 81 der Technischen Universität München.

Singh, V.P. (Ed.) (1995): Computer models of watershed hydrology. Water Resources Publications, Highlands Ranch, Colorado, USA.

Singh, V.P., Frevert, D.K. (eds) (2002): Mathematical models of large watershed hydrology. Water Resources Publications, Highlands Ranch, Colorado, USA.

Sinokrot, B.A., Stefan, H.G. (1993): Stream Temperature Dynamics: Measurements and Modeling. Water Resources Research, 29(7), pp 2299-2312.

Soulis E.D., Kouwen, N., Pietroniro, A., Seglenieks, F.R., Snelgrove, K.R., Pellerin, P., Shaw, D.W., Martz L.W. (2004): A Framework for Hydrological Modelling. In: Prediction in Ungauged Basins: Approaches for Canada's Cold Regions (ed. by C. Spence, J.W. Pomeroy & A. Pietroniro). CWRA ACRH Press, Ontario, Canada.

Tebrügge, F. & Düring, R.A. (1999): Reducing tillage intensity – a review of results from long-term studies in Germany. Soil and Till. Res., 53, pp 15-28.

Thompson, N., Barrie, I. A. & Ayles, M. (1981): The Meterological Office rainfall and evaporation calculation system: MORECS (July 1981). Hydrological Memorandum No. 45.

Tucci, C.E.M., Clarke, R.T., Collischonn, W., da Silva Dias, P.L., de Oliveira, G.S. (2003): Longterm flow forecasts based on climatic and hydrologic modeling: Uruguay river basin. Water Resources Research, Vol. 39

UBA (Hrsg.) (1995): Entwicklung eines mathematischen Modells zur Untersuchung des Einflusses von Klima- und Landnutzungsänderungen auf den Hoch- und Niedrigwasserabfluss im Einzugsgebiet der Mosel sowie zur Echtzeitvorhersage unter Verwendung von Fernerkundungstechniken. Forschungsbericht UBA-FB Wasser 102 01 304, Umweltforschungsplan des Bundesministers für Umwelt, Naturschutz und Reaktorsicherheit.

USGS (U.S. Geological Survey) (1993): Digital elevation models, data user guide 5. Reston, Virginia, 50 p.

Weiler, M.H. (2001): Mechanisms controlling macropore flow during infiltration. Dye tracer experiments and simulations. Dissertation ETH Zürich, Diss. ETHZ Nr. 14237.

Weischet, W. (1983): Einführung in die allgemeine Klimatologie. Physikalische und meteorologische Grundlagen. Verlag Teubner, Stuttgart.

Wigmosta, M.S., Lance, L.W., Lettenmaier, D.P. (1994): A distributed hydrology-vegetation model for complex terrain. Water Resources Research, 30 (6), pp 1665-1679.

Williams, J.R. (1969): Flood routing with variable travel time or variable storage coefficients. Transactions of the ASAE, p. 100.

WMO (World Meteorological Organization) (1988a): Concept of the Global Energy and Water Cycle Experiment. Technical report, WCRP-5, WMO/TD No. 215, Geneva, Switzerland.

WMO (World Meteorological Organization) (1988b): Analyzing long time series of hydrological data with respect to climate variability. WCAP-3, WMO/TD-No. 224, Geneva, Switzerland.

Wohlrab, B., Ernstberger, H., Meuser, A., Sokollek, V. (1992): Landschaftswasserhaushalt. Wasserkreislauf und Gewässer im ländlichen Raum. Verlag Paul Parey, Hamburg und Berlin.

Zeller, J. (1965): Die „Regime-Theorie“, eine Methode zur Bemessung stabiler Flussgerinne. In: Schweizerische Bauzeitung, 83. Jahrgang, Teil 1: S. 67-72 in Heft 5 und Teil 2: S. 87-93 in Heft 6.

Zhao, R.J. (1977): Flood forecasting method for humid regions of China. East China Institute of Hydraulic Engineering, Nanjing, China.

Zhao, R.J., Zhang, Y.-L., Fang, L.-R., Liu, X.-R. & Zhang, Q.-S. (1980): The Xinanjiang model. In: Hydrological Forecasting (Proc. Oxford Symposium, April 1980), pp 351-356. IAHS Publ. 129, IAHS Press, Wallingford, UK.

Zimmerling, B., Schmidt, W.A., (2002): Vorbeugender Hochwasserschutz in landwirtschaftlich genutzten Gebieten. In: Sieker F. Endber., DBU Projekt AZ 15877, Osnabrück., pp 43-70.

Zingg, Th. (1951): Beziehungen zwischen Temperatur und Schmelzwasser und ihre Bedeutung für Niederschlags- und Abflussfragen. IAHS Publ. No. 32, pp 266-269.